Organic semiconductors blended into a cross-linkable insulator: Separating processability from optoelectronic functionality

Dissertation
zur Erlangung des Grades
„Doktor
der Naturwissenschaften“
am Fachbereich Physik, Mathematik und Informatik
der Johannes Gutenberg-Universität
in Mainz

Christian Kasparek

Geb. in Erbach(Odenwald)
Mainz, den 28.09.2017

Tag der mündlichen Prüfung: 01.02.2018

Berichterstatter:

Prof. Dr. Paul Blom

Prof Dr. Mathias Kläui

Abstract

Fabrication of multilayer solution-processed polymer light-emitting diodes (PLEDs) is still a major problem. In this work, functional polymers are blended with a cross-linkable host matrix. After deposition the matrix is made insoluble by UV-light. The solubility of blends of poly[2-methoxy-5-(2-ethylhexyloxy)-1,4-phenylenevinylene] (MEH-PPV) and two different matrices in different weight ratios has been investigated. It was found that only 10 wt. % of the matrix is necessary in order to make the whole blend layer insoluble. As a next step the charge transport was analyzed. One matrix (NOA83H) showed an injection problem for holes from the PEDOT:PSS anode into MEH-PPV. This problem did not occur when SR540 was used as matrix. For only 10 wt. % of matrix, the hole and electron transport are barely affected. Consequently, PLEDs consisting of an insoluble 90:10 MEH-PPV:SR540 blend exhibited the same optoelectronic properties as pristine and soluble MEH-PPV based devices.

Using this method, a multilayer PLED with two emissive layers and a hole-blocking layer was fabricated. To investigate the intermixing of the two emissive layers the electroluminescence spectrum was measured and compared to a drift-diffusion simulation that assumed a sharp interface with two distinct layers. A good agreement was found between measurement and simulation, which indicates that there is no significant intermixing at the interface.

Multilayer PLEDs with charge blocking layers were fabricated to achieve an increased efficiency as compared to a single layer PLED. For a trilayer PLED poly[N,N'-bis(4-butylphenyl)-N,N'-bis(phenyl)-benzidine] (poly-TPD) was used as electron-blocking layer, SuperYellow-PPV (SY-PPV) as emissive layer and poly(9,9-di-n-octylfluorenyl-2,7-diyl) (PFO) as hole-blocking layer. The PLED consisting of 90:10 poly-TPD:SR540/90:10 Super Yellow:SR540/PFO showed a 23% increased efficiency a low voltage that decreased again with increasing voltage. To study this in more detail, a two-layer PLED with MEH-PPV and PFO was fabricated that showed the same increase in efficiency at low voltage and decrease at higher voltage. Introducing a two-layer hole mobility simulation revealed that the increase in efficiency is mainly due to the elimination of quenching and charge accumulation at the MEH-PPV/PFO interface. The decrease in efficiency is because holes can overcome the hole-blocking barrier at high voltage. This could be simulated with a field dependent hole mobility in the PFO layer.

Table of Contents

1 Introduction

The invention of the light bulb revolutionized the modern life. The availability of lighting extended the utilizable time beyond dawn and dusk. The principle of a light bulb is incandescence. An electric current is flowing through a tungsten filament such that it is heating up. The filament starts to emit electromagnetic radiation as a result of its temperature. However, most of the emission is in the infrared spectrum, which is a loss process and makes an incandescent bulb very inefficient as a light source. Nevertheless, the light bulb was used for more than a century.

Newer technologies are the fluorescent and the compact fluorescent lamp where the efficiency is markedly increased but still lots of heat is produced. Since recently, semiconducting light-emitting diodes (LEDs) are commercially available. These new solid-state light sources have an efficiency of around 100 lm/W which is considerably higher than the incandescence bulb (15 lm/W) and compact fluorescent lamp (60 lm/W).(*1*) A new class of LEDs is organic light-emitting diodes (OLEDs) that are made of organic instead of inorganic materials. OLEDs are very thin, typically only a few hundred nanometers, and can be fabricated in various shapes and sizes. In OLEDs almost no heat is produced. Usually the temperature during operation of OLEDs is around 30°C instead of 90°C and 60°C for incandescent bulbs and fluorescent tubes, respectively.(*2*) Additionally, they are mercury-free, have the potential for large areas and can be processed on flexible substrates. More importantly, OLEDs facilitate new design concepts such as transparent lighting panels and luminescent wallpapers.(*2, 3*)

In the beginning of this century the development of thermally evaporated small molecule based OLEDs advanced rapidly and first displays were commercially available. For example Sony offered the first 11 inch OLED TV in 2008. Most notably, Samsung incorporated active matrix OLED displays in their Galaxy smartphone, which was the second most-sold smartphone in 2010. Nowadays, OLED displays are integrated in many different smartphones and TVs.

One of the advantages of OLED displays compared to conventional liquid crystal display (LCD) is the image quality. In a LCD, a white backlight is used that is filtered in order to have red, green and blue pixels. To realize a black pixel, the light is filtered completely. These filters do not block the light perfectly and there is always some background illumination. Consequently, the contrast is not

optimal. In an OLED display the pixels are emitting the red, green and blue light. Therefore, the light emission can be simply turned off to create black color and no background illumination is visible, which increases the contrast. Furthermore, a high brightness, a broad viewing angle and big color range can be achieved. Additionally to the image quality, the power consumption is lower compared to LCD, the display is very thin and has the potential for flexible and transparent displays. The disadvantage of OLED displays is the high manufacturing cost. The displays also show a lower lifetime. This is especially a problem in blue pixels. However, the lifetime has improved a lot recently. LG Display reported that their OLED TVs have a lifetime of 100 000 hours.

The pioneering work that led to today's OLEDs was done in the 1950s, when the conductive properties of anthracene crystals and other organic materials were studied and the first electroluminescence (EL) was found, first by applying an alternating current, later by a direct current.(*4-9*) Typically, these films were about 10-20 µm thick such that very high voltages above 400 V had to be applied to observe the EL. A breakthrough was achieved in 1987 when Tang and van Slyke reported a thermally evaporated double layer OLED.(*10*) The device consisted of an aromatic diamine and Aluminium-tris(8-hydroxychinolin) (Alq_3). By keeping the film thickness low (about 135 nm) a high luminous efficiency of 1.5 lm/W and a brightness of over 1000 cd/m^2 were achieved at a driving voltage below 10 V. In 1990 the first polymer light-emitting diode (PLED) was fabricated using a poly(p-phenylene vinylene) based on a solution-processable precursor.(*11*) Solution processing simplified the fabrication process and was the basis for the development of large area light-emitting displays. By adding side chains to the PPV backbone, the material could be made soluble in common organic solvents and the precursor route was not necessary anymore. The solubility of the materials enabled simple and cheap fabrication methods like spin-coating, slot-die coating or inkjet printing, amongst others.

State-of-the-art OLEDs consist of a stack of layers that each have specific functions. Injection layers decrease the energy difference between the injecting contact and the emissive layer. By adding doped layers, the charge carrier mobility is increased and consequently the voltage drop across the device lowered.(*12-14*) Blocking layers for holes and electrons confine the charge carriers in the emissive layers which increases the efficiency.

The simplest structure is a single layer OLED as shown Figure 1.1a), where the emissive layer is sandwiched between anode and cathode. Holes are injected

from the anode in the highest occupied molecular orbital (HOMO) of the emissive layer and electrons are injected from the cathode to the lowest unoccupied molecular orbital (LUMO). If an electric field is applied, electrons flow towards the anode and holes towards the cathode. If an electron and hole are close together they form an exciton and recombine by emitting a photon. In organic semiconductors the recombination is of Langevin type, which means that the recombination is limited by the diffusion of the carriers towards each other due to the charge carrier mobility. The Langevin recombination and the emission of a photon are shown by the black arrows in Figure 1.1a). In most organic semiconductors the charge transport is highly unbalanced due to the presence of electron traps.(*15*) It was found that additionally to the Langevin recombination, there is another type of recombination, namely the Shockley-Read-Hall (SRH) recombination. The SRH recombination is trap-assisted recombination where a trapped electron recombines with a free hole. The energy is exchanged by the releasing phonons, making it a non-radiative recombination.(*16, 17*) The SRH recombination is indicated by the blue arrows in Figure 1.1a). Holes are not affected by the traps and can move freely through the material, while electrons move slowly because they can fall in trap states where they are immobilized. A consequence is that at low voltages, where the traps are empty, most electrons are trapped and the recombination zone where electrons and holes form excitons is very close to the metallic cathode. In this case the excitons can transfer their energy non-radiatively via long range dipole-dipole interactions to the metallic cathode.(*18*) This is schematically shown in Figure 1.1a) by the dotted lines.

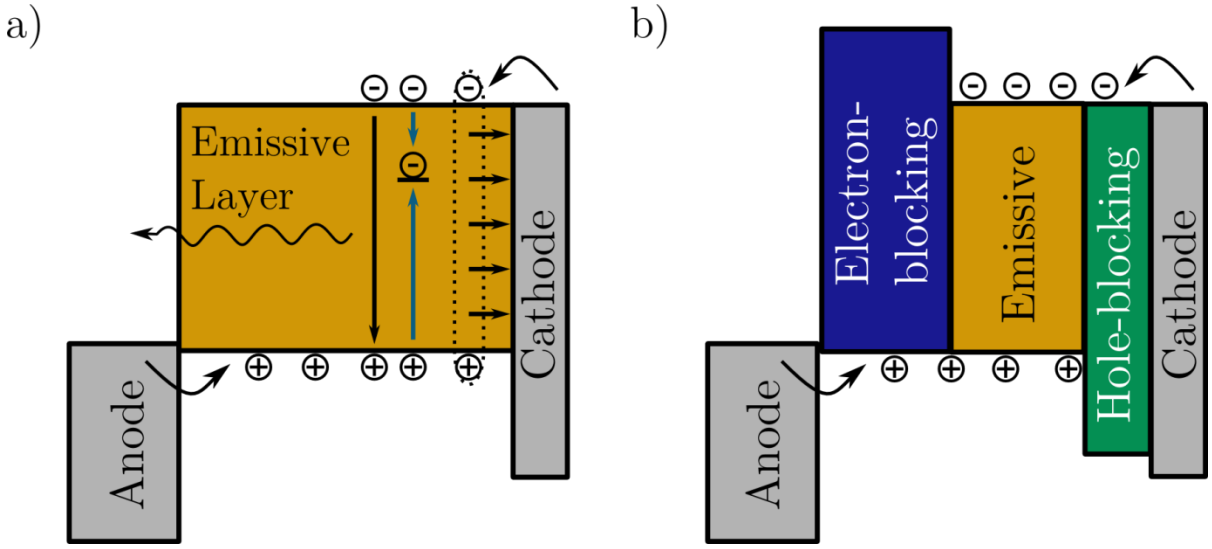

Figure 1.1: a) Schematic energy diagram of a single layer PLED. Radiative Langevin recombination is indicated by the black arrows, non-radiative SRH recombination is indicated by the blue arrows and quenching is indicated by the dotted line. b) Energy diagram of multilayer

PLED with an electron-blocking, emissive and hole-blocking layer. Because of the blocking layers the charge carriers are confined in the emissive layer. They are forced to recombine there and quenching at the metal electrodes is prevented.

By including blocking layers, the charge carriers are confined in the emissive layer. This is done by making use of an energy offset between the HOMO of the emissive layer and the hole-blocking layer and an energy offset between the LUMO of the emissive layer and the electron-blocking layer. The energy diagram of such a structure is shown in Figure 1.1b). Here, holes are injected from the anode into the multilayer stack and subsequently flow through the electron-blocking layer and emissive layer, but get blocked at the interface of the hole-blocking layer. Electrons are injected from the cathode and travel through the hole-blocking layer and emissive layer until they get blocked at the interface of the electron-blocking layer. Consequently, electrons and holes cannot leave the emissive layer without forming an exciton and recombine by emitting light, thereby eliminating the quenching at the cathode.

Recently, Kuik *et al.* investigated the non-radiative loss mechanisms in a single layer poly[2-methoxy-5-(2-ethylhexyloxy)-1,4-phenylenevinylene] (MEH-PPV) PLED.(*19*) In the report the current efficiency versus the applied voltage was simulated and the effect of the loss mechanisms was analyzed. These included SRH recombination and cathode quenching. The same simulation was done for the batch of MEH-PPV used in this thesis and is shown in Figure 1.2. The bimolecular Langevin recombination is the recombination of a free hole and free electron that diffuse towards each other in their mutual Coulomb field. It can be seen that the trap-assisted SRH recombination has the strongest influence on the current efficiency. However, at low voltage the loss due to cathode quenching increases strongly and at 3 V about 25 % of the current efficiency is lost due to cathode quenching. By confining the charge carriers with blocking layers in the emissive layer as shown in Figure 1.1b), this loss mechanism can be eliminated and the efficiency of the PLED can be increased.

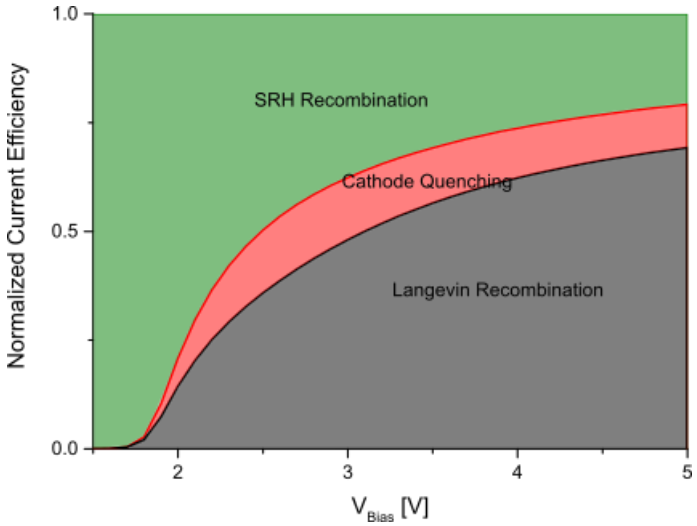

Figure 1.2: Simulation of the current efficiency as a function of the applied voltage of a single layer MEH-PPV PLED. The green and red line show the influence of non-radiative recombination losses and the black line the Langevin recombination.

State-of-the-art multilayer OLEDs fabricated by thermal evaporation of small molecule materials include these charge blocking layers. These devices facilitate a low operating voltage and a high efficiency. This is schematically shown in Figure 1.3a) where the emissive layer (EML) is simply evaporated on top of the previously evaporated electron-blocking layer (EBL).

In addition to display technology with separate red, green and blue pixels, white OLEDs have the potential to replace common light bulbs in future ambient lighting.(*20, 21*) While OLEDs are already commercially available in displays, the technology is not used for lighting applications, yet. A major reason is that the displays are manufactured by thermal evaporation of the organic semiconductor. With this method, it is easy to fabricate small areas that are used as a pixel in a display. If used for lighting applications, point sources like in an OLED display are not suitable but rather large areas are necessary so that the total luminous intensity increases. Evaporating large areas in a vacuum is challenging and moreover expensive. Despite the technological progress, an OLED display is still more expensive than an LCD. In order to compete with cheap commercially available lamps or to realize luminescent wallpapers, large areas have to be manufactured and the costs have to be lowered by a few orders of magnitude.

The route towards lower cost is solution processing. As mentioned before, polymers have been modified so that they are soluble in common organic solvents which enables solution processing. In solution processing, cheap manufacturing methods like roll-to-roll production, which is being used to print newspapers, inkjet printing, spin-coating and spray-coating can be used. Furthermore, large areas can

be deposited relatively easily, even on flexible substrates.(*22-27*) Consequently, PLEDs have the potential for large-area and low-cost manufacturing which are exactly the requirements for lighting application.

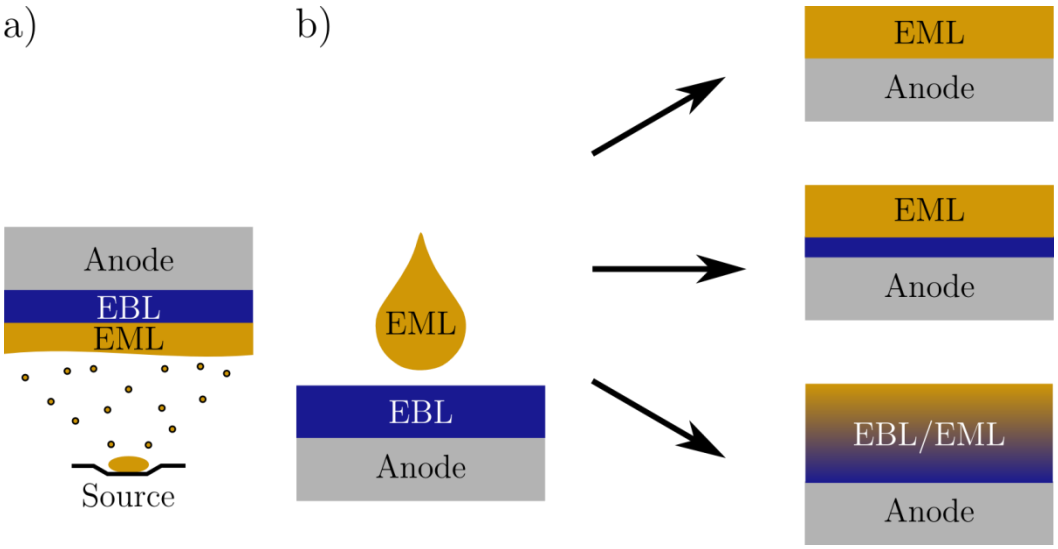

Figure 1.3: a) Fabrication of multilayers by thermal evaporation can be easily done by subsequent evaporation of the materials. B) Fabrication of multilayers by solution is difficult because the first layer, here the electron-blocking layer (EBL) redissolves in the solvent of the emissive layer (EML). Thus, the EBL can be either completely washed off, reduced or both layers can intermix.

As previously mentioned, multilayers are inevitable for PLEDs to be efficient. However, a major challenge in solution processing is the stack integrity. Typical organic semiconductors are soluble in common organic solvents. Consequently, when a subsequent layer is coated on top of a previously deposited layer, the first layer redissolves in the solvent of the second layer. The first layer can then either be completely washed off, reduced or intermixed with the second layer which affects the functionality of the stack. This is shown for an emissive layer (EML) that is deposited by solution on an electron-blocking layer (EBL) in Figure 1.3b)

In the past few years lots of approaches have been developed to realize solution-processed multilayer OLEDs. One of the most common approaches is to use orthogonal solvents to deposit the materials of two adjacent layers. By subsequently depositing materials that are dissolved in polar and non-polar solvents the second solution will not redissolve the first layer. (*28-35*) A very popular example is poly(3,4-ethylenedioxythiophene) polystyrene sulfonate (PEDOT:PSS) that is soluble in water and often used as hole injection layer in organic electronics. However, the success of this approach relies on the ability to reproducibly synthesize materials with the required solubility without affecting the optical and

electrical properties. Furthermore, it is not possible to add another layer in between the layers, because the polarity of all subsequent solvents has to be changed.

An alternative approach is to add cross-linkable side chains to the functional material. The side chains are cross-linked after deposition using ultra violet (UV) light. This prevents redissolution during the deposition of a subsequent layer.(*36-41*) In order to achieve the cross-linking, the side chains have to contain reactive groups. These groups can affect the charge transport, luminescence and stability of the material in a negative way. Additionally, this approach also depends on the ability to synthesize the materials reproducibly with the required optical, electrical and chemical properties.

A different method is to bake an organic layer after the deposition such that it does not dissolve anymore. This has been shown for a hole transport layer in between PEDOT:PSS and the emissive layer. The material was hard baked at high temperatures of around 200°C before the next layer was deposited from an organic solvent.(*42-44*) Typically, this can only be done for one layer in the stack and does not work for flexible plastic substrates because the baking temperature is above the melting point of the substrate.

Another proposed option is the usage of a liquid buffer layer of propylene glycol. This buffer layer is deposited on top of the first layer and does not dissolve in the solvent of the subsequent layer. The second layer then floats on top of the buffer layer that evaporates either during the deposition or during a subsequent baking step. At that point the top layer has dried and an intermixing has been prevented. A challenge here is that some of the propylene glycol may remain in the device and affect the performance and it has only been shown to work for small samples.(*45, 46*)

Furthermore, it is possible to use very high molecular weight polymers that take a long time to dissolve when a second layer is deposited from solution on top.(*47*) Here, the problem is that polymers with a very high molecular weight are difficult to process from solution. A similar technique is to optimize the processing conditions in such a way that the top layer dries very fast and prevents intermixing. (*48, 49*)

Another approach is to achieve multilayers by using a stamp transfer process (*50, 51*) or to make two halves of a device and laminating the dry layers together.(*52*) Recently, He *et al.* reported that cross-linking the surface using a mixed acetylene and argon plasma makes it possible to resist redissolution in

organic solvents.(*53*) An excellent review of the recent progress of solution-processed multilayer OLEDs is given by So *et al.(54)*

All these approaches exhibit certain disadvantages, for example multilayer structures based on solvent polarity or cross-linkable units typically rely on elaborate and often cumbersome synthetic strategies. Consequently, these concepts only work for a specific set of materials. An alternative approach has been published by Zhou *et al.*(*55*). A polyfluorene-based hole transport material was blended with two different insulating, commercially available cross-linkable materials, ethoxylated (4) bisphenol a dimethacrylate (SR540, Sartomer) and NOA83H (Norland Products), to tune the solubility of the resulting blend layer. Upon cross-linking with UV-light these materials form an insoluble host matrix around the semiconductor that makes the whole blend layer insoluble. By blending two materials, the solution processability (insulating matrix) and the optoelectronic functionality (hole transport material) are separated. In contrast to many of the approaches mentioned before, in this approach standard organic semiconductors can be used without the requirement for chemical modifications.

In order to make the layer insoluble in either toluene and chloroform these blends contained nearly 70% of cross-linkable host matrix, which might have a severe effect on the charge transport properties. However, a systematic study on the charge transport was not done. Additionally, the work was limited to only one layer.

In this work, the effect of blending a cross-linkable matrix into a semiconductor and the consequences for the electrical and optical properties are investigated and the approach is extended to more than one layer. If the problem of solution-processed multilayer PLEDs could be solved with this approach, it promises to be a very appealing way to fabricate low cost and large area PLEDs. This is a generic way to make multilayers that is not specific to certain material systems and there is no limitation on how many layers can be stacked as in most of the approaches that were presented before. The general process is sketched in Figure 1.4. A blend of the cross-linkable host matrix and the functional material, in this example a material for the electron-blocking layer, is made. The blend solution is deposited on top of the anode. In this work the solution processing is done by spin-coating but other techniques are possible, too. After deposition, the host matrix is made insoluble by exposure to UV-light. The host matrix forms a cross-linked network around the electron-blocking material, which makes the whole blend layer insoluble. Consecutively, the next layer can be deposited on top of the first

layer without redissolving the layer. The next layer, a blend of matrix and an emissive material are solution-processed and afterwards the host matrix is again cross-linked with UV-light. The resulting blend layer is insoluble and another layer can be processed on top.

The key objective of this thesis is to find a universal approach to process multilayers from solution that is independent of the material concept. Therefore, blends of two different insulating host matrices and poly[2-methoxy-5-(2-ethylhexyloxy)-1,4-phenylenevinylene] (MEH-PPV) are made. MEH-PPV is used as a model material because it has been well-studied in the recent years. The first question that will be addressed is how much matrix is needed in order to make the blend insoluble. To this end, the blends are made in different weight ratios of MEH-PPV and matrix and the solubility is measured after cross-linking by spin-coating solvent on top of the blend. Additionally to being insoluble, the charge transport of the blends should not be affected. Therefore, the charge transport of blends in different weight ratios is analyzed in single carrier devices. Single carrier devices are useful to investigate the effect of the matrix on the hole and electron transport. Furthermore, PLEDs of the blends are fabricated to measure how the matrix affects the efficiency.

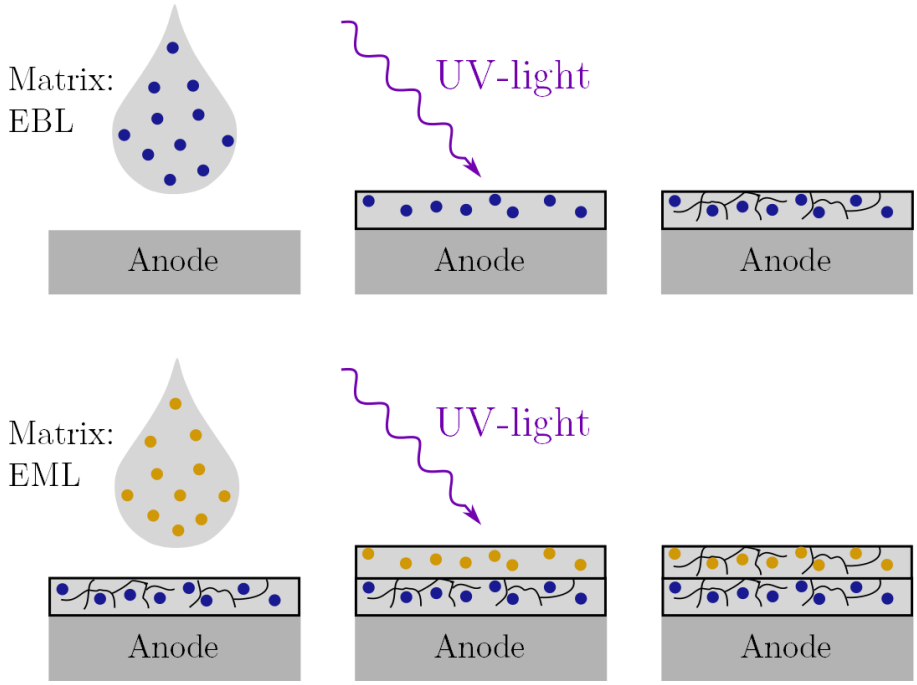

Figure 1.4: Process of multilayer fabrication from solution. The functional material, here electron-blocking material, is blended with the host matrix and solution processed on top of the anode. After deposition the host matrix is cross-linked with UV-light which makes the whole blend insoluble. Consecutively, a next layer can be spin-coated, here the emissive material blended with the host matrix. The blend can again be made insoluble via UV-light and another layer can be processed on top.

As a next step the intermixing of two emissive layers is investigated. Therefore, a blue emitting spiropolybifluorene, SPB-02T is blended with the matrix and made insoluble. In a multilayer PLED including the blue emitting SPB-02T blend, the orange emitting MEH-PPV blend and poly(9,9-di-n-octylfluorenyl-2,7-diyl) (PFO) as a hole-blocking layer, the electroluminescence spectrum was measured and compared to a drift-diffusion simulation that assumed two emitting layers with a sharp interface. By doing this, the intermixing of the two emissive layers is investigated.

As a last step the method is used to fabricate a multilayer PLED with charge blocking layers to increase the efficiency. The desired structure is shown in Figure 1.1b).

The thesis is outlined as follows: the theoretical background to organic semiconductors and the basics that are necessary to understand the device operation of a PLED are explained in Chapter 2. The materials and methods that are used in this work are briefly described in Chapter 3. Chapter 4 discusses the solubility and the charge transport of blends of UV-cross-linkable matrices and MEH-PPV. In Chapter 5 the intermixing of a blue emitting and orange emitting layer in a multilayer PLED is discussed. The fabrication of multilayer PLEDs with charge blocking layers is shown in Chapter 6. A summary is given in Chapter 7.

1.1 References

1. C. J. Humphreys, Solid-State Lighting. *MRS Bulletin* **33**, 459-470 (2008).

2. H. Sasabe, J. Kido, Development of high performance OLEDs for general lighting. *J Mater Chem C* **1**, 1699-1707 (2013).

3. M. Zhang, S. Hofle, J. Czolk, A. Mertens, A. Colsmann, All-solution processed transparent organic light emitting diodes. *Nanoscale* **7**, 20009-20014 (2015).

4. H. Mette, H. Pick, Elektronenleitfähigkeit von Anthracen-Einkristallen. *Zeitschrift für Physik* **134**, 566-575 (1953).

5. H. Akamatu, H. Inokuchi, On the Electrical Conductivity of Violanthrone, Iso-Violanthrone, and Pyranthrone. *The Journal of Chemical Physics* **18**, 810-811 (1950).

6. S. Mrozowski, Semiconductivity and Diamagnetism of Polycrystalline Graphite and Condensed Ring Systems. *Physical Review* **85**, 609-620 (1952).

7. H. Akamatu, H. Inokuchi, Y. Matsunaga, Electrical Conductivity of the Perylene-Bromine Complex. *Nature* **173**, 168-169 (1954).

8. A. Bernanose, Electroluminescence of organic compounds. *British Journal of Applied Physics* **6**, S54 (1955).

9. M. Pope, H. P. Kallmann, P. Magnante, Electroluminescence in Organic Crystals. *The Journal of Chemical Physics* **38**, 2042-2043 (1963).

10. C. W. Tang, S. A. VanSlyke, Organic electroluminescent diodes. *Appl Phys Lett* **51**, 913-915 (1987).

11. J. H. Burroughes *et al.*, Light-emitting diodes based on conjugated polymers. *Nature* **347**, 539-541 (1990).

12. J. Kido, T. Matsumoto, Bright organic electroluminescent devices having a metal-doped electron-injecting layer. *Appl Phys Lett* **73**, 2866-2868 (1998).

13. J. Huang *et al.*, Low-voltage organic electroluminescent devices using pin structures. *Appl Phys Lett* **80**, 139-141 (2002).

14. M. Pfeiffer, S. R. Forrest, K. Leo, M. E. Thompson, Electrophosphorescent p-i-n organic light-emitting devices for very-high-efficiency flat-panel displays. *Adv Mater* **14**, 1633-1636 (2002).

15. H. T. Nicolai *et al.*, Unification of trap-limited electron transport in semiconducting polymers. *Nat Mater* **11**, 882-887 (2012).

16. R. N. Hall, Electron-Hole Recombination in Germanium. *Physical Review* **87**, 387-387 (1952).

17. W. Shockley, W. T. Read, Statistics of the Recombinations of Holes and Electrons. *Physical Review* **87**, 835-842 (1952).

18. R. R. Chance, A. Prock, R. Silbey, Comments on the classical theory of energy transfer. *The Journal of Chemical Physics* **62**, 2245-2253 (1975).

19. M. Kuik, L. J. A. Koster, A. G. Dijkstra, G. A. H. Wetzelaer, P. W. M. Blom, Non-radiative recombination losses in polymer light-emitting diodes. *Org Electron* **13**, 969-974 (2012).

20. J. Kido, M. Kimura, K. Nagai, Multilayer White Light-Emitting Organic Electroluminescent Device. *Science* **267**, 1332-1334 (1995).

21. R. F. Service, Organic LEDs Look Forward to a Bright, White Future. *Science* **310**, 1762-1763 (2005).

22. S. Logothetidis, A. Laskarakis, Towards the optimization of materials and processes for flexible organic electronics devices. *Eur. Phys. J. Appl. Phys.* **46**, 12502 (2009).

23. S. Logothetidis, Flexible organic electronic devices: Materials, process and applications. *Materials Science and Engineering: B* **152**, 96-104 (2008).
24. A. Sandström, H. F. Dam, F. C. Krebs, L. Edman, Ambient fabrication of flexible and large-area organic light-emitting devices using slot-die coating. *Nat Commun* **3**, 1002 (2012).
25. S. Khan, L. Lorenzelli, R. S. Dahiya, Technologies for Printing Sensors and Electronics Over Large Flexible Substrates: A Review. *IEEE Sensors Journal* **15**, 3164-3185 (2015).
26. M. R. Niazi *et al.*, Solution-printed organic semiconductor blends exhibiting transport properties on par with single crystals. *Nat Commun* **6**, 8598 (2015).
27. J.-S. Park *et al.*, Flexible full color organic light-emitting diode display on polyimide plastic substrate driven by amorphous indium gallium zinc oxide thin-film transistors. *Appl Phys Lett* **95**, 013503 (2009).
28. W. L. Ma *et al.*, Water/methanol-soluble conjugated copolymer as an electron-transport layer in polymer light-emitting diodes. *Adv Mater* **17**, 274-+ (2005).
29. T. L. Ye *et al.*, Efficient multilayer electrophosphorescence white polymer light-emitting diodes with aluminum cathodes. *Org Electron* **12**, 154-160 (2011).
30. K. S. Yook, S. E. Jang, S. O. Jeon, J. Y. Lee, Fabrication and Efficiency Improvement of Soluble Blue Phosphorescent Organic Light-Emitting Diodes Using a Multilayer Structure Based on an Alcohol-Soluble Blue Phosphorescent Emitting Layer. *Adv Mater* **22**, 4479-4483 (2010).
31. S. Sax *et al.*, Efficient Blue-Light-Emitting Polymer Heterostructure Devices: The Fabrication of Multilayer Structures from Orthogonal Solvents. *Adv Mater* **22**, 2087-+ (2010).
32. C. M. Zhong, C. H. Duan, F. Huang, H. B. Wu, Y. Cao, Materials and Devices toward Fully Solution Processable Organic Light-Emitting Diodes. *Chem Mater* **23**, 326-340 (2011).
33. C. Tanase, J. Wildeman, P. W. M. Blom, Luminescent poly(p-phenylenevinylene) hole-transport layers with adjustable solubility. *Adv Funct Mater* **15**, 2011-2015 (2005).
34. R. Trattnig *et al.*, Bright Blue Solution Processed Triple-Layer Polymer Light-Emitting Diodes Realized by Thermal Layer Stabilization and Orthogonal Solvents. *Adv Funct Mater* **23**, 4897-4905 (2013).

35. S. Xue *et al.*, Fully solution-processed and multilayer blue organic light-emitting diodes based on efficient small molecule emissive layer and intergrated interlayer optimization. *Org Electron* **27**, 35-40 (2015).
36. N. Aizawa *et al.*, Solution-processed multilayer small-molecule light-emitting devices with high-efficiency white-light emission. *Nat Commun* **5**, 5756 (2014).
37. L. Derue *et al.*, All-Solution-Processed Organic Light-Emitting Diodes Based on Photostable Photo-cross-linkable Fluorescent Small Molecules. *Acs Appl Mater Inter* **8**, 16207-16217 (2016).
38. M. C. Gather, A. Kohnen, A. Falcou, H. Becker, K. Meerholz, Solution-processed full-color polymer organic light-emitting diode displays fabricated by direct photolithography. *Adv Funct Mater* **17**, 191-200 (2007).
39. C. Gu *et al.*, Multilayer Polymer Stacking by In Situ Electrochemical Polymerization for Color-Stable White Electroluminescence. *Adv Mater* **23**, 527-+ (2011).
40. A. Haldi *et al.*, Optimization of Orange-Emitting Electrophosphorescent Copolymers for Organic Light-Emitting Diodes. *Adv Funct Mater* **18**, 3056-3062 (2008).
41. A. Kohnen *et al.*, The Simple Way to Solution-Processed Multilayer OLEDs - Layered Block-Copolymer Networks by Living Cationic Polymerization. *Adv Mater* **21**, 879-+ (2009).
42. J.-S. Kim, R. H. Friend, I. Grizzi, J. H. Burroughes, Spin-cast thin semiconducting polymer interlayer for improving device efficiency of polymer light-emitting diodes. *Appl Phys Lett* **87**, 023506 (2005).
43. L. Duan *et al.*, Multilayer blue polymer light-emitting devices with spin-coated interlayers. *Synthetic Met* **157**, 343-346 (2007).
44. T.-W. Lee *et al.*, Hole-transporting interlayers for improving the device lifetime in the polymer light-emitting diodes. *Appl Phys Lett* **89**, 123505 (2006).
45. S. R. Tseng *et al.*, General method to solution-process multilayer polymer light-emitting diodes. *Appl Phys Lett* **88**, (2006).
46. S. R. Tseng *et al.*, High-efficiency blue multilayer polymer light-emitting diode fabricated by a general liquid buffer method. *Synthetic Met* **158**, 130-134 (2008).
47. H. A. Al-Attar, A. P. Monkman, Solution processed multilayer polymer light-emitting diodes based on different molecular weight host. *J Appl Phys* **109**, 074516 (2011).

48. J.-D. You *et al.*, All-solution-processed blue small molecular organic light-emitting diodes with multilayer device structure. *Org Electron* **10**, 1610-1614 (2009).
49. S.-R. Tseng, H.-F. Meng, K.-C. Lee, S.-F. Horng, Multilayer polymer light-emitting diodes by blade coating method. *Appl Phys Lett* **93**, 153308 (2008).
50. K. S. Yook, C. W. Joo, S. O. Jeon, J. Y. Lee, Small molecule based mixed interlayer for color control of solution processed multilayer white polymer light-emitting diodes. *Org Electron* **11**, 184-187 (2010).
51. K.-H. Kim, S.-Y. Huh, S.-m. Seo, H. H. Lee, Solution-based formation of multilayers of small molecules for organic light emitting diodes. *Appl Phys Lett* **92**, 093307 (2008).
52. A. R. Duggal, C. M. Heller, J. J. Shiang, J. Liu, L. N. Lewis, Solution-Processed Organic Light-Emitting Diodes for Lighting. *Journal of Display Technology* **3**, 184-192 (2007).
53. K. D. He *et al.*, Solution processed organic light-emitting diodes using the plasma cross-linking technology. *Appl Surf Sci* **382**, 288-293 (2016).
54. S. Ho, S. Liu, Y. Chen, F. So, Review of recent progress in multilayer solution-processed organic light-emitting diodes. *PHOTOE* **5**, 057611-057611 (2015).
55. Z.-L. Zhou *et al.*, Multilayer structured polymer light emitting diodes with cross-linked polymer matrices. *Appl Phys Lett* **96**, 013504 (2010).

2 Theory

In this chapter the basic knowledge that is necessary to understand the working principle of polymer light-emitting diodes (PLEDs) is presented. First, a short overview on the electronic properties of conjugated polymers is given. In the next section, the basics of the device operation of PLEDs are presented. First, the charge transport and the development of charge carrier mobility models in the last decade are discussed. As a next step the electron transport, which differs substantially from the hole transport due to trapping, is explained. The results of hole and electron transport are subsequently combined in a PLED device model that also takes charge recombination into account. Finally, the loss mechanisms in a PLED will be discussed.

2.1 Conjugated Polymers

Usually polymers show insulating properties, common polymers/plastics like polyethylene are used to insulate the conducting core of an electricity cable. However, polymers can also be semiconducting. For this, the backbone of the polymer has to be conjugated. The term conjugated means that the polymer has alternating single and double bonds along the carbon backbone. This is schematically shown in Figure 2.1a) for the most simple conjugated polymer polyacetylene. These alternating bonds are the origin of the semiconducting properties. In this case, the orbitals of the carbon atoms are sp^2 hybridized, meaning that the 2s and 2p orbitals form three sp^2 orbitals that have the same energy. One of the p orbitals (p_z) remains in its original state with a higher energy than the sp^2 hybrid orbitals. The energy diagram of the sp^2 hybridization is shown Figure 2.1b).

The formation of bonds between atoms can be described by the linear combination of atomic orbitals (LCAO). In Figure 2.1c) this is shown for the case of two sp^2 hybridized carbon atoms that bind together and form ethene (C_2H_4). Here, only the four valence electrons are regarded. Two electrons in a sp^2 orbital can bind together and form a σ bond that has a lower energy than the sp^2 orbital. In the case of ethene three σ bonds are formed, however only one is shown here. Similarly, the electrons in the p orbital can form a bond that is called π bond. The σ bonds are the in-plane bonds between the carbon and hydrogen atoms. The π bond is the out-of-plane bond and the electrons are delocalized. This delocalization is the reason why conjugated polymers are conductive.

Furthermore, for each linear combination there is an additional molecular orbital, namely the σ^* and the π^* orbital. These orbitals have a higher energy than σ and π orbitals and are based on anti-bonding electrons. The case of bonding (lower picture) and anti-bonding (upper picture) in the case of ethene is shown in Figure 2.1d). In the ground state the σ^* and π^* orbitals are empty. Consequently, the π orbital is called the highest occupied molecular orbital (HOMO) and the π^* orbital is called the lowest unoccupied molecular orbital (LUMO). Electrons can be excited from the HOMO to the LUMO by absorbing energy and also relax from the LUMO to the HOMO by releasing energy.

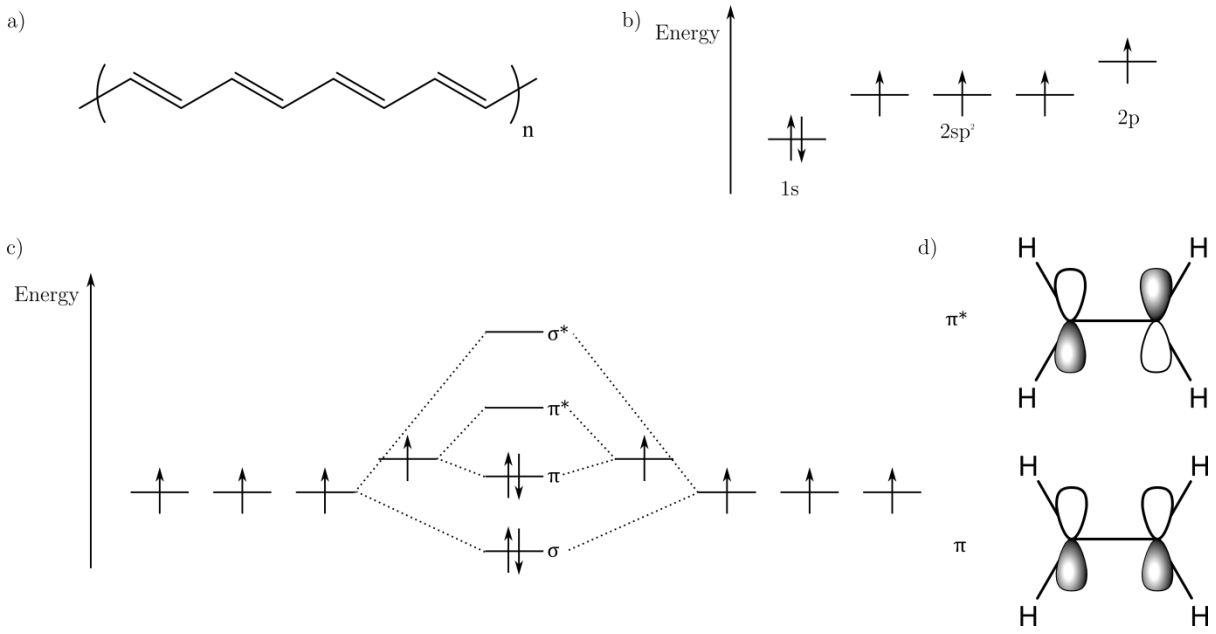

Figure 2.1 a) Chemical structure of polyacetylene with alternating single and double bonds. b) Energetic structure of the sp^2 hybridization in carbon. c) Linear combination of atomic orbitals of the valence electrons for the case of ethene. d) π orbitals in the case of bonding (π) and anti-bonding (π^*)

In the case of a polymer, there are more than two carbon atoms that have alternating single and double bonds. With increasing number of carbon atoms the number of π electrons increases. The influence of the amount of π electrons, which is equivalent to the chain length, on the electronic structure is shown in Figure 2.2. In the case of ethene with only two carbon atoms, the difference between π and π^* levels or the HOMO and LUMO level is rather big. With increasing number of carbon atoms the number of energy states is increasing and the HOMO-LUMO gap is decreasing. In the HOMO-LUMO gap there are no energetic states for electrons, what makes it equivalent to the band gap in inorganic semiconductors. For common conjugated polymers, e.g. MEH-PPV, the HOMO-LUMO gap is around

2.4 eV. Consequently, if an electron relaxes from the LUMO to the HOMO it emits light in the visible spectrum.

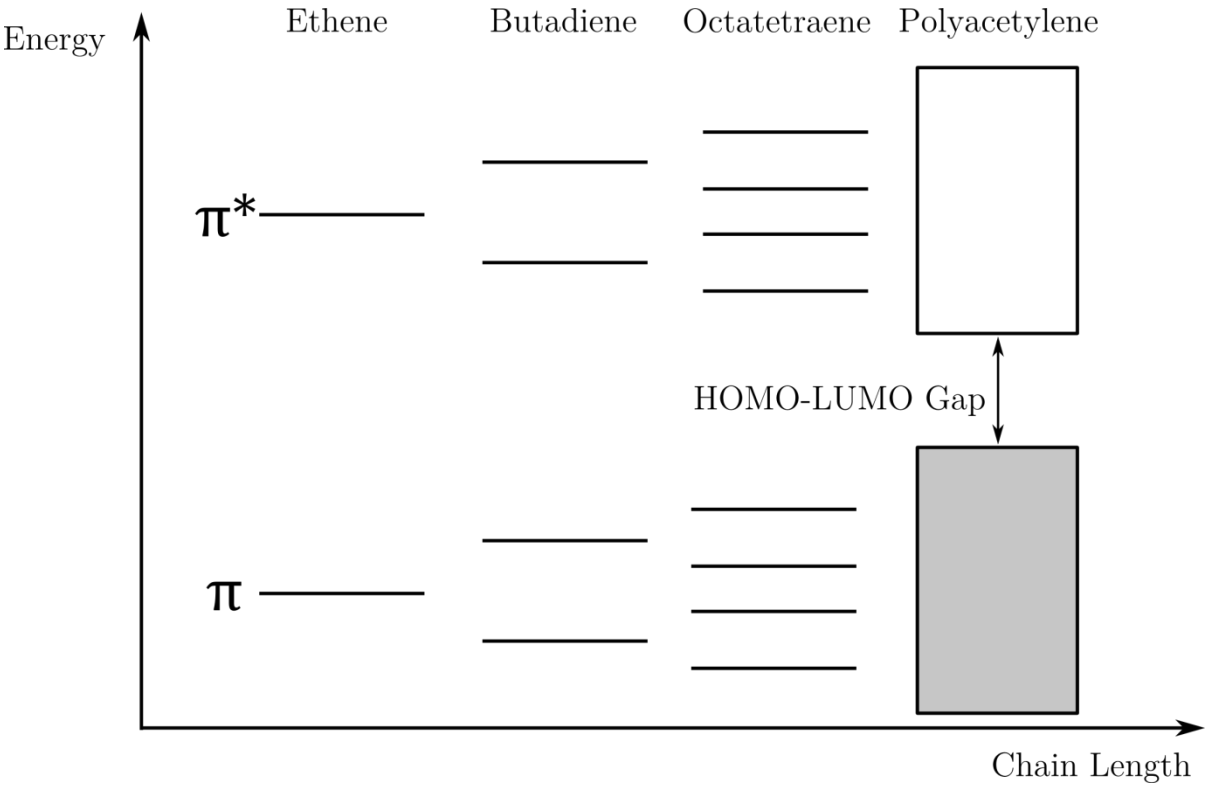

Figure 2.2: Energy states as a function of the chain length in a conjugated polymer. With increasing chain length HOMO-LUMO gap is decreasing.

2.2 Device operation of polymer light emitting diodes

The general structure of a PLED consists of an organic semiconductor that is sandwiched between an anode and cathode. This is schematically shown in Figure 2.3.

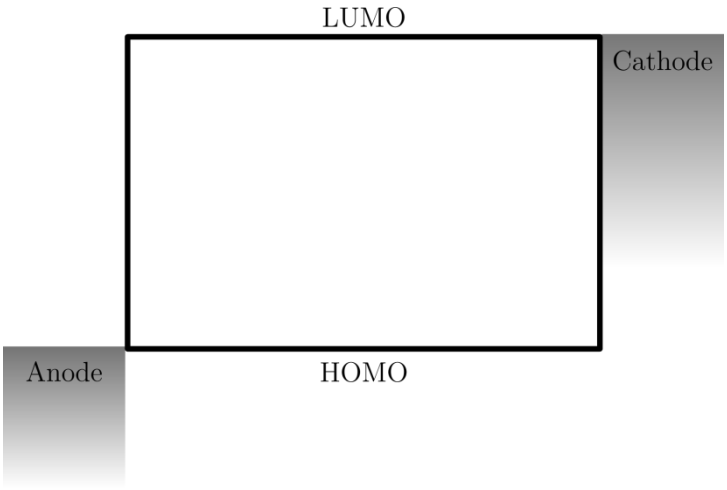

Figure 2.3: General structure of a PLED. The emissive material is sandwiched between an anode and cathode, of which the work functions each match the energy level of the HOMO and LUMO, respectively.

The device characteristics of a PLED in operation are dependent on the conductive and emissive properties. The most important features of the operation are charge injection, charge transport and recombination. (*1, 2*) The working principle is schematically shown in Figure 2.4. In order to achieve emission of light, several processes in the PLED have to take place. First, the charge carriers have to be injected in the material. Electrons are injected from the cathode in the LUMO and holes are injected from the anode into the HOMO of the organic semiconductor. To achieve an efficient charge injection the materials of the electrodes have to be carefully chosen. The work functions of the electrodes have to match the HOMO and LUMO levels. Otherwise, the resulting energy barrier will limit the flow of carriers into the semiconductor. If the injection barrier φ is smaller than 0.3 eV, the contact can supply sufficient carriers to the organic semiconductor and the transport becomes bulk-limited. In this case, the contact is defined as an ohmic contact.(*3-6*) Typical materials for the anode and cathode are indium tin oxide (ITO) and barium, respectively.

Because of the work functions of the electrodes, holes can only be injected from the anode and electrons only from the cathode. In reverse operation, electrons and hole have to overcome a large energy barrier at the electrodes and there is no injection of carriers at all. This means that the device is only conductive in one direction, which is why it is called a diode.

In spite of a difference in the work function between anode and cathode, in thermal equilibrium the Fermi levels in the structure will align. This leads to a built-in voltage in the PLED. Consequently, the structure shown in Figure 2.3 is the special case where the built-in voltage is equal to the applied voltage, such that the internal electrical field is zero. If the applied voltage is smaller than the built-in voltage the electric field is against the direction of the current. In that case the current is dominated by diffusion of charge carriers. If a voltage higher than the built-in voltage of the device is applied, the current is dominated by drift.

In this case, once electrons and holes are injected, they drift to the opposite electrode because of the driving force of an applied electric field. When an electron and a hole come in close distance they form an exciton because of the Coulombic attraction. An exciton is a bound excited state between a hole and electron. The electron is in a higher energetic state and decays radiatively by releasing a photon. This process is called bimolecular recombination. The color of the emitted light is determined by the energy difference of the HOMO and LUMO minus the exciton binding energy.

The generated light in the semiconductor must be coupled out of the PLED. Therefore, typically the cathode is reflecting and the anode is transparent. The PLED is then called bottom emitting.

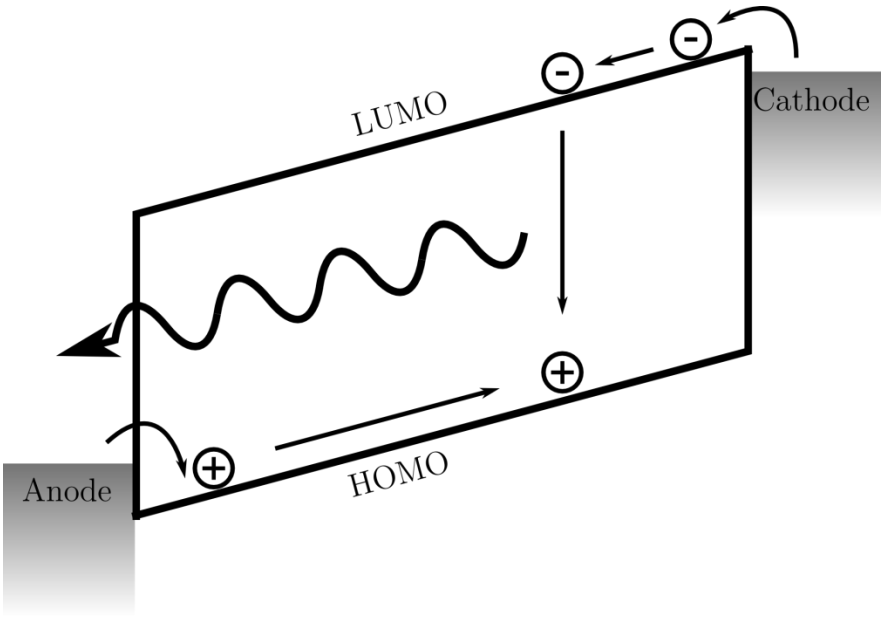

Figure 2.4: Working principle of a PLED. Holes are injected from the anode and are transported towards the cathode due to the applied electric field. Electrons are injected from the cathode and are transported towards the anode. When a hole and an electron are in close distance they form an exciton that recombines by emitting a photon.

2.3 Charge Transport in organic semiconductors

The charge transport in an organic semiconductor is usually characterized by the charge carrier mobility μ. The mobility is a characteristic for the average drift velocity v of charge carriers under the influence of an applied electric field E:

$$v = \mu E \qquad 1)$$

As mentioned in the previous section, for a working PLED the materials for anode and cathode have to be carefully chosen to avoid energy barriers that limit the charge transport. On the other hand, by deliberately blocking one type of charge carrier, so-called single carrier devices can be fabricated. In the case of a hole-only device two materials with a high work function, such as ITO/PEDOT:PSS and MoO_3 enable the injection of holes from both electrodes. Due to a large energy barrier no electrons can be injected. For electron-only devices two low work function materials are used that only enable the injection of electrons. Using these single carrier devices helps to disentangle the transport

properties of both charge carriers that are present in a PLED and study the charge transport of one type of charge carrier individually.

Figure 2.5 shows the current density J as a function of the applied voltage V corrected for the built-in voltage V_{bi} of a PLED (black), hole-only (red) and electron-only (green) device of MEH-PPV. The thickness of all devices is around 120 nm. Figure 2.5 shows an important feature of PLEDs. The current density of PLEDs is dominated by the hole transport. The current density of the PLED and the hole-only device are almost equal, but the current density of the electron-only device is orders of magnitudes lower. In the next sections the different contributions to the transport and recombination of charge carriers, that lead to this difference will be disentangled and explained.

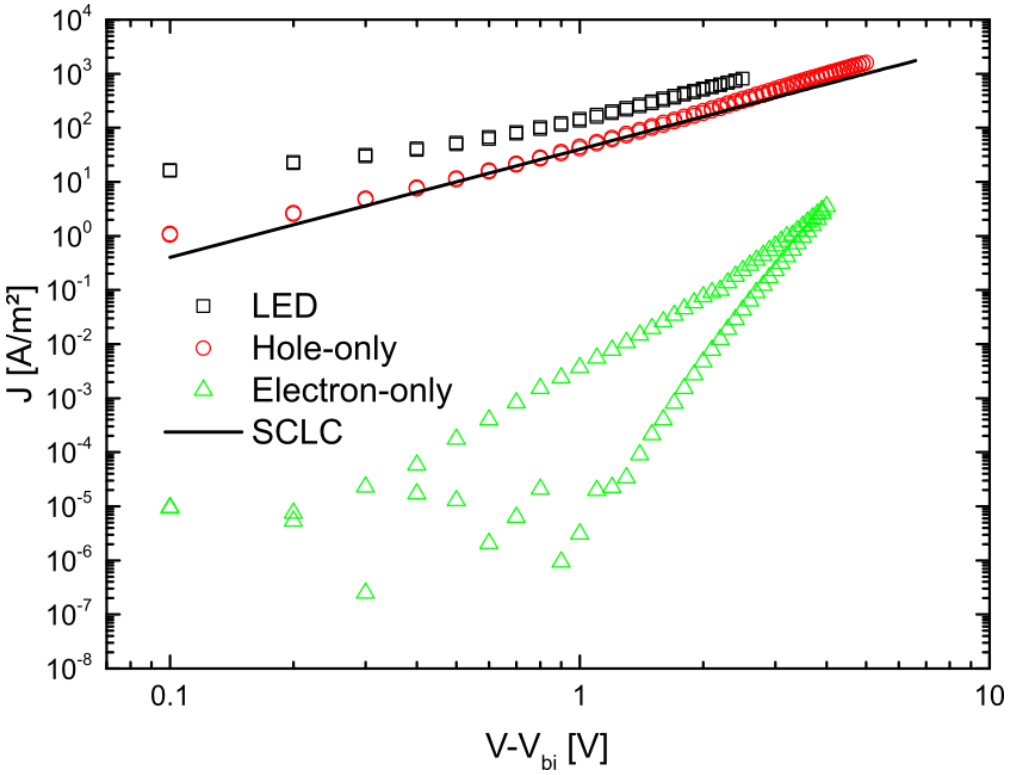

Figure 2.5: J-V characteristics of a MEH-PPV based PLED (black), hole-only (red) and electron-only (green) device, showing that the PLED is dominated by the hole transport. The hole transport is space-charge limited but the fit with a constant mobility is not valid at high voltage.

2.3.1 Hole transport

Conjugated polymers are undoped semiconductors with a very low conductivity, so they can be considered as insulators. In a hole-only device only positive charge carriers are injected from the anode. Since the charges are not screened or neutralized by electrons, a space-charge will be built up. The unscreened space charge builds up an electric field inside the device. This electrostatically limits the amount of charges that can be injected in the materials.

The resulting current is called space-charge limited current (SCLC) and is described by the Mott-Gurney law (7)

$$J = \frac{9}{8}\varepsilon_0\varepsilon_r\mu\frac{V^2}{L^3} \qquad 2)$$

where ε_0 is the permittivity of vacuum, ε_r is the relative dielectric constant of the organic semiconductor, μ is the mobility of the organic semiconductor, V the applied voltage and L the layer thickness. A consequence of the SCLC is that the current density scales with V^2 instead of V as in the case of an ohmic current. In Figure 2.6 the electric field (black) and the carrier density (red) are shown as a function of the distance from the injecting contact of a SCL device. The electric field scales with $E \sim \sqrt{x}$ and the carrier density scales with $p \sim \frac{1}{\sqrt{x}}$.

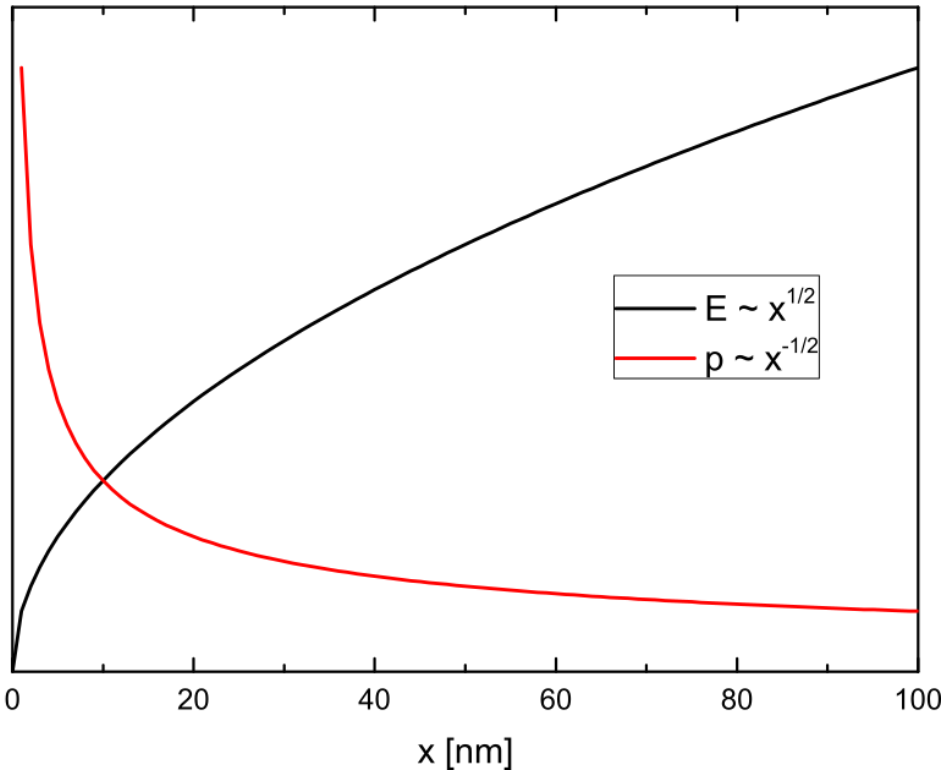

Figure 2.6: Electric field (black) and carrier density (red) as a function of the distance from the injecting contact of a SCL device

The solid line in Figure 2.5 shows a fit using Equation 2 for the SCL hole current of MEH-PPV. In contrast to the electron current, the hole current can be well described with the SCLC. However, at high voltages, the hole current increases stronger than the SCLC predicts. In the derivation of Equation 2 it is assumed that the mobility is a constant, so not dependent on electric field or carrier density. This is not necessarily the case in an organic semiconductor and lots of effort has been

done to find a suitable model for the mobility in the past. A brief overview will be given in the following.

A possible explanation that the current density at high voltages is higher than the SCLC could be that the mobility is dependent on the electric field. In 1972 Gill proposed a Poole-Frenkel like mobility that scales with the electric field and the temperature according to (*8-10*)

$$\mu_{PF} = \mu(T,E) = \mu_0 \exp\left(-\frac{\Delta}{k_B T}\right) \exp\left(\gamma\sqrt{E}\right), \qquad 3)$$

where μ_0 is the mobility at zero field, Δ is the activation energy, k_B the Boltzmann constant, T the absolute temperature and γ a field enhancement factor. The temperature and field dependent mobility in combination with the SCLC was successfully used by Blom *et al.* in 1997 to describe the hole current in MEH-PPV at high fields and different temperatures and by Auweraer *et al.* in time-of-flight measurements. (*11, 12*)

In inorganic semiconductors there is a periodic lattice structure which leads to delocalized charge carriers and band-like transport. The mean free path of the charge carriers is high and limited by the scattering of phonons. Consequently, the mobility of the charge carriers is decreasing with increasing temperature.

The charge transport in organic semiconductors has different properties compared to inorganic semiconductors. In semiconducting polymers the charge carriers are delocalized along the polymer backbone. However, due to chemical impurities or twists and kinks in the chain, the conjugation of the polymer is broken. As mentioned before, the energy gap and thus the energy of the HOMO and LUMO are dependent on the conjugation length. The variation in the conjugation length leads to distribution of HOMO and LUMO levels, also termed as the energetic disorder of the polymer. A disordered conjugated polymer can therefore be considered as a system consisting of many conjugated parts that are localized with different energy levels. The transport in such a material can be described as a hopping process between these localized states that are spread in energy. This greatly affects the charge transport of organic semiconductors and leads to mobilities that are orders of magnitudes lower than their inorganic counterparts.

The hopping process between localized states is assisted by phonons. A hop to a site at higher energy needs to be assisted by absorption of a phonon, while a hop to a site in lower energy releases a phonon. This process was already described

by Conwell and Mott in 1954.(*13, 14*) Miller and Abrahams described a model for the hopping rates, taking into account the energy difference and the spatial overlap between an occupied and unoccupied state.(*15*) The resulting transition rate W_{ij} from an occupied state i to an unoccupied state j with energies ε_i and ε_j, respectively is given by:(*15*)

$$W_{ij} = \nu_0 \exp(-2\alpha R_{ij}) \begin{cases} \exp\left(-\frac{\varepsilon_j - \varepsilon_i}{k_B T}\right) & \text{for } \varepsilon_j > \varepsilon_i \\ 1 & \text{for } \varepsilon_j < \varepsilon_i \end{cases} \quad 4)$$

with ν_0 the attempt-to-jump frequency, R_{ij} the distance between the states i and j, α the inverse localization length, k_B the Boltzmann constant and T the absolute temperature.

In 1993 Bässler proposed a charge transport model for disordered organic semiconductors. In the model, the hopping rate is described by the Miller and Abrahams formalism of Equation (4). Both, positional and energetic disorder is taken into account. The energetic disorder is approximated by a Gaussian distribution $\rho(\varepsilon)$

$$\rho(\varepsilon) = \frac{1}{\sqrt{2\pi}\sigma} \exp\left(\frac{\varepsilon^2}{2\sigma^2}\right) \quad 5)$$

where σ is the width of the Gaussian density of states (DOS). The energy ε is measured relative to the center. This transport model is known as the Gaussian disorder model (GDM) and is schematically shown in Figure 2.7.(*16*) Since the charge transport cannot be solved analytically, Monte Carlo simulations have been used.

A result of these simulations is that the carriers relax to an equilibrium level below the center of the Gaussian DOS at $-\frac{\sigma^2}{k_B T}$. For transport the carriers have to be thermally activated to a level with higher energy, which is called transport level. Here, the DOS is higher and the hopping is easier. The transport level is basically a compromise between the activation energy and the number of available states. This is indicated in Figure 2.7 for a localized carrier (grey) that is thermally activated to a higher energy from where it participates in the charge transport (white). The activation energy explains the temperature dependence of the mobility at low electric field. The mobility is additionally dependent on the electric field, because the applied electric field is tilting the energy landscape as shown in Figure 2.8. This

makes it easier for charge carriers to overcome energy barriers in direction of the applied electric field.

From the Monte Carlo simulations Bässler derived a temperature and field dependent mobility according to:(*16*)

$$\mu_{GDM}(T,E) = \mu_0 \exp\left[-\left(\frac{2}{3}\hat{\sigma}\right)^2\right] \times \begin{cases} \exp\left(C(\hat{\sigma}^2 - \Sigma^2)\sqrt{E}\right) \text{ for } \Sigma \geq 1.5 \\ \exp\left(C(\hat{\sigma}^2 - 2.25)\sqrt{E}\right) \text{ for } \Sigma \leq 1.5 \end{cases} \quad 6)$$

where $\hat{\sigma} \equiv \frac{\sigma}{k_B T}$, C is a constant that depends on the site spacing and Σ is the degree of positional disorder.

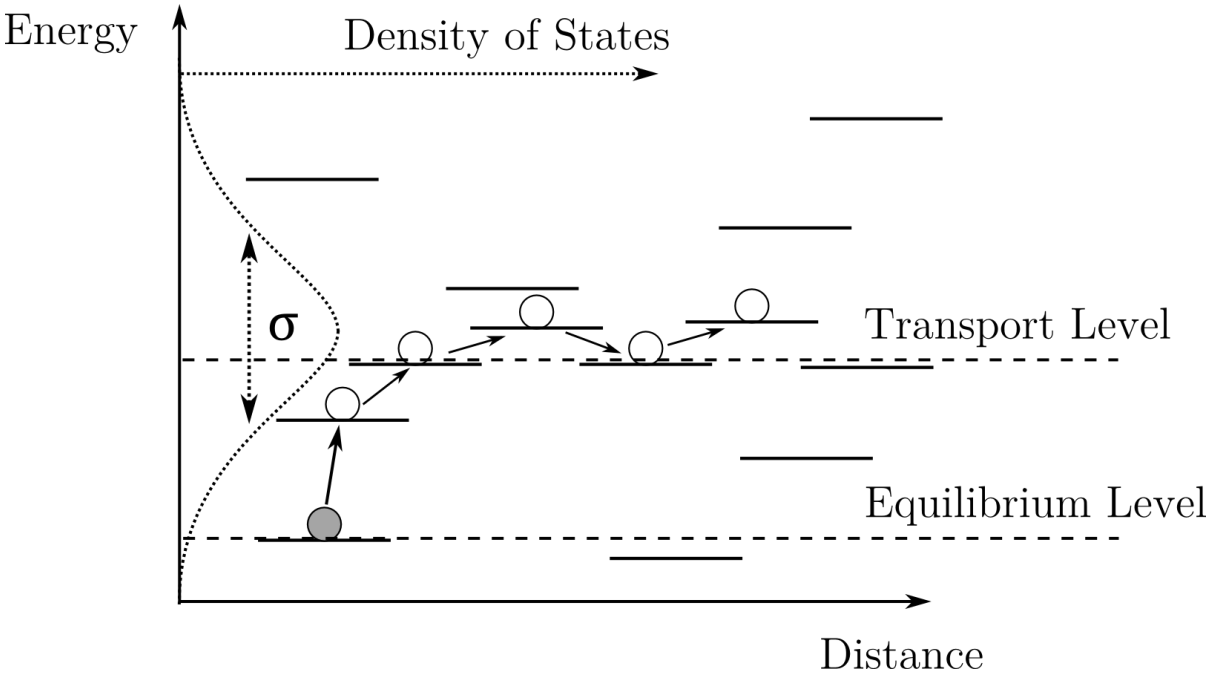

Figure 2.7: Schematic representation a Gaussian distribution of energy sites. The density of states is indicated by the dotted line. Localized charge carrier (grey) is thermally activated from localized state to the transport level (white) where it can participate in the charge transport.

It is important to note that in the GDM it is assumed that the electron-phonon coupling is weak and consequently the influence of polarons is neglected.

The mobility description of Bässler gave some important insights into the charge transport in disordered systems. The mobility is increasing with temperature in contrast to classical semiconductors, where the mobility is limited by phonon scattering when the temperature is increased. Since the hopping mechanism is phonon-assisted, the transport is temperature activated. Additionally, the mobility is field dependent because the energy barriers between the localized states are easier to overcome with an external electric field. Using the GDM the observed activation energy could be linked to the amount of disorder, represented by the width of the DOS σ.

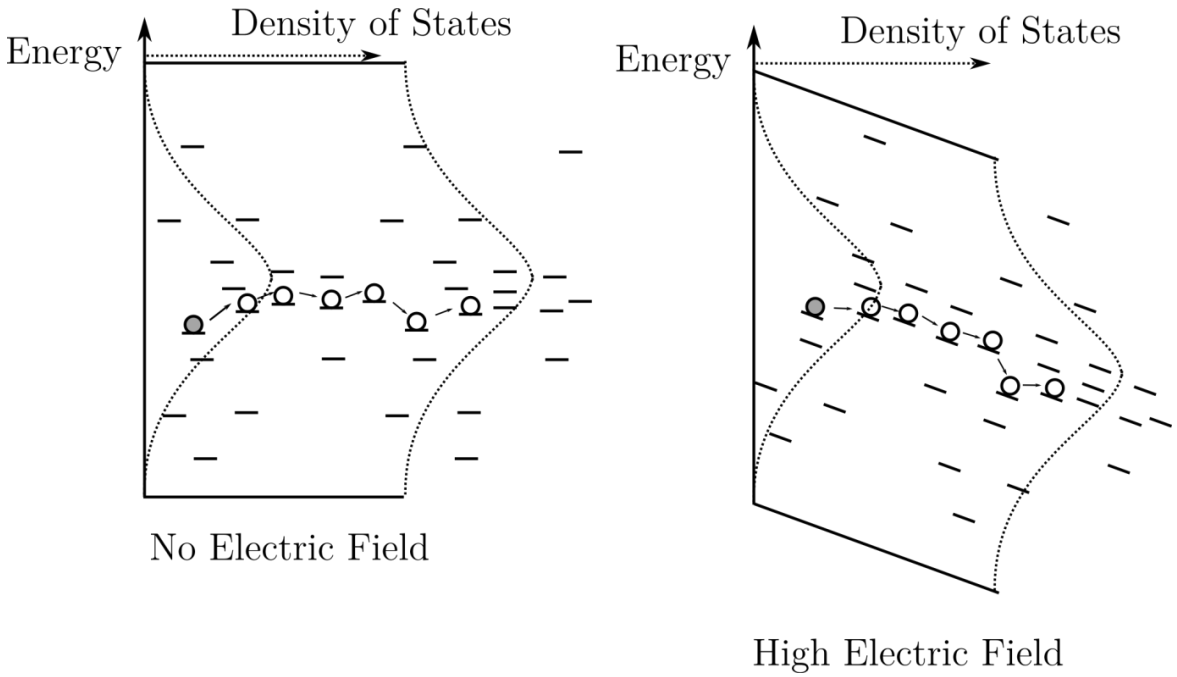

Figure 2.8: Hopping transport in the case of no electric field (left). Hopping transport in the case of high electric field (right). The energy landscape is tilted by the electric field, enabling higher charge carrier mobility.

In the considerations of Bässler the dependence of the transport on charge carrier density was not taken into account. In a space-charge-limited device the electric field and the charge carrier density are simultaneously increased by increasing the applied voltage. Disentangling the two contributions at high voltages is therefore difficult. To this end, measurements on field-effect transistors (FET) and light-emitting diodes have been combined. The geometry of FETs and LEDs is different. In a FET the distance between source and drain is in the order of micrometers while in an LED the distance between anode and cathode is around 100 nm. Because of the thin layer, the electric field in a LED is much higher than in a FET. Furthermore, in a FET by applying a voltage at the gate electrode, charge carriers accumulate in the organic semiconductor in close vicinity of the insulator interface, leading to high volume concentrations of carriers.(*17*) By varying the gate voltage a change of the mobility has been found.(*18, 19*) This dependence has been explained by the dependence of the mobility on carrier density.(*20, 21*) At low carrier densities only the deep, localized states in the tail of the DOS are occupied. Carriers that occupy a state deep in the tail need high activation energy to hop to a neighboring site. This is schematically shown in Figure 2.9a) for an exponential DOS. As the carrier density increases the deep states are more and more filled. Then more charges occupy states at a higher energy, which means that less activation energy is needed to reach a next site. This

case is shown in Figure 2.9b). In this case the mobility is increased and depends on the charge carrier density.

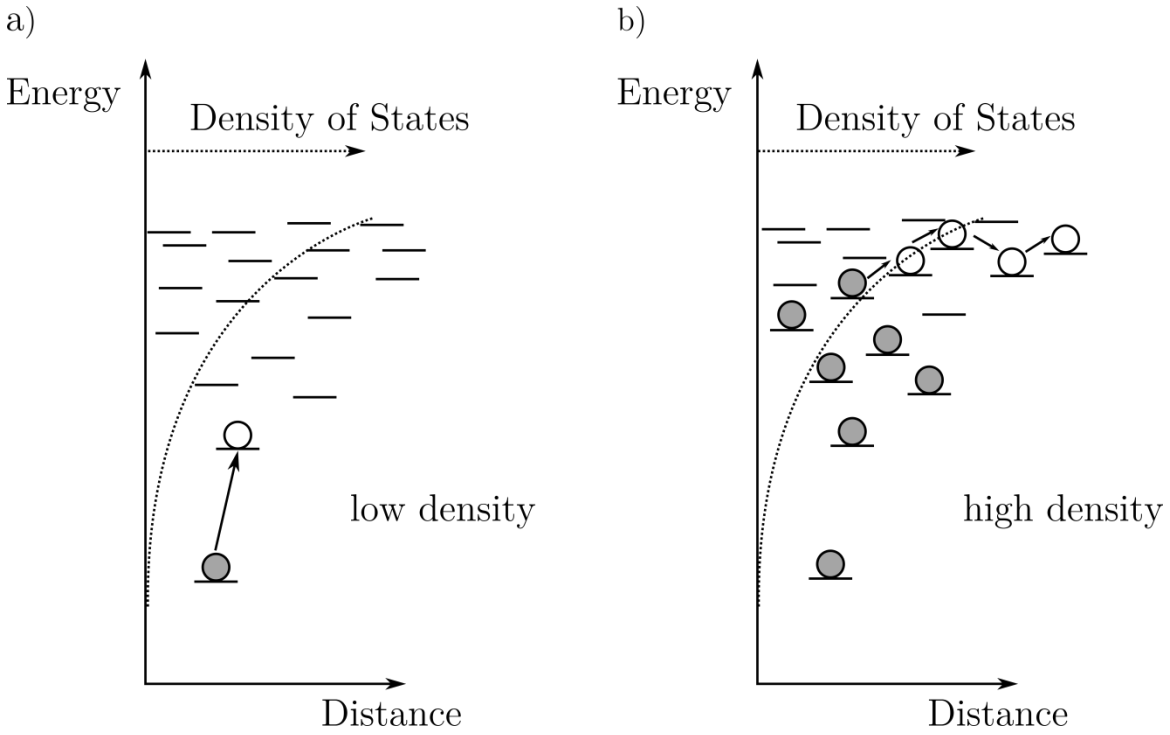

Figure 2.9: a) Effect of the carrier density on the mobility of charge carriers. At low density carriers relax to the deep states in the tail where the density of states is low. b) At high carrier densities the deep states are filled and charge carriers hop at a higher density of states where energy difference of neighboring sites is low. Consequently, the mobility is increased.

Experiments on MDMO-PPV showed that the mobility measured in FETs is approximately three orders of magnitude higher as compared to measurements in LED geometry.(*22*) The reason for this difference in mobility is the much higher volume charge carrier density in FETs. In order to explain the charge transport in FETs Vissenberg and Matters derived an analytic equation based on hopping in an exponential DOS that describes the mobility as a function of the charge carrier density p:(*23*)

$$\mu_h(p,T) = \mu_0 + \frac{\sigma_0}{e}\left(\frac{\left(\frac{T_0}{T}\right)^4 \sin\left(\pi\frac{T}{T_0}\right)}{(2\alpha)^3 B_c}\right)^{T_0/T} p^{\frac{T_0}{T}-1} \qquad 7)$$

where μ_0 is the hole mobility at low densities, σ_0 a prefactor for the conductivity, T_0 the characteristic temperature describing the decay of the exponential distribution, α the inverse overlap parameter between localized states and B_c the critical number for the onset of percolation.

As mentioned before, it is difficult to disentangle the influences of the electric field and the charge carrier concentration on the mobility. However, in 2003

Tanase et al. described a uniform charge carrier mobility description for PLEDs and FETs.(*22*) The difference in the observed mobilities of PLEDs and FETs was explained by the much higher charge carrier density in FETs, such that states in the tail of the DOS are all filled. This increases the mobility by orders of magnitude. Additionally, it has been found that the charge carrier dependence influences the mobility more at room temperature than the field dependence. The field dependence however, is more significant at low temperatures.(*24*)

For a consistent description of the transport of organic semiconductors it is important to include both field and carrier density effects. In 2005, based on the experiments of Tanase *et al.*, Pasveer *et al.* developed the extended Gaussian disorder model (EGDM) that gave a complete description of the mobility, including temperature-, field- and carrier density dependence.(*25*) This was done by solving the master equation for hopping transport on a cubic lattice with a site spacing a. The analytical data was numerically described with the following parametrization scheme:

$$\begin{aligned}
\mu(T,p,E) &\approx \mu_p(T,p) f(T,E) \\
\mu_p(T,p) &= \mu_0(T)\exp\left[\frac{1}{2}(\hat{\sigma}^2 - \hat{\sigma})(2pa^3)^{\delta}\right] \\
\mu_0(T) &= \mu_0 \exp[-0.42\hat{\sigma}^2] \\
\delta &\equiv 2\,\frac{\ln(\hat{\sigma}^2 - \hat{\sigma}) - \ln(\ln(4))}{\hat{\sigma}^2} \\
f(T,E) &= \exp\left\{0.44\left(\hat{\sigma}^{\frac{3}{2}} - 2.2\right)\left[\sqrt{1 + 0.8\left(\frac{Eea}{\sigma}\right)^2} - 1\right]\right\}
\end{aligned} \tag{8}$$

with μ_0 the mobility prefactor, $\hat{\sigma} = \frac{\sigma}{kT}$, p the charge carrier density, a the hopping distance and e the elementary charge. A result of this model is that the carrier dependence is stronger at room temperature and low electric fields. At low temperature or high electric fields the field dependence is stronger. Additionally, the carrier dependence becomes more important if the disorder is increased.

While the mobility model of Vissenberg and Matters assumes an exponential shape of the DOS, the (E)GDM assumes a Gaussian shape. During the operation of a PLED only a small part of the DOS is filled. In the case of a Gaussian DOS only the tail of the distribution is filled. In this case the Gaussian DOS may be approximated with an exponential distribution and the other way around.

The mobility model proposed by Pasveer is used to describe the mobility of charge carriers in this thesis. This is shown for a MEH-PPV hole-only device for different temperatures ranging from 295 K down to 213 K (symbols) in Figure 2.10.

To obtain the fits (solid line) the parameters $\mu_0 = 11000\ \mathrm{m^2/Vs}$, $a = 1.6\ \mathrm{nm}$ and $\sigma = 0.14\ \mathrm{eV}$ were used. A zero-field mobility at room temperature of $\mu_0(295\ \mathrm{K}) = 5.81 \times 10^{-11}\mathrm{m^2/Vs}$ was determined which is in excellent agreement to literature.(*26*)

The EGDM predicts a temperature dependence of the mobility of $\ln \mu \sim \frac{1}{T^2}$ in the limit of zero field and zero carrier density. A comparison of the temperature dependence of hole-only devices of several organic semiconductors showed that the temperature dependence can be described by a universal Arrhenius behavior:(*27*)

$$\mu_h = \mu_0 \exp\left(-\frac{\Delta}{k_B T}\right) \tag{9}$$

where Δ is the activation energy. The difference in the temperature dependence can be explained by considering two cases, zero charge carrier density ($p = 0$ in Equation 8)) and at a finite carrier density ($p = 1 \times 10^{21}\mathrm{m^{-3}}$). It can be seen that at zero carrier density the mobility scales with $1/T^2$ and at finite carrier density it scales with $1/T$.

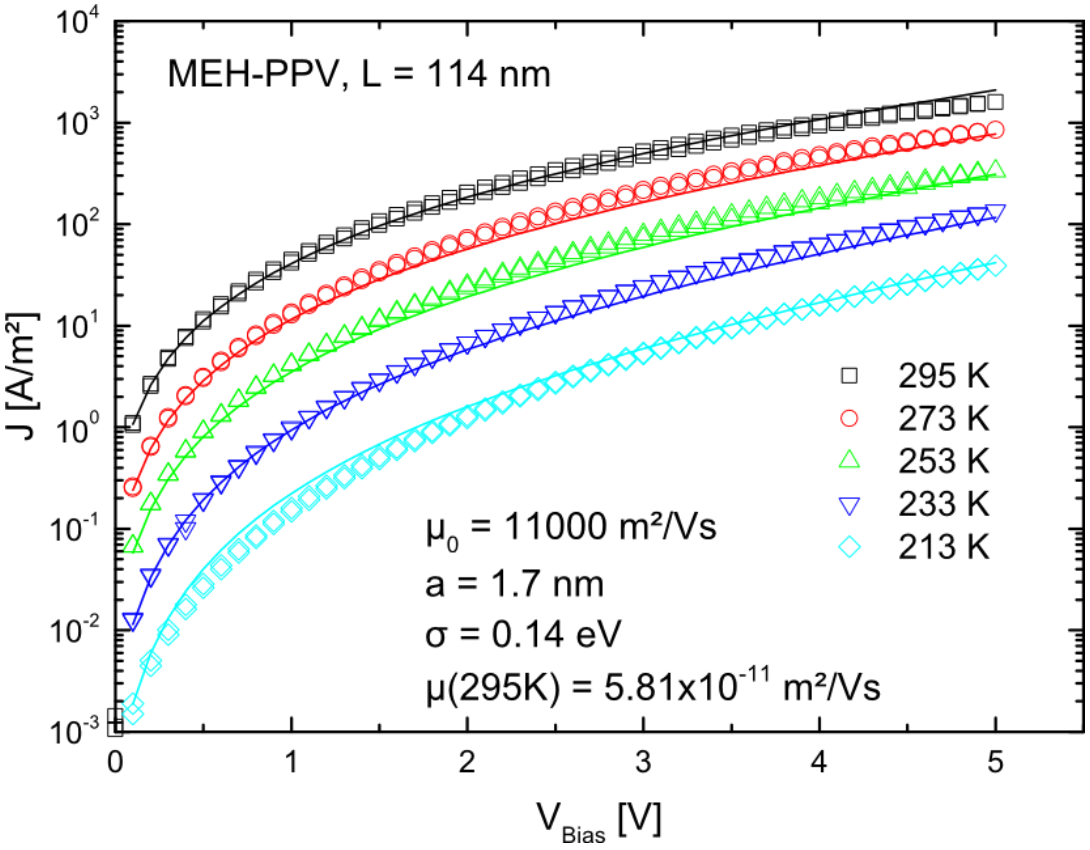

Figure 2.10: Measured (symbols) and simulated (solid lines) *J-V* characteristics of a MEH-PPV hole-only device using the mobility model of Pasveer *et al.* The current density is described very well across a broad voltage and temperature range.

2.3.2 Electron transport

With the combination of a field- and density dependent mobility and space-charge limited current, the hole current of conjugated polymers can be fully explained. Although the hole and electron mobility is similar in many organic semiconductors, the electron current is typically several orders of magnitude lower than the hole current. Furthermore, the electron current cannot be explained with the mobility model presented so far. However, the electron transport is crucial for the understanding of double carrier devices, such as PLEDs. In contrast to the hole transport, that usually shows a quadratic dependence of the current density on the voltage, the electron current shows a very strong voltage- and thickness dependence.(*28*) The reason for the lower current is that the electron current is limited by the presence of traps. Electron traps are localized defect sites inside the band gap. Because the energy of the traps is lower than the LUMO, electrons can fall in a trapping site and are immobilized. This is shown in Figure 2.11 in the case of a Gaussian distribution for both LUMO and trap level. In the LUMO electrons can hop to neighboring energy sites. However, if they approach a lower lying trap they will be captured and are immobilized. Trapping of charge carriers markedly affects the charge transport in a negative way. The traps can also explain a very distinct feature of the electron current in Figure 2.5. In the electron current there is a strong clockwise hysteresis. This means that the current density in the forward scan is higher than in the backward scan. This is different from the current density in hole-only devices and PLEDs, where the current density is the same in forward and reverse direction. In the case of a trap-limited electron transport the traps are filled in the forward scan. When the traps are deep in energy the detrapping of electrons takes longer than the duration of a voltage sweep, there are too many trapped electrons in the device during the back scan leading to a lowering of the current density.

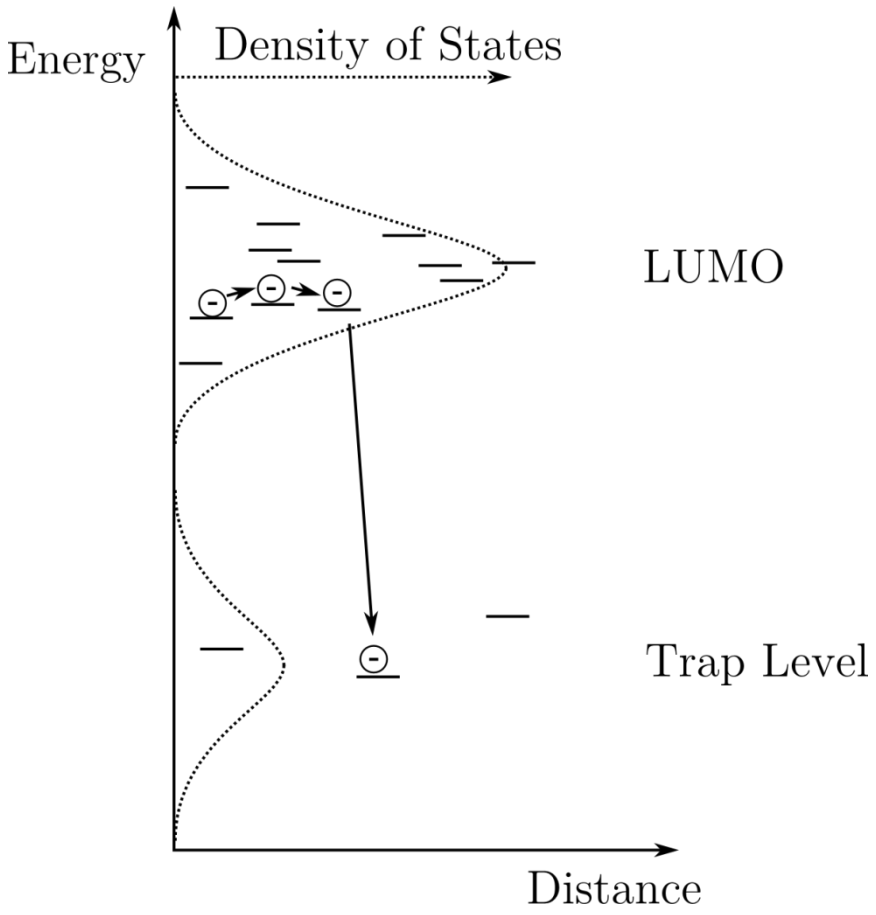

Figure 2.11: Hopping transport of an electron in a Gaussian DOS, followed by trapping of the electron in a trap site that is Gaussianly distributed, too. In the trap, the electron is immobilized.

The aforementioned strong voltage and thickness dependence of the electron current was initially explained using an exponential distribution of trapping sites:

$$n_t(\varepsilon) = \left(\frac{N_t}{k_B T_t}\right) \exp\left(\frac{\varepsilon - \varepsilon_c}{k_B T_t}\right) \qquad 10)$$

with $n_t(\varepsilon)$ the trap density of states at an energy ε, N_t the total trap density, $k_B T_t$ an energy characterizing the trap distribution and ε_c the energy of the conduction band. For the case of a trap-limited current with exponential traps an analytical equation was found by Mark and Lampert: (*29*)

$$J = N_c e\, \mu \left(\frac{\varepsilon_0 \varepsilon_r}{e N_t}\right)^{r+1} \left(\frac{2r+1}{r+1}\right)^{r+1} \left(\frac{r}{r+1}\right)^{r} \frac{V^{r+1}}{L^{2r+1}} \qquad 11)$$

with N_c the DOS in the conduction band and $r = T_t/T$. Using this equation, the electron current of MDMO-PPV could be described for several thicknesses. However, the temperature dependence of the trap-limited current was much weaker

than the exponential trap model predicted. In organic semiconductors the transport is described by a hopping in a Gaussian DOS. The model proposed by Mark and Lampert however, assumes a sharp conduction band edge. By taking into account a Gaussian distribution of the LUMO also the temperature dependence of the trap-limited electron current can be described. The classical Mark and Lampert equation is then modified to (*30*)

$$J = N_c e\,\mu \left(\frac{\varepsilon_0 \varepsilon_r}{e N_t \exp\left(\frac{E_t - E_a}{k_B T_t}\right)} \right)^{r+1} \left(\frac{2r+1}{r+1}\right)^{r+1} \left(\frac{r}{r+1}\right)^{r} \frac{V^{r+1}}{L^{2r+1}} \qquad 12)$$

With E_t, the trap energy and E_a, a characteristic energy located $\frac{\sigma^2}{2k_B T}$ below the center of the Gaussian DOS. With this modification it was possible to consistently describe the temperature dependent electron current of PPV-derivates.(*31*)

When it comes to the characterization of trap-limited electron transport using *J-V* characteristics there is however the problem that the electron mobility, the trap energy and the total amount of traps are all in the prefactor of Equation 112). For this reason they cannot be determined independently. Zhang *et al.* used dimethylcobaltocene as a n-type dopant of MEH-PPV to fill its trap states. Once all the traps were filled by the dopant, the trap-free electron current was the same as the hole current. This proves that the intrinsic mobility of holes and electrons is the same in MEH-PPV.(*32*)

Recently Nicolai *et al.* gave a full description of a Gaussian trap distribution.(*33*) Since the charge transport is characterized by hopping in a Gaussian DOS, it is plausible to use a Gaussian distribution for the traps as well. The work unified previous reports of shallow and deep Gaussianly-shaped traps that were only valid in a limited voltage range.(*34, 35*) The trap-limited electron current of three PPV derivates could be described equally well as with an exponential trap distribution. Additionally, in contrast to the exponential trap distribution, the trap energy and the total amount of the traps could be disentangled. Remarkably, the trap-limited electron transport could be described with one fixed set of parameters of a total amount of traps $N_t = 1 \times 10^{23}\mathrm{m}^{-3}$ with a width of $\sigma_t = 0.1\,\mathrm{eV}$ that have a trap energy $E_t = 0.7 - 0.8\,\mathrm{eV}$ below the LUMO of the PPV derivatives.(*33*)

This is a remarkable result because when the trap-limited result was described with an exponential trap distribution, different parameters for various PPV derivatives were obtained. This can be explained if it is taken into account, that during a voltage sweep the trap distribution is only partially filled. The partially filled tail of a Gaussian DOS can be approximated with an exponential DOS. However, this has to be done for each PPV derivate individually by adjusting N_t and T_t to agree with the experiment.

The fact that the traps for these three PPV derivates have the same parameters might indicate that the traps have the same origin. In order to elaborate this, electron transport of a series of nine polymers was analyzed by Nicolai *et al.* using the Gaussian trap model.

Remarkably, for all polymers that showed a trap-limited current the amount of traps is almost the same with a value of $3 \times 10^{23}\ \mathrm{m}^{-3}$. The only value that was different between the polymers was the trap energy E_t below the LUMO. After relating the trap energy to the LUMO levels of each polymer, it was found that the all traps are located at a common energy level of around 3.6 eV below the vacuum level. Note that the width of the trap distribution σ_t was assumed to be equal to the width of the Gaussian distribution of the LUMO because both will result from the same disorder in the material. This essentially allows for predictive modelling of the trap-limited electron current if the hole mobility and the LUMO of a material is known.(*36*)

The nature of the traps is still not fully understood and under debate. The findings of Nicolai *et al.* however indicate that the origin cannot be from structural defects like kinks and twists in the polymer chain, because polymers with different chemical structure as PPVs, thiophenes and fluorenes have been investigated. Since for all polymers the electron transport could be modeled with almost the same parameters it is likely that the traps all have a common origin that is extrinsic. Quantum chemical calculations suggested that water and oxygen complexes could be a possible origin of electron traps in organic semiconductors.(*36*)

2.4 Device Model for Polymer Light-Emitting Diodes

So far, the transport for single carrier devices has been explained. Charge carriers hop from localized states that are Gaussianly distributed in energy. The mobility of the carriers is temperature, field and carrier density dependent. The intrinsic mobility of electrons and holes is the same. However, the electron transport is affected by traps, resulting in a trap-limited current.

A PLED is a double carrier device, where both, holes and electrons are injected. In a double carrier device the charge carrier recombination and the charge neutralization additionally play an important role. Due to the neutralization of electrons and holes, the total charge may exceed the net charge. The net charge is the difference between the hole and electron concentration. Because of this, the current density in a double carrier device is always higher than in a single carrier device.

Because the charge carrier mobility is temperature, field and density dependent and the electron transport is trap-limited, the current density of a PLED cannot be described by an analytical equation. Therefore, Koster *et al.* developed a numerical device model with the basic equations based on double-carrier semiconductor devices such as the current equations:(*29, 37*)

$$J = J_n + J_p \tag{13}$$

$$J_n = e\mu_n[E(x), n(x), T]n(x)E(x) + eD_n \frac{\partial}{\partial x} n(x) \tag{14}$$

$$J_p = e\mu_p[E(x), p(x), T]p(x)E(x) - eD_p \frac{\partial}{\partial x} p(x) \tag{15}$$

The Poisson equation:

$$\frac{\varepsilon_0 \varepsilon_r}{e} \frac{dE(x)}{dx} = p(x) - n(x) - n_t(x) \tag{16}$$

And the particle-conservation equation:

$$\frac{1}{e}\frac{dJ_n}{dx} = -\frac{1}{e}\frac{dJ_p}{dx} = Bp(x)n(x) \tag{17}$$

Where J_n and J_p is the electron and hole current density, respectively, $E(x)$ is the electric field at the position x, $n(x)$ and $p(x)$ are the density of mobile electrons and holes, n_t the density of trapped electrons, D_n and D_p the diffusion coefficient of electrons and holes and B the bimolecular recombination constant. Note that the diffusion coefficients follow the Einstein relation $D = \frac{\mu k_B T}{e}$. The term $Bp(x)n(x)$ is the bimolecular rate at which charge carriers recombine and form excitons.

The recombination of charge carriers will be discussed more detailed in the following part. In organic semiconductors the bimolecular recombination is of Langevin type. This means that it is limited by the diffusion of the carriers towards each other due to their Coulombic attraction. Typically, this is the case if the mean free path of the carriers is smaller than the critical Coulomb binding radius

$$r_c = \frac{e^2}{4\pi\varepsilon_0\varepsilon_r k_B T} \tag{18}$$

at which the Coulombic attraction is equal to the thermal energy. Typical hopping lengths of charge carriers are in the order of 1-3 nm. The Coulomb binding radius at a Temperature of 300 K is about 18.5 nm, which is much larger than the hopping distance. As a result the Langevin recombination rate is

$$R_L = B_L np \tag{19}$$

with the Langevin recombination constant (*38*)

$$B_L = \frac{e}{\varepsilon_0\varepsilon_r}\left[\mu_n(n,E,T) + \mu_p(p,E,T)\right] \tag{20}$$

From this equation it follows that an increase in the mobility automatically increases the probability that the charge carriers find each other in the Coulomb field and recombine. The Langevin recombination was used to model the current-voltage characteristics of PPV-based PLEDs. Only considering the Langevin type of recombination was not sufficient to describe the PLED. The calculated Langevin recombination constant was by a factor of 3 to 4 lower than in the experiment.(*39*)

This suggests that other recombination processes than the Langevin type have to be taken into account. When looking at the open-circuit voltage V_{OC} of organic solar cells it was found that the slope of the V_{OC} versus the natural logarithm of the light intensity was different for trap-free electron transport as compared to trap-limited electron transport.(*40*) This difference could be explained by considering trap-assisted recombination, where a trapped electron can recombine with a free hole.(*41-44*) The recombination constant for trap-assisted recombination is given by the Shockley-Read-Hall (SRH) equation (*45, 46*)

$$B_{SRH} = \frac{C_n C_p N_t}{C_n(n + n_1) + C_p(p + p_1)} \quad 21)$$

Where C_n and C_p are capture coefficients for electrons and holes, respectively, n and p are the hole and electron density in the conduction band and valence band, respectively and their product in equilibrium conditions: $p_1 n_1 = N_{CV} \exp\left(-\frac{E_g}{k_B T}\right) = n_i^2$, where N_{CV} is the effective density of states and n_i^2 the intrinsic carrier concentration.

For the total recombination in a PLED the SRH recombination rate is added to the Langevin recombination rate and Equation 17) becomes:

$$\frac{1}{e}\frac{dJ_n}{dx} = -\frac{1}{e}\frac{dJ_p}{dx} = R = (B_L + B_{SRH})(np - n_i^2) \quad 22)$$

In order to analyze the capture coefficient that is necessary to describe the SRH recombination the V_{OC} versus light intensity of a MEH-PPV PLED for different temperatures was measured. It was found that the temperature activation of the capture coefficient was the same as activation energy in a hole-only device of MEH-PPV.(*47*) This shows that the capture coefficient is related to the hole mobility. It was found that the rate limiting step is the diffusion of holes towards a trapped electron, meaning that $C_p \ll C_n$. The capture coefficient is given by (*47*)

$$C_p = \frac{q}{\varepsilon}\mu_p. \quad 23)$$

The SRH recombination is similar to Langevin recombination with the difference that the mobility of a trapped electron is zero. In a working PLED the SRH recombination can be approximated by (*47*)

$$R_{SRH} = \frac{q}{\varepsilon}\mu_p N_t p \quad 24)$$

This means that the recombination of electrons and holes in organic semiconductors is only dependent on the mobilities $\mu_n(n, E, T)$ and $\mu_p(n, E, T)$ of electrons and holes, respectively and the total amount of traps.

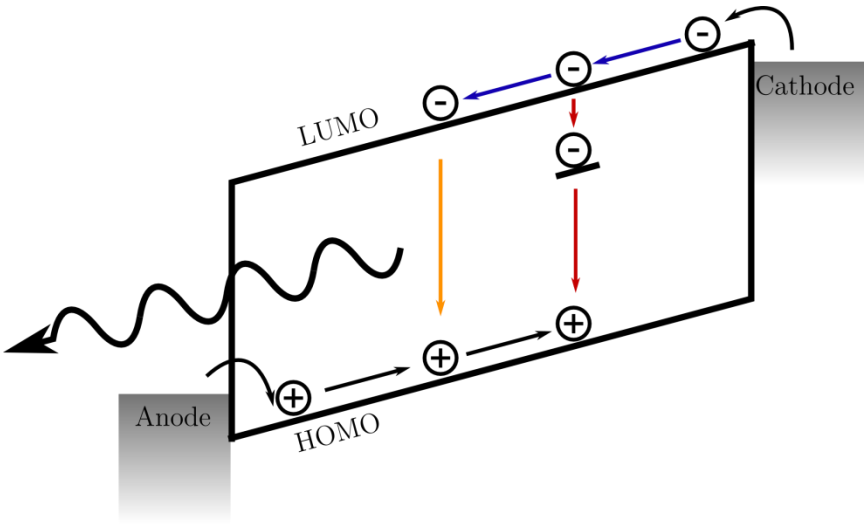

Figure 2.12: Overview of device operation of an PLED including SRH recombination: Trap-free hole transport (black), trap-limited electron transport (blue), non-radiative SRH recombination (red) and emissive Langevin recombination (orange).

Figure 2.12 gives an overview of the processes of recombination in organic semiconductors: Trap-free hole transport (black), trap-limited electron transport (blue) trap-assisted SRH (red) and Langevin recombination (orange).

2.5 Loss mechanisms in single layer PLEDs

Knowing the basics of charge transport and recombination in organic semiconductors, the next section will focus on how non-radiative loss mechanisms influence the operation of a PLED. The two main loss mechanisms are non-radiative trap-assisted recombination (SRH) and exciton quenching at a metallic electrode. When an exciton is quenched, its energy is transferred non-radiatively to an electrode via long range dipole-dipole interactions. Because of that, there is a concentration gradient of excitons with less excitons close to the electrode than in the bulk of the material. Consequently, excitons diffuse towards the electrode thereby increasing the effect of quenching. Typically the electron transport is inferior to the hole transport due to the presence of traps. Consequently, most of the light is generated at the cathode and the quenching is mainly observed at the cathode. To analyze the exciton quenching a one dimensional continuity equation for the exciton density distribution $E(x,t)$ is used*(48-50)*

$$\frac{\partial E(x,t)}{\partial t} = D\frac{\partial^2 E(x,t)}{\partial x^2} - \frac{E(x,t)}{\tau_\infty}\left(1+\frac{x_0^3}{x^3}\right) + R_L \qquad 25)$$

where x is the distance from the electrode. The first term, with D the diffusion coefficient of the excitons, describes the one dimensional exciton diffusion. The second term, with τ_∞ is the exciton lifetime describes the exciton decay in the polymer. This is further enhanced by the non-radiative exciton energy transfer to the electrode mentioned above characterized by an inverse cubic distance dependence, with x_0 a characteristic length for energy transfer.(*49, 51*) The last term is the Langevin recombination rate that describes the exciton generation process as discussed in the last section. Typical values for the exciton diffusion coefficient D and the exciton lifetime τ_∞ that were obtained by time-resolved photoluminescence measurements are $2.2 \times 10^{-7}\mathrm{m}^2/\mathrm{s}$ and $600\,\mathrm{ps}$, respectively. This leaves the range of the energy transfer x_0 as the only unknown parameter.(*51*)

Quenching of excitons at the electrodes has been included in the PLED device model and the effect of the various loss mechanisms on the device efficiency was analyzed. The current efficiency, that is the light-output divided by the current, was simulated for a MEH-PPV PLED by Kuik *et al.* including the effect of emissive Langevin and non-radiative SRH recombination, as well as quenching at the cathode.(*26, 52*) The current efficiency basically is a measure on how efficient electrons and holes are converted into photons. The simulation was repeated for the batch of MEH-PPV used in this thesis for a 100 nm PLED with $x_0 = 10\,\mathrm{nm}$ and is shown in Figure 2.13. It shows how the contributions of the non-radiative SRH recombination and exciton quenching at a cathode compare in magnitude and how they relate to the current efficiency.

From the simulation it can be seen that at low voltages the PLED is completely dominated by the non-radiative SRH recombination. This is because at low voltages the trap states are empty and get filled. Since the total amount of traps N_t is fixed in a sample, the traps get filled more and more at higher voltages. Therefore, the probability of the Langevin recombination increases and is the dominant recombination process at high voltage. The voltage at which Langevin recombination is stronger than the SRH recombination mainly depends on the film thickness. The traps additionally enhance the loss mechanism of cathode quenching. Especially at low voltages, where the traps are mainly empty, the electron transport is inferior to the hole transport. Consequently, the recombination zone is close to the cathode which leads to an increased exciton quenching at the cathode. This can be seen in Figure 2.13 where the cathode quenching increases strongly at low voltages. Overall, at 5 V only 70 % of the excitons recombine

radiatively, 20 % recombine non-radiatively via electron traps and around 10% are quenched at the cathode.

In order to avoid cathode quenching, typically hole-blocking layers are used. Here, a material with a HOMO that is deep compared to the HOMO of the emissive material is put between the emissive layer and the cathode. Because of the energy barrier between both HOMOs, holes are blocked and the recombination zone is shifted away from the cathode to the interface of the emissive layer and the hole-blocking layer.

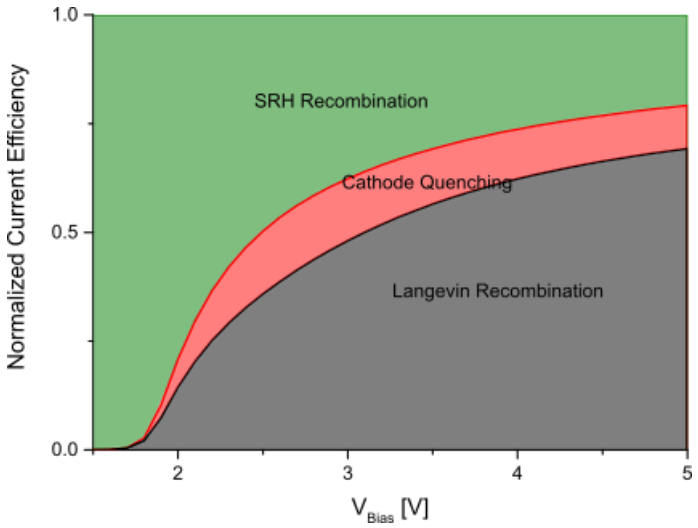

Figure 2.13: Current efficiency plotted versus the applied voltage showing the contribution of the loss mechanisms of non-radiative SRH recombination and cathode quenching for a MEH-PPV PLED of 100 nm. Picture adapted from Kuik *et al. (26)*

In summary in this chapter all processes and parameters that are necessary to describe the charge transport and recombination in a PLED were explained. The hole transport is trap-free and the hole current limited by a buildup of space charge in the device (space-charge limited current). The mobility depends on the temperature, the electric field and the carrier density, which was explained by a hopping mechanism in a Gaussian density of states. The electron transport usually is trap-limited, which means that electrons can fall into localized states in the band gap where they are immobilized. It was found that the trap distribution can be described as a Gaussian dependence on energy and is similar for all polymers. The typical electron trap density amounts to $N_t = 3 \times 10^{23}\mathrm{m}^{-3}$ at an energy of 3.6 eV below vacuum level and a width of 0.1 eV. The recombination of free holes with trapped electrons is determined by a capture coefficient that is thermally activated. The activation energy is equal to the activation energy of holes, which indicates that the trap-assisted recombination is limited by the diffusion of a hole towards an immobile, trapped electron. This is similar to the Langevin recombination where

both carriers diffuse towards each other. By incorporating Langevin and SRH recombination and cathode quenching in the device model the electrical properties of a PLED can be fully modeled.

2.6 References

1. P. W. M. Blom, M. C. J. M. Vissenberg, Charge transport in poly(p-phenylene vinylene) light-emitting diodes. *Materials Science and Engineering: R: Reports* **27**, 53-94 (2000).

2. H. Bässler, Injection, transport and recombination of charge carriers in organic light-emitting diodes. *Polymers for Advanced Technologies* **9**, 402-418 (1998).

3. Y. Shen, A. R. Hosseini, M. H. Wong, G. G. Malliaras, How To Make Ohmic Contacts to Organic Semiconductors. *ChemPhysChem* **5**, 16-25 (2004).

4. I. H. Campbell, P. S. Davids, D. L. Smith, N. N. Barashkov, J. P. Ferraris, The Schottky energy barrier dependence of charge injection in organic light-emitting diodes. *Appl Phys Lett* **72**, 1863-1865 (1998).

5. B. K. Crone, P. S. Davids, I. H. Campbell, D. L. Smith, Device model investigation of single layer organic light emitting diodes. *J Appl Phys* **84**, 833-842 (1998).

6. G. G. Malliaras, J. C. Scott, Numerical simulations of the electrical characteristics and the efficiencies of single-layer organic light emitting diodes. *J Appl Phys* **85**, 7426-7432 (1999).

7. N. F. Mott, R. W. Gurney, *Electronic Processes in Ionic Crystals.* (Oxford University Press, London, 1940).

8. W. D. Gill, Drift mobilities in amorphous charge-transfer complexes of trinitrofluorenone and poly-n-vinylcarbazole. *J Appl Phys* **43**, 5033-5040 (1972).

9. D. M. Pai, Transient Photoconductivity in Poly(N-vinylcarbazole). *The Journal of Chemical Physics* **52**, 2285-2291 (1970).

10. J. Frenkel, On Pre-Breakdown Phenomena in Insulators and Electronic Semi-Conductors. *Physical Review* **54**, 647-648 (1938).

11. P. W. M. Blom, M. J. M. de Jong, M. G. van Munster, Electric-field and temperature dependence of the hole mobility in poly(p-phenylene vinylene). *Physical Review B* **55**, R656-R659 (1997).

12. M. Van der Auweraer, F. C. De Schryver, P. M. Borsenberger, H. Bässler, Disorder in Charge Transport in doped polymers. *Adv Mater* **6**, 199-213 (1994).

13. E. M. Conwell, Impurity Band Conduction in Germanium and Silicon. *Physical Review* **103**, 51-61 (1956).

14. N. F. Mott, On the Transition to Metallic Conduction in Semiconductors. *Canadian Journal of Physics* **34**, 1356-1368 (1956).

15. A. Miller, E. Abrahams, Impurity Conduction at Low Concentrations. *Physical Review* **120**, 745-755 (1960).

16. H. Bässler, Charge Transport in Disordered Organic Photoconductors a Monte Carlo Simulation Study. *physica status solidi (b)* **175**, 15-56 (1993).

17. C. Tanase, E. J. Meijer, P. W. M. Blom, D. M. de Leeuw, Local charge carrier mobility in disordered organic field-effect transistors. *Org Electron* **4**, 33-37 (2003).

18. G. Horowitz, M. E. Hajlaoui, R. Hajlaoui, Temperature and gate voltage dependence of hole mobility in polycrystalline oligothiophene thin film transistors. *J Appl Phys* **87**, 4456-4463 (2000).

19. A. R. Brown, C. P. Jarrett, D. M. de Leeuw, M. Matters, Field-effect transistors made from solution-processed organic semiconductors. *Synthetic Met* **88**, 37-55 (1997).

20. G. Horowitz, R. Hajlaoui, D. Fichou, A. El Kassmi, Gate voltage dependent mobility of oligothiophene field-effect transistors. *J Appl Phys* **85**, 3202-3206 (1999).

21. C. D. Dimitrakopoulos, S. Purushothaman, J. Kymissis, A. Callegari, J. M. Shaw, Low-Voltage Organic Transistors on Plastic Comprising High-Dielectric Constant Gate Insulators. *Science* **283**, 822-824 (1999).

22. C. Tanase, E. J. Meijer, P. W. M. Blom, D. M. de Leeuw, Unification of the Hole Transport in Polymeric Field-Effect Transistors and Light-Emitting Diodes. *Phys Rev Lett* **91**, 216601 (2003).

23. M. C. J. M. Vissenberg, M. Matters, Theory of the field-effect mobility in amorphous organic transistors. *Physical Review B* **57**, 12964-12967 (1998).

24. C. Tanase, P. W. M. Blom, D. M. de Leeuw, Origin of the enhanced space-charge-limited current in poly(p-phenylene vinylene). *Physical Review B* **70**, 193202 (2004).

25. W. F. Pasveer *et al.*, Unified Description of Charge-Carrier Mobilities in Disordered Semiconducting Polymers. *Phys Rev Lett* **94**, 206601 (2005).

26. M. Kuik, L. J. A. Koster, A. G. Dijkstra, G. A. H. Wetzelaer, P. W. M. Blom, Non-radiative recombination losses in polymer light-emitting diodes. *Org Electron* **13**, 969-974 (2012).

27. N. I. Craciun, J. Wildeman, P. W. M. Blom, Universal Arrhenius Temperature Activated Charge Transport in Diodes from Disordered Organic Semiconductors. *Phys Rev Lett* **100**, 056601 (2008).

28. P. W. M. Blom, M. J. M. de Jong, J. J. M. Vleggaar, Electron and hole transport in poly(p-phenylene vinylene) devices. *Appl Phys Lett* **68**, 3308-3310 (1996).

29. M. A. Lampert, P. Mark, *Current Injection in Solids.* (Academic Press, New York, 1970).

30. P. Mark, W. Helfrich, Space-Charge-Limited Currents in Organic Crystals. *J Appl Phys* **33**, 205-215 (1962).

31. M. M. Mandoc, B. de Boer, G. Paasch, P. W. M. Blom, Trap-limited electron transport in disordered semiconducting polymers. *Physical Review B* **75**, 193202 (2007).

32. Y. Zhang, B. de Boer, P. W. M. Blom, Trap-free electron transport in poly(p-phenylene vinylene) by deactivation of traps with n-type doping. *Physical Review B* **81**, 085201 (2010).

33. H. T. Nicolai, M. M. Mandoc, P. W. M. Blom, Electron traps in semiconducting polymers: Exponential versus Gaussian trap distribution. *Physical Review B* **83**, 195204 (2011).

34. W. Hwang, K. C. Kao, Studies of the theory of single and double injections in solids with a Gaussian trap distribution. *Solid-State Electronics* **19**, 1045-1047 (1976).

35. S. Nešpůrek, P. Smejtek, Space-charge limited currents in insulators with the Gaussian distribution of traps. *Czechoslovak Journal of Physics B* **22**, 160-175 (1972).

36. H. T. Nicolai *et al.*, Unification of trap-limited electron transport in semiconducting polymers. *Nat Mater* **11**, 882-887 (2012).

37. L. J. A. Koster, E. C. P. Smits, V. D. Mihailetchi, P. W. M. Blom, Device model for the operation of polymer/fullerene bulk heterojunction solar cells. *Physical Review B* **72**, 085205 (2005).

38. P. Langevin, *Ann. Chim. Phys.* **28**, 433 (1903).

39. P. W. M. Blom, M. J. M. de Jong, S. Breedijk, Temperature dependent electron-hole recombination in polymer light-emitting diodes. *Appl Phys Lett* **71**, 930-932 (1997).

40. L. J. A. Koster, V. D. Mihailetchi, R. Ramaker, P. W. M. Blom, Light intensity dependence of open-circuit voltage of polymer:fullerene solar cells. *Appl Phys Lett* **86**, 123509 (2005).

41. M. M. Mandoc, F. B. Kooistra, J. C. Hummelen, B. de Boer, P. W. M. Blom, Effect of traps on the performance of bulk heterojunction organic solar cells. *Appl Phys Lett* **91**, 263505 (2007).

42. M. M. Mandoc, W. Veurman, L. J. A. Koster, B. de Boer, P. W. M. Blom, Origin of the Reduced Fill Factor and Photocurrent in MDMO-PPV:PCNEPV All-Polymer Solar Cells. *Adv Funct Mater* **17**, 2167-2173 (2007).

43. N. C. Giebink, G. P. Wiederrecht, M. R. Wasielewski, S. R. Forrest, Ideal diode equation for organic heterojunctions. I. Derivation and application. *Physical Review B* **82**, 155305 (2010).

44. D. Cheyns *et al.*, Analytical model for the open-circuit voltage and its associated resistance in organic planar heterojunction solar cells. *Physical Review B* **77**, 165332 (2008).

45. W. Shockley, W. T. Read, Statistics of the Recombinations of Holes and Electrons. *Physical Review* **87**, 835-842 (1952).

46. R. N. Hall, Electron-Hole Recombination in Germanium. *Physical Review* **87**, 387-387 (1952).

47. M. Kuik, L. J. A. Koster, G. A. H. Wetzelaer, P. W. M. Blom, Trap-Assisted Recombination in Disordered Organic Semiconductors. *Phys Rev Lett* **107**, 256805 (2011).

48. D. E. Markov, J. C. Hummelen, P. W. M. Blom, A. B. Sieval, Dynamics of exciton diffusion in poly(p-phenylene vinylene)/fullerene heterostructures. *Physical Review B* **72**, 045216 (2005).

49. R. R. Chance, A. Prock, R. Silbey, Comments on the classical theory of energy transfer. *The Journal of Chemical Physics* **62**, 2245-2253 (1975).

50. A. L. Burin, M. A. Ratner, Exciton Migration and Cathode Quenching in Organic Light Emitting Diodes. *The Journal of Physical Chemistry A* **104**, 4704-4710 (2000).

51. D. E. Markov, C. Tanase, P. W. M. Blom, J. Wildeman, Simultaneous enhancement of charge transport and exciton diffusion in poly(p-phenylene vinylene) derivatives. *Physical Review B* **72**, 045217 (2005).
52. M. Kuik *et al.*, Determination of the trap-assisted recombination strength in polymer light emitting diodes. *Appl Phys Lett* **98**, 093301 (2011).

3 Materials and Methods

This chapter briefly introduces the organic semiconductors and matrix materials that are used in this work. The preparation of the substrates and the device fabrication is explained, as well as the device layout. In the end the methods that are used to characterize the devices are explained.

3.1 Materials

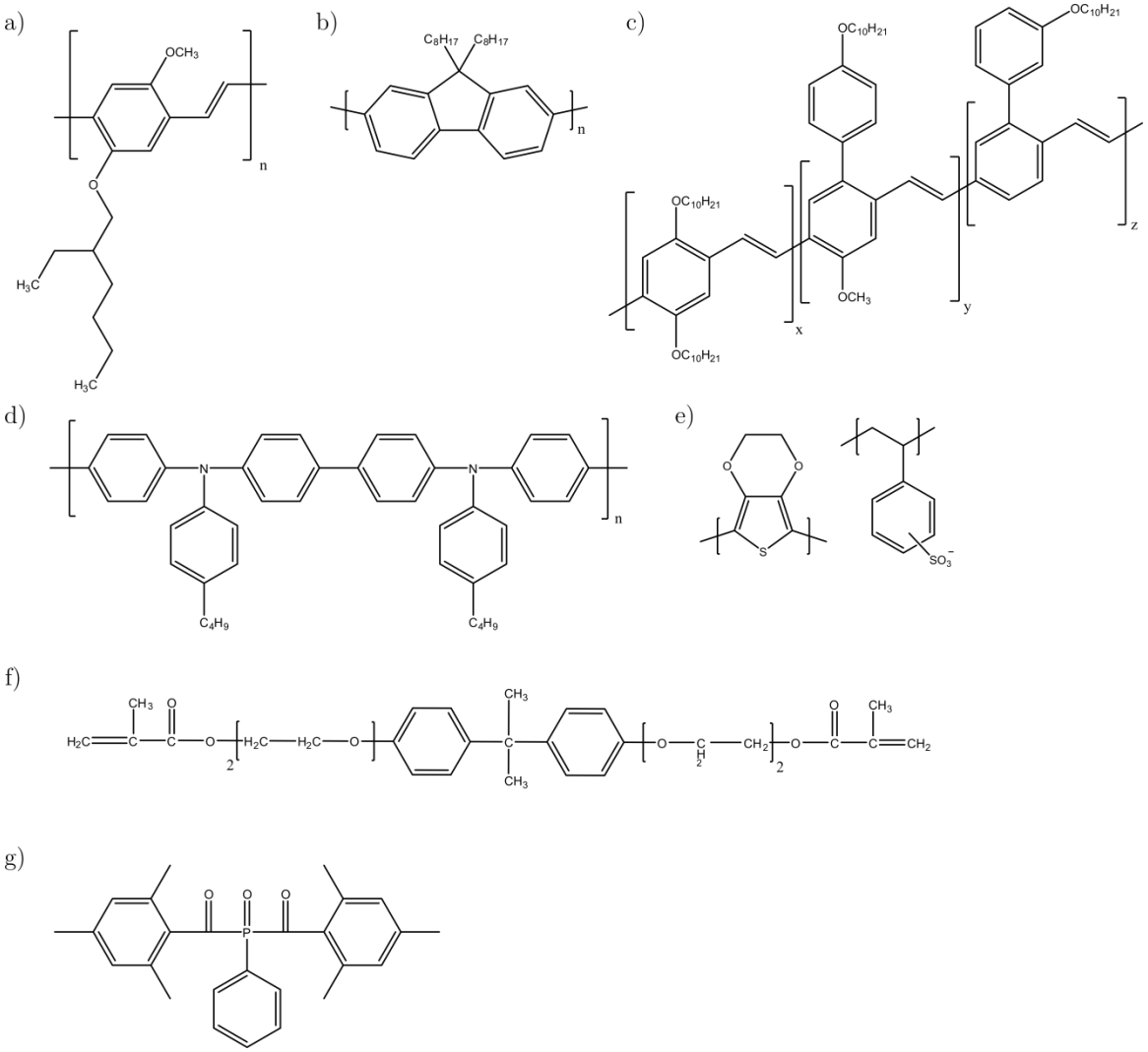

Figure 3.1: Overview of the materials used in this thesis: a) MEH-PPV, b) PFO, c) SY-PPV, d) poly-TPD, e) PEDOT:PSS, f) SR540 and g) Irgacure 819

Poly[2-methoxy-5-(2-ethylhexyloxy)-1,4-phenylenevinylene] (MEH-PPV) is a PPV-derivate with two asymmetric alkyl side chains. The chemical structure is shown in Figure 3.1a). It has been used as a working horse in the last decades and is therefore an ideal model material for our study. The highest occupied molecular orbital (HOMO) and lowest unoccupied molecular orbital (LUMO) levels are reported to be around 5.0 - 5.3 eV and 2.7 - 3.0 eV below vacuum level.(*1-3*) In the multilayer PLEDs demonstrated in this work MEH-PPV is used as an emissive layer. The emitted light has a characteristic orange color with the peak emission at 590 nm. The absorption and electroluminescence (EL) spectra of a MEH-PPV film are shown in Figure 3.2. The molecular weight of this batch is $M_w = 370\,000 \frac{\mathrm{g}}{\mathrm{mol}}$ with a polydispersity index of 3.4.

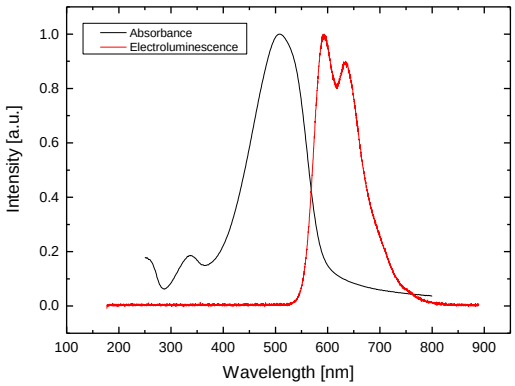

Figure 3.2: Absorption and electroluminescence spectra of an MEH-PPV layer.

Another PPV-derivative used is the so-called Super Yellow PPV (SY-PPV). Its chemical structure is shown in Figure 3.1c). SY-PPV was bought from Merck KGaA. SY-PPV shows a characteristic yellow emission and the EL spectrum is shown in Figure 3.3 in yellow. The molecular weight is $M_w = 975\,000 \frac{\mathrm{g}}{\mathrm{mol}}$. The LUMO and HOMO levels of Super Yellow are reported to be at 3.0 and 5.4 eV below vacuum level, respectively.(*4*)

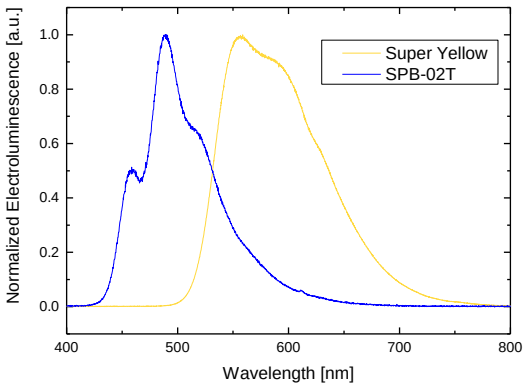

Figure 3.3: Electroluminescence spectrum of Super Yellow (yellow) and SPB-02T (blue)

In a multilayer device poly(9,9-di-n-octylfluorenyl-2,7-diyl) (PFO) is used as a hole-blocking layer. PFO was bought from TNO/Holst Center. The structure is shown in Figure 3.1b). The HOMO level of PFO is at 5.8 eV below vacuum level.(*5*) Compared to the HOMO levels of MEH-PPV and Super Yellow, there is a substantial energy barrier that block holes efficiently.

For the experiments reported in Chapter 5, which include two emissive layers, the blue-emitting polymer SPB-02T has been used. SPB-02T is a poly(spirobifluorene) and was bought from Merck KGaA, but the detailed chemical structure is not provided. The EL spectrum of the blue emitting polymer is shown in Figure 3.3 in blue. The molecular weight of SPB-02T is $M_w = 750\,000 \frac{g}{mol}$. The

LUMO and HOMO are located at 2.5 and 5.2 eV below vacuum level, respectively.(*6*)

In the tri-layer device reported in Chapter 6, poly[N,N'-bis(4-butylphenyl)-N,N'-bis(phenyl)-benzidine] (poly-TPD) is used as an electron-blocking layer. The chemical structure is shown in Figure 3.1d). The LUMO and the HOMO of poly-TPD are at 2.3 and 5.1 eV below vacuum level, giving rise to an energy barrier to the LUMO of Super Yellow PPV.(*7*) Consequently, poly-TPD can block electrons efficiently.

As insulating cross-linkers the commercially available NOA83H (Norland Products) and ethoxylated (4) bisphenol A dimethacrylate that is sold under the name SR540 from Sartomer were used. The structure of SR540 is shown in Figure 3.1d). The structure of NOA83H is not known. NOA83H is typically used as a liquid adhesive that cures upon exposure to ultraviolet (UV) light, in order to bond optical components together. SR540 is a monomer that is used in free radical polymerization.

In order to activate the cross-linking for SR540, an additional photoinitiator is necessary. Therefore, Irgacure 819 that was bought from BASF. Irgacure 819 is bis(2,4,6-trimethylbenzoyl)-phenylphosphineoxide and the structure is shown in Figure 3.1e). Irgacure 819 is strongly absorbing light below 400 nm. The bonds between the carbon and phosphor atoms can break and thus three radicals per molecule can be created. These radicals can break one of the C-C double bond at the ends of SR540, thereby creating a new radical. The new radical can again break a C-C double bond and consequently, the molecule polymerizes. During this process two polymer chains can be linked together. This is called cross-linking. When a polymer chain is cross-linked, its properties can change drastically. One example is the ability of the chains to move freely. SR540 in the initial state is a resin, because the chains are flowing freely. When SR540 is cross-linked the chain mobility is drastically reduced and the material turns from liquid to solid. Furthermore, the solubility in solvents is decreased. Typically, cross-linked polymers are not soluble in most of their initial solvents.

To initiate the cross-linking process a UV-flood lamp (Dymax, EC-2000) is used. The spectral output of the lamp is shown in Figure 3.4. A mercury halide lamp is used that shows an emission in the UV-A and visible spectrum. In order to prevent photo-oxidation of the organic semiconductors, the cross-linking is done in nitrogen atmosphere.

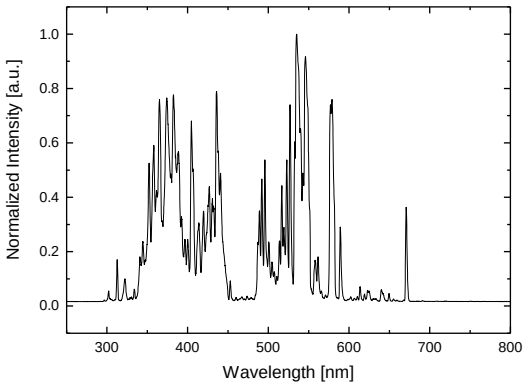

Figure 3.4: Emission spectrum of the Dymax EC-2000 UV-flood lamp

One of the electrodes has to be transparent in a PLED so that the light can get out of the device. This is typically the anode. The transparent anode material that is used is indium tin oxide (ITO). ITO is a well-known transparent conductive oxide and the standard material for anodes in organic electronics because of its good transparency and low resistivity.(*8*) By treating the ITO with UV-ozone, the work function can be increased from 4.7 to 5.6 eV below vacuum level.(*9*) Organic contaminations are removed and the surface is oxidized, resulting in a hydrophilic surface.(*10*)

On top of ITO, poly(3,4-ethylenedioxythiophene) polystyrene sulfonate (PEDOT:PSS) is spin-coated. PEDOT:PSS has been commonly used as a hole injection layer in organic electronics.(*11*) The chemical structure is shown in Figure 3.1f). PEDOT:PSS was bought from Heraeus (Clevios P VP Al 4083). The work function is approximately 5.2 eV below vacuum level(*12, 13*) and the weight ratio between PEDOT and PSS is 1 to 6. Furthermore, PEDOT:PSS is not soluble in organic solvents and dispersed in water. In a PLED it is commonly used to decrease the energy difference between ITO and the organic semiconductor.(*11*) Additionally, the transparency is high and by spin-coating a PEDOT:PSS layer on top of ITO the ITO surface is planarized.

As a cathode barium is used in this work. Barium is a low work function metal (2.7 eV) and can efficiently inject electrons in the LUMO of common organic semiconductors.(*14*) Barium is thermally evaporated at a pressure of 10^{-7} mbar with a thickness of 5 nm. Since barium is very reactive, an aluminum capping layer of 100 nm is evaporated on top to prevent a reaction of barium with oxygen or water.

For hole-only devices molybdenum tri-oxide (MoO_3) is used as a hole injecting top contact. MoO_3 is a transition metal oxide and is commonly used because of its exceptional electronic properties.(*15, 16*) MoO_3 has a very high work

function of 6.9 eV below vacuum level, which makes it an ideal hole injecting contact.(*15*) MoO_3 is evaporated at a pressure of 10^{-6} mbar with a thickness of 10 nm, followed by a 100 nm aluminum capping layer.

For MEH-PPV water-free chlorobenzene has been used as solvent, for all other materials water-free toluene has been used. Solutions were prepared in a nitrogen atmosphere and left for stirring overnight. A detailed description of the concentrations and the resulting film thicknesses is given in each chapter separately.

MEH-PPV and SY-PPV solutions were stirred at 55°C, in order to increase the dissolution in the solvent. After stirring, the solutions were filtered with a Rezist 5 µm PTFE filter. The matrix and photoinitiator solutions were filtered with a 1 µm filter.

3.2 Device Fabrication

The film thickness of the spin-coated films is typically in the order of 100 nm and therefore much smaller than dust particles that are µm-sized. Already a single dust particle can cause a short circuit in the device. To this end, the devices are generally fabricated in a cleanroom environment.

The devices are fabricated on a 3×3 cm glass substrate with a pre-patterned ITO layer. The pre-patterned glass substrates are cleaned by scrubbing with a 10 wt. % solution of Extran MA 02 (VWR) in deionized water. The substrates are then put in a flow bath of deionized water with a temperature of 50°C. Consecutively, the substrates are cleaned in a 5 min ultrasonic bath in acetone followed by isopropanol. After drying at a temperature of 140°C for 10 min, the substrates are cleaned in a UV-ozone cleaner for 20 min.

In order to reduce the roughness of ITO and improve the hole injection, a PEDOT:PSS layer is spin-coated with a speed of 500 rpm for 10 s followed by 1500 rpm for 60 s. Before deposition, the solution is filtered with a 0.45 µm pore size PVDF filter. After spin-coating, the film is dried at 140°C for 10 min to remove the water. The resulting film thickness is around 45 nm.

All following steps were carried out in a nitrogen atmosphere. After coating PEDOT:PSS on the substrate, the light-emitting polymers are spin-coated on the substrate. The typical spin-coating program is 1000 rpm for 20 s followed by 250 rpm for 60 s. If chlorobenzene is used as solvent instead of toluene, the last step is 120 s instead of 60 because chlorobenzene evaporates more slowly. In case that blends with a cross-linkable matrix are fabricated, the blends are illuminated with

UV-light with a dose of approximately 40 J/cm^2. The fabrication of multilayers using the crosslinked blends is described in more detail in chapter 5 and 6.

Finally, the top contact is thermally evaporated at a pressure of 10^{-6} mbar. For a PLED and electron-only device, the top contact consists of 5 nm barium, followed by a 100 nm aluminum capping layer. For a hole-only device, the top contact is 10 nm MoO_3 followed by 100 nm of aluminum. Electron-only devices are fabricated on clean glass substrates without ITO and PEDOT:PSS. As a bottom contact 30 nm of aluminum is evaporated through a shadow mask that is subsequently oxidized in air for 10 min.

The overlap of the bottom contact and the top contact is the active area in the final device. The contacts are designed in such a way that they cover a range of 10^{-5} m^2 to 10^{-4} m^2. The general structure is shown as a side view and top view in Figure 3.5a) and b), respectively. Figure 3.5c) shows a photograph of an MEH-PPV PLED. The typical orange emission is visible on a 1 cm^2 sample.

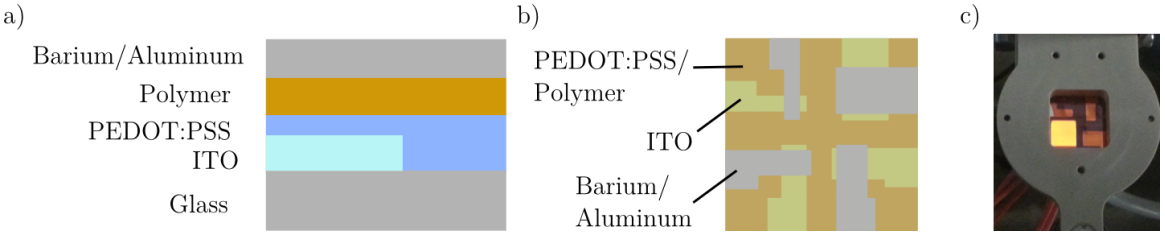

Figure 3.5: Structure of a PLED: a) side view and b) top view. c) Photograph of a MEH-PPV PLED in operation showing the characteristic orange emission.

3.3 Device layout

Single carrier devices such as hole-only and electron-only devices help to disentangle the charge transport in a PLED where both carriers are present. In a PLED the work functions of anode and cathode match the energy levels of the HOMO and LUMO, respectively. The energy diagram of a PLED is shown in Figure 3.6a). Therefore ITO, covered with a PEDOT:PSS layer is used as anode and hole-injection layer, respectively, and barium with an aluminum capping layer is used as cathode.

In a hole-only device, the injection of electrons must be blocked. Therefore it is suitable to have two hole-injecting contacts. The energy diagram of a hole-only device is schematically shown in Figure 3.6b). As a bottom contact ITO with a PEDOT:PSS layer is used. As a top contact, MoO_3 is used as a thermally evaporated hole injecting contact.

In an electron-only device, the injection of holes has to be blocked. Therefore, the ITO contact is replaced by an oxidized aluminum contact. The work

function of the oxidized aluminum is around 3.2 eV below vacuum level and prevents the injection of holes. As a top contact, the electron-injecting barium covered with an aluminum capping layer is used.

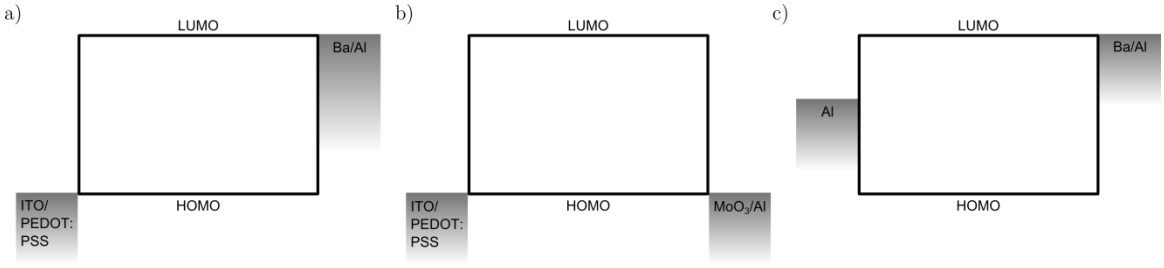

Figure 3.6: a) Schematic energy diagram of a PLED with hole-injecting bottom contact and electron-injecting top contact. b) Hole-only device with ITO/PEDOT:PSS as bottom contact and MoO_3 as a top contact that enables hole injection, too. c) Electron-only device with Al bottom contact that blocks the hole injection and electron-injecting Ba/Al top contact.

3.4 Device characterization

In order to analyze the charge transport in organic semiconductors, the current-voltage characteristics (J-V) of both, single carrier and double carrier devices are measured. Therefore, a Keithley 2400 source meter is used. To measure the light output of a PLED, a silicon photodiode that is connected to a Keithley 6514 electrometer is used. To measure the luminance (L), a Konica Minolta LS-100 luminance meter was used. The EL spectrum of the PLEDs is measured with an Ocean Optics USB400-UV-VIS-ES spectrometer.

The J-V characteristics of a PLED are measured by applying a voltage sweep starting from 0 to typically 5 V with a step size of 0.1 V. At 5 V the voltage is decreased to -2 V and then increased again to 0 V. A J-V curve of a typical MEH-PPV PLED is shown black in Figure 3.7. Measuring the reverse bias shows the leakage current of the device that is also visible at very low voltage in forward bias. The leakage current is labeled with a 1 in Figure 3.7. Here the device current in the device is dominated by leakage that scales linearly with the applied voltage. At voltages above 1.5 V the current follows an exponential increase. Because of the different work functions of the electrodes, at 0 V electrons will flow from the cathode to the anode to equilibrate the Fermi levels. The resulting built-in voltage gives rise to an internal electric field that is in opposite direction of the drift current. For voltages lower than the built-in voltage the current is dominated by diffusion, which leads to an exponential dependence of the current density on voltage. This regime is labeled with a 2 in Figure 3.7. Above the built-in voltage,

the current density shows a quadratic dependence on the voltage that is due to the drift current. This is labeled with a 3.

In hole-only devices there is usually hole injection from both contacts and consequently hole current in forward and reverse bias. In this case, the voltage sweep is applied from 0 to 5 to -5 to 0 V. This is shown in red Figure 3.7. In case both contacts are Ohmic the curve is symmetric in forward and reverse bias.

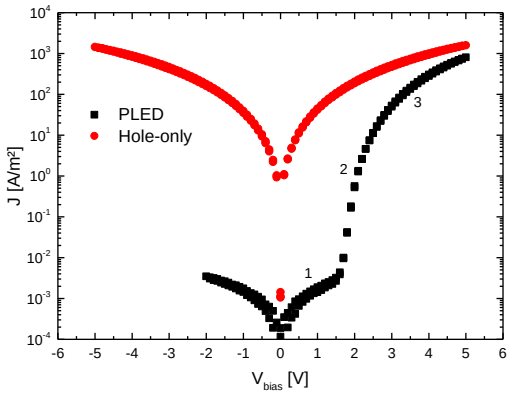

Figure 3.7: J-V charateristics of a MEH-PPV PLED (black) and a MEH-PPV hole-only device (red)

The charge transport is dependent on the film thickness. Therefore, the thickness of every sample has to be measured. The film thickness is measured using a Bruker DektakXT Stylus Profiler. The polymer film is scratched with a needle, exposing the glass substrate. The surface profiler can then measure the height difference between the polymer film and the glass substrate.

3.5 References

1. I. H. Campbell, T. W. Hagler, D. L. Smith, J. P. Ferraris, Direct Measurement of Conjugated Polymer Electronic Excitation Energies Using Metal/Polymer/Metal Structures. *Phys Rev Lett* **76**, 1900-1903 (1996).

2. A. L. Holt, J. M. Leger, S. A. Carter, Electrochemical and optical characterization of p- and n-doped poly[2-methoxy-5-(2-ethylhexyloxy)-1,4-phenylenevinylene]. *The Journal of Chemical Physics* **123**, 044704 (2005).

3. Y. Li *et al.*, Electrochemical properties of luminescent polymers and polymer light-emitting electrochemical cells. *Synthetic Met* **99**, 243-248 (1999).

4. M. Zhang, S. Hofle, J. Czolk, A. Mertens, A. Colsmann, All-solution processed transparent organic light emitting diodes. *Nanoscale* **7**, 20009-20014 (2015).

5. S. Janietz *et al.*, Electrochemical determination of the ionization potential and electron affinity of poly(9,9-dioctylfluorene). *Appl Phys Lett* **73**, 2453-2455 (1998).
6. J. Yang, Y. Kwon, J. Kwak, C. Lee, P.119: High-Performance Polymer Light-Emitting Diodes with a Conjugated Polyelectrolyte. *SID Symposium Digest of Technical Papers* **44**, 1431-1433 (2013).
7. Q. J. Sun *et al.*, White light from polymer light-emitting diodes: Utilization of fluorenone defects and exciplex. *Appl Phys Lett* **88**, 163510 (2006).
8. D. S. Ginley, C. Bright, Transparent Conducting Oxides. *MRS Bulletin* **25**, 15-18 (2000).
9. P. Destruel *et al.*, Influence of indium tin oxide treatment using UV–ozone and argon plasma on the photovoltaic parameters of devices based on organic discotic materials. *Polymer International* **55**, 601-607 (2006).
10. S. Y. Kim, J.-L. Lee, K.-B. Kim, Y.-H. Tak, Effect of ultraviolet–ozone treatment of indium–tin–oxide on electrical properties of organic light emitting diodes. *J Appl Phys* **95**, 2560-2563 (2004).
11. L. Groenendaal, F. Jonas, D. Freitag, H. Pielartzik, J. R. Reynolds, Poly(3,4-ethylenedioxythiophene) and Its Derivatives: Past, Present, and Future. *Adv Mater* **12**, 481-494 (2000).
12. Y. Zhang, L. Chen, X. Hu, L. Zhang, Y. Chen, Low Work-function Poly(3,4-ethylenedioxylenethiophene): Poly(styrene sulfonate) as Electron-transport Layer for High-efficient and Stable Polymer Solar Cells. *Scientific Reports* **5**, 12839 (2015).
13. T. M. Brown *et al.*, Built-in field electroabsorption spectroscopy of polymer light-emitting diodes incorporating a doped poly(3,4-ethylene dioxythiophene) hole injection layer. *Appl Phys Lett* **75**, 1679-1681 (1999).
14. C.-J. Lee, M.-G. Kwak, D.-K. Choi, D.-G. Moon, Influence of the Performance of Organic Light Emitting Devices by Chemical Reaction at the Interface between Electron Transport Material and Ba Cathode. *MATERIALS TRANSACTIONS* **52**, 1316-1319 (2011).
15. J. Meyer *et al.*, Transition Metal Oxides for Organic Electronics: Energetics, Device Physics and Applications. *Adv Mater* **24**, 5408-5427 (2012).
16. T. Shizuo, N. Koji, T. Yasunori, Metal oxides as a hole-injecting layer for an organic electroluminescent device. *Journal of Physics D: Applied Physics* **29**, 2750 (1996).

4 Solubility and Charge Transport in Blends of poly-dialkoxy-p-phenylene vinylene and UV-cross-linkable Matrices

In this chapter poly[2-methoxy-5-(2-ethylhexyloxy)-1,4-phenylenevinylene] (MEH-PPV) is blended with two different inert UV-cross-linkable matrices to tune the solubility of the solution-processed films . It is found that only 10 wt. % of theses matrices is required to make the blend layer insoluble after cross-linking. The addition of only 10 wt. % matrix only slightly reduces the hole mobility, whereas the electron transport is not affected. Polymer light-emitting diodes (PLEDs) with an insoluble 90:10 MEH-PPV:matrix blend layer exhibit the same current density and photocurrent as pristine and soluble MEH-PPV PLEDs.

The content of this chapter was published in:
C. Kasparek, R. Rohloff, J. J. Michels, N. I. Crăciun, J. Wildeman, P. W. M. Blom, Adv. Electron. Mater. 2017, 3, 1600519

4.1 Introduction

As mentioned in the general introduction in Chapter 1, organic light-emitting diodes (OLEDs) consist of a stack of small molecule-based layers that each have specific functions.(*1*) These functions include hole transport, electron-blocking, emission of one or more colors, hole-blocking and electron transport. Conventionally, such a stack of layers is deposited by thermal evaporation in a high vacuum. The route towards lower cost is to process these layers from solution, such that a cost efficient roll-to-roll process can be used. However, a major challenge is the stack integrity; when a subsequent layer is coated on top of a previously deposited layer, the first layer will redissolve in the solvent of the second layer.

In the last years several different approaches that typically rely on elaborate synthetic strategies and only work for a certain set of materials have been presented.(*2-17*) A general concept to make layers insoluble that enables multilayer application form solution still has to be developed. In this work, a general concept is used where the functional material is blended with a cross-linkable host matrix. In this chapter the solubility and the charge transport of blends of a functional material and two different cross-linkable host matrices are analyzed. To this end poly[2-methoxy-5-(2-ethylhexyloxy)-1,4-phenylenevinylene] (MEH-PPV) is blended with two different cross-linkable host matrices, NOA83H (Norland Products) and SR540 (Sartomer). The matrix is cross-linked after deposition with UV-light which makes the whole blend layer insoluble. The solubility of blends in different weight ratios and the effect of the cure time are investigated. Furthermore the charge transport in hole-only and electron-only devices is analyzed. Finally, from the insoluble blend layers polymer light-emitting diodes (PLEDs) with the same optoelectronic functionality as pristine and soluble MEH-PPV are fabricated.

4.2 Experimental

Water-free chlorobenzene is used as solvent for all materials. For MEH-PPV a concentrations of 5.5 mg/ml was used, whereas for the matrices NOA83H and SR540 20 mg/ml and 40 mg/ml were used, respectively. In order to activate the cross-linking process of SR540, the photoinitiator Irgacure 819 (BASF) was added with a concentration of 2 wt. % relative to the total material in the blend solution. PLEDs as well as hole-only devices were processed on a glass substrate with a pre-patterned indium tin oxide (ITO) layer. The substrates were cleaned using soap

followed by an ultrasonic acetone and isopropanol bath. After that they were dried and treated with UV-ozone. Poly(3,4-ethylenedioxythiophene) polystyrene sulfonate (PEDOT:PSS, Clevios P VP Al 4083, Heraeus) was spin-coated with a speed of 250 rpm for 10 s followed by a drying step with 1500 rpm for 50s. The layer was baked at 140°C for 10 min, resulting in 45 nm thick films. The MEH-PPV:matrix blends were spin-coated in a nitrogen atmosphere with a speed of 1000 rpm for 20 s and then dried at 250 rpm for 90 s. The blend was then cross-linked in a nitrogen atmosphere with a UV flood lamp (Dymax 2000-EC). Cathodes were thermally evaporated at a pressure of 10^{-6} mbar. For electron-only and PLEDs cathodes consist of 5 nm Barium and 100 nm Aluminum as a capping layer. For electron-only devices the anode consisted of a 30 nm Aluminum layer that was slightly oxidized. For hole-only devices the top electrode is made of 10 nm MoO_3 followed by a 100 nm Al capping layer. The devices were characterized in nitrogen atmosphere using a Keithley 2400 source meter and a 6514 system electrometer connected to a Si-photodiode. The film thickness was measured with a Bruker DektakXT Stylus Profiler.

4.3 Results and discussion

4.3.1 Tuning the solubility of a MEH-PPV:Matrix blend layer

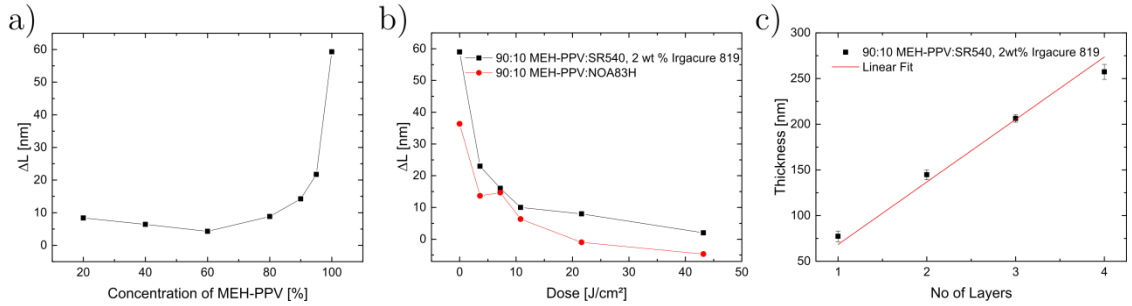

Figure 4.1: a) Film thickness difference after spin-coating chlorobenzene on top of the cross-linked MEH-PPV:SR540 blends (dose 3 J/cm²) for different ratios of MEH-PPV and SR540. b) Film thickness difference of MEH-PPV blended with SR540 (black) and NOA83H (red) in a 90:10 ratio for different doses. c) Film thickness of 90:10 MEH-PPV:SR540 layers that were each cross-linked with a dose of 43 J/cm² stacked on top of each other.

Blends of MEH-PPV and SR540 in different concentrations, ranging from 20:80 MEH-PPV:SR540 to pristine MEH-PPV (100%), were made and spin-coated on a glass substrate. The notation 20:80 MEH-PPV:SR540 means that there is 20 wt. % MEH-PPV and 80 wt. % SR540 in the blend. The blends were cross-linked with a dose of 3 J/cm² in a nitrogen atmosphere. The film thickness of all blends was around 100 nm after cross-linking. To test the effectiveness of the cross-linking

procedure, chlorobenzene was spin-coated on top of the cured blend films to remove any dissolvable material, followed by measurement of the film thickness. Since MEH-PPV is well soluble in chlorobenzene, parts of the MEH-PPV in the blend that are not surrounded by matrix can be washed off. The difference in film thickness ΔL before and after spin-coating chlorobenzene on top is plotted as a function of the concentration of MEH-PPV in Figure 4.1a). From the 100 nm of the pristine MEH-PPV film around 60 nm were washed off. The wash-off is not complete due to the relatively high molecular weight (M_w = 350 000 g/mol) of the MEH-PPV used. Adding only 5 % of the SR540 matrix decreased the wash-off to 20 nm after cross-linking. The wash off for a blend containing 10 % SR540 was around 15 nm. Further increasing the amount of SR540 to 20 % decreased the wash-off to 10 nm. The blends from 80:20 down to 20:80 MEH-PPV:SR540 showed a wash-off of less than 10 nm. We note that such small wash off approaches the accuracy of the profilometric thickness measurement, which is typically 5 nm. Surprisingly, only small concentrations of 10-20 % SR540 in the blend are sufficient to drastically reduce the solubility of the film. In this case MEH-PPV is in excess of SR540, however the term matrix for SR540 and NOA83H will be further used.

To investigate the influence of the UV-illumination dose, blends of 90:10 MEH-PPV:SR540 and 90:10 MEH-PPV:NOA83H were cross-linked with different doses. Again, the film thickness of the cross-linked samples was measured before and after spin-coating chlorobenzene on top. The resulting difference in film thickness ΔL is plotted against the UV dose in Figure 4.1b). For both matrices (SR540 in black and NOA83H in red) the thickness difference of the blend decreases with increasing dose. For a sufficiently high dose of typically 40 J/cm^2, the wash-off for the 90:10 MEH-PPV:matrix blend can even be decreased close to 0 nm, resulting in completely insoluble films.

To show that the solubility is low enough to allow for sequential solution processing, four layers of a 90:10 MEH-PPV:SR540 blend were stacked on top of each other. To this end, first a single layer was spin-coated and cross-linked with a dose of 43 J/cm^2 and the film thickness was measured. Afterwards, a subsequent layer was spin-coated on top of the first one and the total thickness was measured again after cross-linking. This was repeated for four layers in total. The total film thickness is plotted against the number of layers in Figure 4.1c). As expected for an insoluble film, the film thickness increases linearly with the number of deposited layers. The red line shows a linear fit with a slope of 70 nm per layer. This is in good agreement with the measured thickness of the first layer of 75 nm. As a

result, for both matrices we demonstrated that with a sufficiently large UV-illumination dose the 90:10 MEH-PPV:matrix blends are completely insoluble.

4.3.2 Hole transport in the MEH-PPV:matrix blends

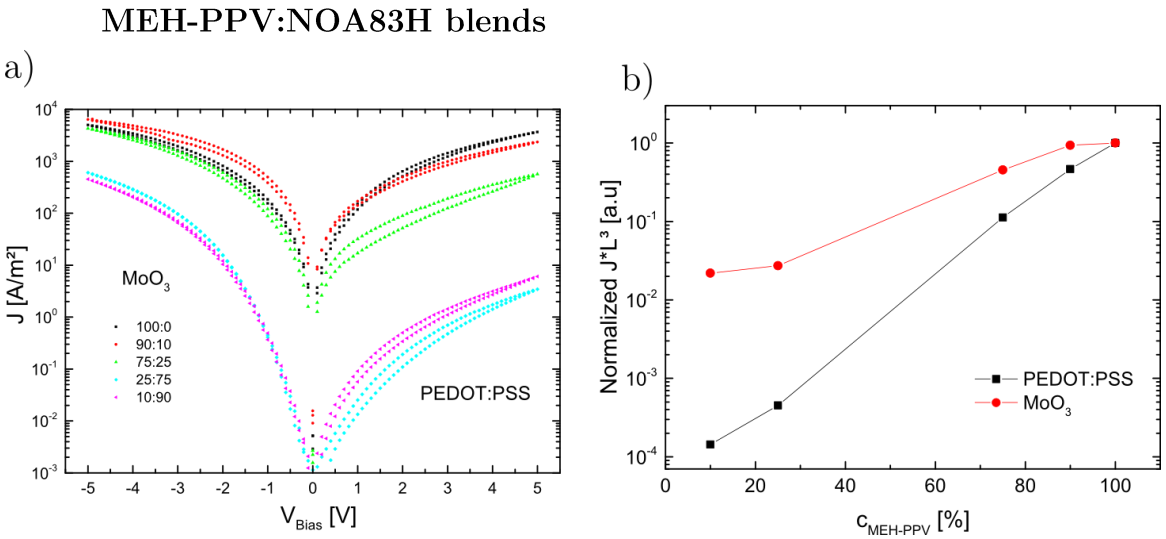

Figure 4.2: a) Current density-voltage characteristics at room temperature of MEH-PPV:NOA83H hole-only devices. Forward bias shows injection from PEDOT:PSS, reverse bias shows injection from MoO_3. b) Current density at +2 V (injection from PEDOT:PSS, black) and -2 V (injection from MoO_3, red) corrected for the film thickness. The blends were cross-linked with a dose of 43 J/cm²

As a next step it was investigated how the presence of the electrically inert matrix affects the transport of holes through the MEH-PPV:matrix blend. Figure 4.2a) shows the *J-V* characteristics at room temperature of hole-only devices of MEH-PPV:NOA83H blends from pristine MEH-PPV (100:0) all the way down to 10:90 blends with only 10 % of the conducting MEH-PPV. The device structure of the hole-only devices is ITO/PEDOT:PSS/MEH-PPV:NOA83H/MoO_3/Al. The blends were cross-linked with a dose of 43 J/cm². The *J-V* curve of the pristine MEH-PPV hole-only device (black squares) is symmetric in forward and reverse bias. This is in agreement with the observation that PEDOT:PSS and MoO_3 both form an ohmic contact to the HOMO of MEH-PPV.(*18*) However, if there is only 10 % of NOA83H in the blend, the curve becomes asymmetric. When the holes are injected from the MoO_3 top contact (reverse bias), the current density is higher as compared to hole injection from the PEDOT:PSS bottom contact (forward bias). The asymmetry is small for the 90:10 MEH-PPV:NOA83H device, but for blends with a higher concentration of NOA83H the asymmetry steadily grows. For the 10:90 MEH-PPV:NOA83H blend a difference of more than two orders of magnitude between forward and reverse bias is observed.

To visualize the effect of the NOA38H on the magnitude of the hole current in Figure 4.2b), current density at +2 and -2 V is plotted as a function of the concentration of MEH-PPV in the blend. For pristine MEH-PPV the (symmetric) current is known to be space-charge limited, following the Mott-Gurney law $J = \frac{9}{8}\varepsilon_0\varepsilon_r\mu\frac{V^2}{L^3}$ at low voltages.(*19*) Not all film thicknesses are identical for the different blend ratios. Therefore, we correct for the effect of thickness variation by multiplying the measured current density J at +2 V and -2 V with the film thickness L to the third power, according to the Mott-Gurney law. As mentioned above, the current density at +2 V shows the current when holes are injected from the PEDOT:PSS contact, whereas the current density at -2 V shows the hole current injected from the MoO_3 contact. For hole injection from the PEDOT:PSS contact the current density strongly decreases with decreasing amount of MEH-PPV in the blend. The difference in current density between 100 % MEH-PPV and 10:90 MEH-PPV:NOA83H amounts to four orders of magnitude. In contrast, the current density for hole injection from the MoO_3 contact hardly changes for concentrations of 100 % MEH-PPV down to 75:25 MEH-PPV:NOA83H. Only if the concentration of MEH-PPV is further reduced to 25% the current density decreases by two orders of magnitude.

The strong decrease of the hole current from the PEDOT:PSS contact with increasing content of inert matrix, combined with the much less affected hole current injected from the MoO3 contact, indicates that there is a hindered injection of holes from the PEDOT:PSS into the MEH-PPV:NOA83H blend. A possible origin might be a vertical phase segregation in the blend such that there is an enriched NOA83H composition at the PEDOT:PSS interface. In a typical PLED the anode consists of ITO covered with a layer of PEDOT:PSS. Consequently, for application in a PLED a MEH-PPV:NOA83H blend with limited hole injection is not really suitable.

MEH-PPV:SR540 blends

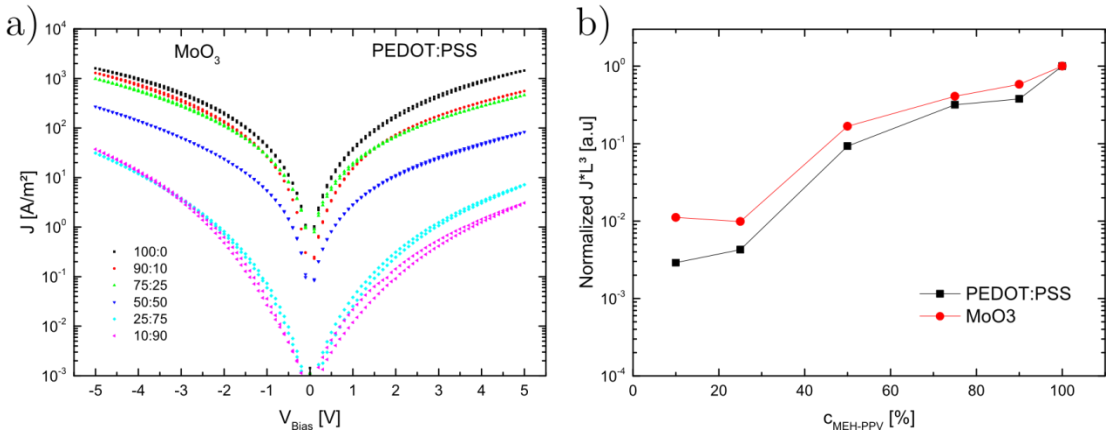

Figure 4.3: a) Current density-voltage characteristics at room temperature of MEH-PPV:SR540 hole-only devices. Forward bias shows injection from PEDOT:PSS, reverse bias shows injection from MoO_3. b) Current density at +2 V (injection from PEDOT:PSS, black) and -2 V (injection from MoO_3, red) corrected for the film thickness.

To verify whether this PEDOT:PSS contact problem is characteristic for NOA83H, the hole transport of blends using a different cross-linkable matrix, SR540, is investigated. To this end, hole-only devices of MEH-PPV:SR540 blends with the same device structure were made and cross-linked with a dose of 43 J/cm^2. Figure 4.3a) shows the *J-V* characteristics at room temperature of MEH-PPV:SR540 hole-only devices from pristine (100:0) MEH-PPV down to 10:90 MEH-PPV:SR540. The curve of the pristine MEH-PPV (black squares) is again symmetric in forward- and reverse bias. In contrast to the mixtures based on NOA83H, here the current density of all blends is symmetric in forward- and reverse bias. In Figure 4.3b) the current density at +2 (PEDOT:PSS) and -2 V (MoO3), corrected for the film thickness, is plotted as a function of MEH-PPV concentration. From pristine MEH-PPV towards a 50:50 MEH-PPV:SR540 blend the current density, gradually decreases one order of magnitude. For blends with a higher concentration of SR540 (25:75 and 10:90 MEH-PPV:SR540) the current density decrease is more pronounced. This shows that SR540 does not affect the hole injection in the blend and both contacts remain ohmic.

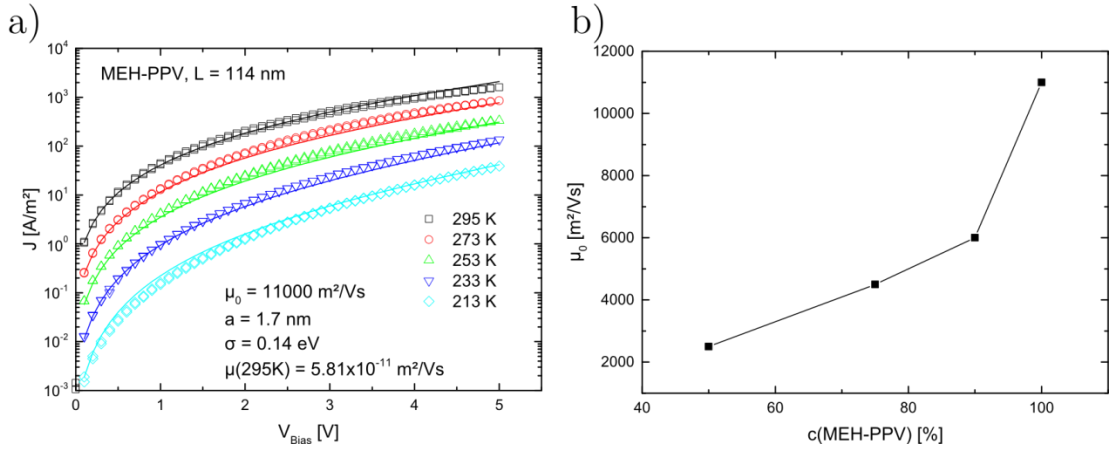

Figure 4.4: a) Current density-voltage characteristics of MEH-PPV for different temeperatures (symbols) and drift-diffusion simulations using a temperature, field and carrier density dependent mobility (lines). b) Mobility prefactor μ_0 as a function of the MEH-PPV concentration in the blend with SR540.

The absence of contact problems allows us to further investigate the hole transport of the MEH-PPV:SR540 blends. To this end, temperature dependent *J-V* measurements were carried out. The *J-V* curves were fitted using drift-diffusion simulations (*20*), that include a temperature-, electric field- and carrier density dependent mobility.(*21*) The mobility is characterized by the following parameters; the mobility prefactor μ_0, the distance between transport sites a and the width of the Gaussian density of states (DOS) σ. The *J-V* characteristics for pristine MEH-PPV at different temperatures from 295 K down to 213 K are shown in Figure 4.4a). The *J-V* characteristics of 90:10, 75:25 and 50:50 MEH-PPV:SR540 blends can be found in the Figure 1 in Appendix A . The room temperature mobility at zero field for pristine MEH-PPV is $5 \times 10^{-11} \frac{\mathrm{m}^2}{\mathrm{Vs}}$. The temperature dependence of the *J-V* characteristics is well described by the mobility parameters $\mu_0 = 11000 \frac{\mathrm{m}^2}{\mathrm{Vs}}$, $a = 1.7\,\mathrm{nm}$ and $\sigma = 0.14\,\mathrm{eV}$. These values are in agreement with earlier reported values in literature. (*21*), (*22*)

The *J-V* characteristics of the 90:10 to 50:50 MEH-PPV:SR540 blend hole-only devices have a similar voltage- and temperature dependence as that of the pristine MEH-PPV, except that the current is lower. As a result, the hole transport in the blends can be described with the same parameters $a = 1.7\,\mathrm{nm}$ and $\sigma = 0.14\,\mathrm{eV}$ as in pristine MEH-PPV. Only the mobility prefactor μ_0 had to be lowered to fit the reduced current density. The values of μ_0 versus the concentration of MEH-PPV in the blend are plotted in Figure 4.4b). With increasing amount of SR540 the mobility gradually decreases. In a blend with little amount of SR540, e.g. 90:10, the mobility is about half of the value for the pristine

device. For the 50:50 MEH-PPV:SR540 blend the mobility decrease by a factor of 5 compared to pristine MEH-PPV. The identical temperature dependence of pristine MEH-PPV as compared to the MEH-PPV:SR540 blends, reflected by the unchanged σ, shows that the energetic disorder is not really affected by the addition of the SR540 matrix in this concentration regime.

4.3.3 Electron transport in MEH-PPV:SR540 blends

In MEH-PPV the intrinsic electron and hole mobility are equal.(*23*) With the hole mobility known, we can further investigate the electron transport in the blends. Since addition of the matrix SR540 does not give rise to injection problems at the PEDOT:PSS contact, that might hinder the performance of blend-based PLEDs, we focus on MEH-PPV:SR540 blends.

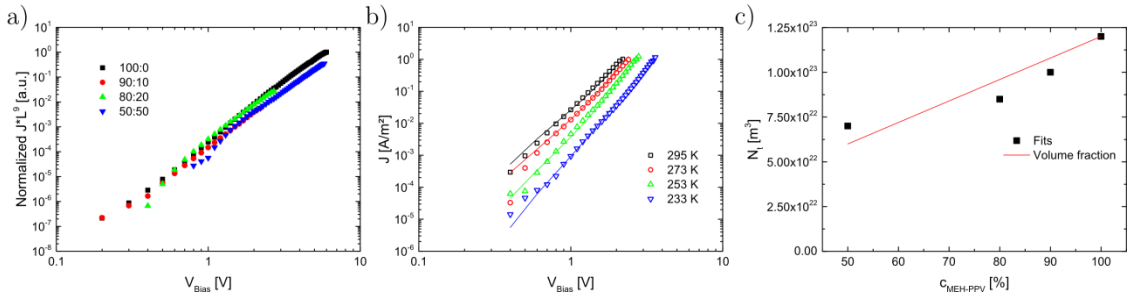

Figure 4.5: a) Current density-voltage characteristics at room temperature of MEH-PPV:SR540 electron-only devices after correction for the film thickness. b) Temperature dependent current density-voltage characteristics of 90:10 MEH-PPV:SR540 electron-only devices. The solid lines show fits with N_t = 1.0x10^{23} m^{-3}, E_t = 0.7 eV and σ_t = 0.05eV. c) Trap density versus the MEH-PPV concentration from the simulations (black) compared to the decrease of volume fraction of MEH-PPV (red).

Electron-only devices of MEH-PPV:SR540 blends were fabricated and the current density versus voltage was measured at different temperatures. The blends were cross-linked with a dose of 43 J/cm^2 The device structure of the electron-only devices is Al/MEH-PPV:SR540/Ba/Al. The electron current in organic semiconductors is known to be trap-limited. (*24*) The current density does not scale with $\frac{V^2}{L^3}$, like in the trap-free space-charge limited case (*22*), but with $\frac{V^{r+1}}{L^{2r+1}}$.(*25*) The coefficient r relates to the width of the energy distribution of the traps and can be determined from the slope of the *J-V* characteristics on a double logarithmic axis. For MEH-PPV the coefficient r is typically equal to 4, leading to a thickness dependence scaling of L^9. To exclude the influence of a variation in film thickness on the *J-V* characteristics of the MEH-PPV:SR540 electron-only blend devices, the current density was multiplied by L^9 and normalized to the current density of pristine MEH-PPV at 6 V.

For the different blend concentrations ranging from pristine MEH-PPV (100:0) to 50:50 MEH-PPV:SR540, the thickness-corrected electron currents at room temperature are shown in Figure 4.5a). Remarkably, the electron current shows almost no dependence on the amount of SR540 in the blend. This is different to the hole transport, where the current density and mobility decreased with increasing amount of SR540 (Figure 4.3). Such a decrease of the hole and electron mobility is also expected to lead to a decrease of the trap-limited electron transport.

To further investigate the electron transport we performed temperature scans of the electron currents for the various blend composition. Figure 4.5b) shows temperature dependent *J-V* scans of a 90:10 MEH-PPV:SR540 blend based electron-only device. For modeling of the devices, the electron mobility is taken equal to the hole mobility.(*23*) To account for the trapping, traps with a Gaussian distribution in energy were used with the parameters trap density N_t, the trap depth E_t and the width of the trap distribution σ_t.(*24*) A good agreement between simulation and measurement was obtained with $N_t = 1.0 \times 10^{23}\ \mathrm{m^{-3}}$, $E_t = 0.7\ \mathrm{eV}$ and $\sigma_t = 0.05\ \mathrm{eV}$, in agreement with earlier reported values.(*26*) The temperature scans and simulation of the 100:0, 80:20 and 50:50 MEH-PPV:SR540 can be found in Figure 2 in the Appendix A.

The obtained trap density as a function of the MEH-PPV fraction in the blend is shown in Figure 4.5c). It can be observed that with increasing amount of SR540, the trap density decreases. In the simulations the trap energy and width are kept constant at $E_t = 0.7\ \mathrm{eV}$ and $\sigma_t = 0.05\ \mathrm{eV}$, respectively. The decrease of the trap density seems to correlate to the decrease in volume fraction of MEH-PPV in the blend, which is shown in red in Figure 4.5c).

The SR540 matrix is an insulator with a high band gap and is electrically inactive. This trap dilution effect has recently been observed for blends of MEH-PPV and a number of large band gap polymers as polystyrene, polyvinylcarbazole and polyfluorene.(*27*) A condition for trap dilution to occur is that there is no macroscopic phase separation. To check, if phase separation occurs an atomic force microscopy (AFM) topography picture of a 50:50 MEH-PPV:SR540 blend was measured (see Figure 3,Appendix A). We observe that the surface is smooth and featureless and does not indicate any form of phase separation. The same was observed for other blend compositions. So the fact that the trap-limited electron current seems nearly independent on the fraction of insulating SR540 in the blend

is a result of two effects that counteract; the decrease of the charge carrier mobility is compensated by the dilution of the trapping sites.

In summary, the hole and electron transport in the 90:10 MEH-PPV:SR540 blend is nearly identical to the transport in pristine MEH-PPV. This demonstrates that MEH-PPV is not damaged by the exposure to UV-light. MEH-PPV is known to photo-oxidize if illuminated with UV-light in the presence of oxygen.(*28*) In this case the electron transport would be strongly decreased because photo-oxidation generates carbonyl groups that act as electron traps. To check if the carbonyl groups are formed during UV-illumination Fourier transform infrared spectroscopy (FTIR) was done. A reference sample of MEH-PPV was not illuminated with UV light and compared to a MEH-PPV sample that was illuminated with a dose of 40 J/cm^2. The measurement can be found in Figure 4 in the Appendix A. In the case of photo-oxidation, carbonyl groups are formed that show a strong absorption around 1650 cm^{-1}.(*28*) Neither the pristine MEH-PPV nor the UV-illuminated MEH-PPV samples show a strong peak in this region, proving that MEH-PPV is not damaged during the UV-illumination in nitrogen.

4.3.4 90:10 MEH-PPV:SR540 PLED

In order to make MEH-PPV insoluble to chlorobenzene we have observed that only 10 % of the UV-curable SR540 matrix is necessary. These 10 % of SR540 only slightly reduce the charge carrier mobility, resulting in decreased hole current density. On the other hand, the trap density is diluted, giving an increase of the electron current density. To observe how both effects influence the current density in a PLED double carrier devices were made using a 90:10 MEH-PPV:SR540 blend that is cross-linked with a dose of 43 J/cm^2. As a reference, also a PLED of pristine MEH-PPV is simultaneously fabricated. The device structure of the blend PLEDs is ITO/PEDOT:PSS/MEH-PPV:SR450/Ba/Al. Current density, as well as the photocurrent density, are shown in Figure 4.6a) for both, blend and pristine device. The current and photocurrent are equal for both devices. The efficiency, the photocurrent divided by the electric current, is shown in Figure 4.6b) and is also identical. This further confirms that the MEH-PPV is not damaged by the UV treatment. As a result, it is demonstrated that the processability of a standard conjugated polymer as MEH-PPV can be modified without affecting its functional properties. The insoluble MEH-PPV based blend films can as a next step be stacked in a solution-processed multilayer device.

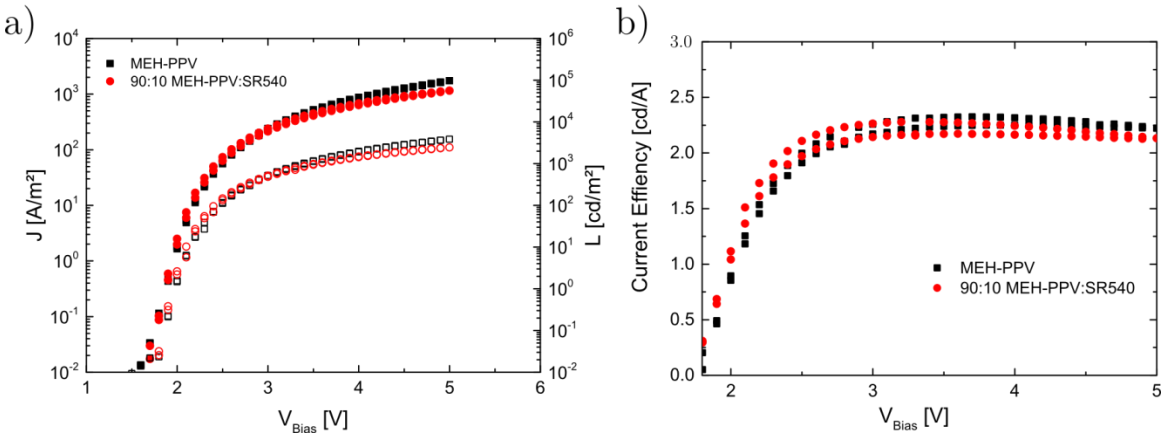

Figure 4.6: a) Current density and photocurrent plotted as a function of voltage for PLED devices based on pristine MEH-PPV (black) and 90:10 MEH-PPV:SR540. (red) b) Current efficiency as a function of voltage of MEH-PPV and 90:10 MEH-PPV:SR540.

4.4 Conclusion

In conclusion, a generic method to tune the solubility of a MEH-PPV layer by blending it with a UV-curable matrix is demonstrated. For two different matrices, NOA83H and SR540, only 10 % of matrix is needed to get an insoluble layer. However, the NOA83H matrix affects the hole injection from the PEDOT:PSS contact, which is not observed when SR540 is used. The hole mobility of 90:10 MEH-PPV:SR540 blends is only slightly lower as compared to pristine MEH-PPV. For the electron transport the mobility decrease is compensated by a dilution of the trap concentration. As a result PLEDs based on an insoluble 90:10 MEH-PPV:SR540 blend exhibit identical current density and photocurrent as compared to pristine MEH-PPV.

4.5 References

1. B. W. D'Andrade *et al.*, High-efficiency yellow double-doped organic light-emitting devices based on phosphor-sensitized fluorescence. *Appl Phys Lett* **79**, 1045-1047 (2001).

2. N. Aizawa *et al.*, Solution-processed multilayer small-molecule light-emitting devices with high-efficiency white-light emission. *Nat Commun* **5**, 5756 (2014).

3. W. L. Ma *et al.*, Water/methanol-soluble conjugated copolymer as an electron-transport layer in polymer light-emitting diodes. *Adv Mater* **17**, 274-+ (2005).

4. S. Sax *et al.*, Efficient Blue-Light-Emitting Polymer Heterostructure Devices: The Fabrication of Multilayer Structures from Orthogonal Solvents. *Adv Mater* **22**, 2087-+ (2010).

5. C. Tanase, J. Wildeman, P. W. M. Blom, Luminescent poly(p-phenylenevinylene) hole-transport layers with adjustable solubility. *Adv Funct Mater* **15**, 2011-2015 (2005).

6. R. Trattnig *et al.*, Bright Blue Solution Processed Triple-Layer Polymer Light-Emitting Diodes Realized by Thermal Layer Stabilization and Orthogonal Solvents. *Adv Funct Mater* **23**, 4897-4905 (2013).

7. S. Xue *et al.*, Fully solution-processed and multilayer blue organic light-emitting diodes based on efficient small molecule emissive layer and intergrated interlayer optimization. *Org Electron* **27**, 35-40 (2015).

8. T. L. Ye *et al.*, Efficient multilayer electrophosphorescence white polymer light-emitting diodes with aluminum cathodes. *Org Electron* **12**, 154-160 (2011).

9. K. S. Yook, S. E. Jang, S. O. Jeon, J. Y. Lee, Fabrication and Efficiency Improvement of Soluble Blue Phosphorescent Organic Light-Emitting Diodes Using a Multilayer Structure Based on an Alcohol-Soluble Blue Phosphorescent Emitting Layer. *Adv Mater* **22**, 4479-4483 (2010).

10. C. M. Zhong, C. H. Duan, F. Huang, H. B. Wu, Y. Cao, Materials and Devices toward Fully Solution Processable Organic Light-Emitting Diodes. *Chem Mater* **23**, 326-340 (2011).

11. L. Derue *et al.*, All-Solution-Processed Organic Light-Emitting Diodes Based on Photostable Photo-cross-linkable Fluorescent Small Molecules. *Acs Appl Mater Inter* **8**, 16207-16217 (2016).

12. M. C. Gather, A. Kohnen, A. Falcou, H. Becker, K. Meerholz, Solution-processed full-color polymer organic light-emitting diode displays fabricated by direct photolithography. *Adv Funct Mater* **17**, 191-200 (2007).

13. C. Gu *et al.*, Multilayer Polymer Stacking by In Situ Electrochemical Polymerization for Color-Stable White Electroluminescence. *Adv Mater* **23**, 527-+ (2011).

14. A. Haldi *et al.*, Optimization of Orange-Emitting Electrophosphorescent Copolymers for Organic Light-Emitting Diodes. *Adv Funct Mater* **18**, 3056-3062 (2008).

15. A. Kohnen *et al.*, The Simple Way to Solution-Processed Multilayer OLEDs - Layered Block-Copolymer Networks by Living Cationic Polymerization. *Adv Mater* **21**, 879-+ (2009).

16. J. Lee, H. Han, J. Lee, S. C. Yoon, C. Lee, Utilization of "thiol-ene" photo cross-linkable hole-transporting polymers for solution-processed multilayer organic light-emitting diodes. *J Mater Chem C* **2**, 1474-1481 (2014).

17. B. W. Ma, B. J. Kim, D. A. Poulsen, S. J. Pastine, J. M. J. Frechet, Multifunctional Crosslinkable Iridium Complexes as Hole Transporting/Electron-blocking and Emitting Materials for Solution-Processed Multilayer Organic Light-Emitting Diodes. *Adv Funct Mater* **19**, 1024-1031 (2009).

18. G. A. H. Wetzelaer, P. W. M. Blom, Ohmic current in organic metal-insulator-metal diodes revisited. *Physical Review B* **89**, (2014).

19. N. F. Mott, R. W. Gurney, *Electronic Processes in Ionic Crystals*. (Oxford University Press, London, 1940).

20. L. J. A. Koster, E. C. P. Smits, V. D. Mihailetchi, P. W. M. Blom, Device model for the operation of polymer/fullerene bulk heterojunction solar cells. *Physical Review B* **72**, 085205 (2005).

21. W. F. Pasveer *et al.*, Unified description of charge-carrier mobilities in disordered semiconducting polymers. *Phys Rev Lett* **94**, (2005).

22. P. W. M. Blom, M. J. M. de Jong, J. J. M. Vleggaar, Electron and hole transport in poly(p-phenylene vinylene) devices. *Appl Phys Lett* **68**, 3308-3310 (1996).

23. Y. Zhang, B. de Boer, P. W. M. Blom, Trap-free electron transport in poly(p-phenylene vinylene) by deactivation of traps with n-type doping. *Physical Review B* **81**, 5 (2010).

24. H. T. Nicolai, M. M. Mandoc, P. W. M. Blom, Electron traps in semiconducting polymers: Exponential versus Gaussian trap distribution. *Physical Review B* **83**, (2011).

25. P. Mark, W. Helfrich, Space-Charge-Limited Currents in Organic Crystals. *J Appl Phys* **33**, 205-215 (1962).

26. H. T. Nicolai *et al.*, Unification of trap-limited electron transport in semiconducting polymers. *Nat Mater* **11**, 882-887 (2012).

27. D. Abbaszadeh *et al.*, Elimination of charge carrier trapping in diluted semiconductors. *Nat Mater* **15**, 628-+ (2016).

28. J. C. Scott *et al.*, Degradation and failure of MEH-PPV light-emitting diodes. *J Appl Phys* **79**, 2745-2751 (1996).

5 Solution-processed multilayer polymeric light-emitting diode without intermixing

In this chapter, the intermixing of two emissive layers in a four-layer solution-processed polymeric light-emitting diode (PLED) with a hole injection, two emissive and one hole-blocking layer is investigated. The relative emission of both emissive layers is measured and compared to a calculated recombination profile across the device using drift-diffusion simulations. A good agreement between the measured and calculated relative emission was found, supporting that there is no intermixing in the two emissive materials.

The content of this chapter was published in:
C. Kasparek and P. W. M. Blom *Appl. Phys. Lett.* **110**, 023302 (2017);

5.1 Introduction

In the last chapter it was shown that by blending poly[2-methoxy-5-(2-ethylhexyloxy)-1,4-phenylenevinylene] (MEH-PPV) with a cross-linkbable host matrix SR540 (ethoxylated (4) bisphenol a dimethacrylate) a blend layer can be made insoluble after cross-linking. Only 10 wt. % of SR540 is necessary to achieve an insoluble blend. This insoluble blend layer can be used to attain multilayer polymer light-emitting diodes (PLEDs).

However, after fabricating a stack of layers it is still possible that the layers are partially intermixed instead of forming a multilayer with distinct interfaces. It is very difficult to experimentally prove if the layers are partially intermixed. In this chapter, the possible occurrence of intermixing of two emissive layers that are solution-processed with this approach is investigated. This is done by fabricating a solution-processed four layer PLED. This device consists of a hole injection layer made of poly(3,4-ethylenedioxythiophene) polystyrene sulfonate (PEDOT:PSS), two emissive layers, a blue-emitting spirobifluorene derivative (SPB-02T, Merck) and orange-emitting MEH-PPV, that are both blended with a cross-linkable host matrix, followed by a hole-blocking layer of poly(9,9-di-n-octylfluorenyl-2,7-diyl) (PFO) sandwiched between an indium tin oxide (ITO) anode and barium/aluminum cathode. The energy diagram of the device is schematically shown in Figure 5.1. The development of the electroluminescence (EL) spectrum is used to investigate whether the emissive layers intermix or not. The measured EL spectrum is finally compared with a numerically simulated Langevin recombination profile across the device that assumes an ideal bilayer structure of the emissive layers without intermixing.

5.2 Intermixing of two emitting layers

The emissive layer in the PLEDs consists of 50 nm of blue-emitting SPB-02T and 15 nm of orange emitting MEH-PPV. If both emitters completely intermix the concentration of MEH-PPV in the intermixed region will be approximate the ratio of the layer thicknesses, typically 30%, as schematically shown in Figure 5.1a). The region of intermixing is indicated by the dotted line. For such a high concentration of MEH-PPV, above the percolation threshold for transport, electrons and holes will be directly injected into the MEH-PPV from the surrounding layers. Even in the case that electrons are injected in the lowest unoccupied molecular orbital (LUMO) of SPB-02T, they will relax to the lower lying LUMO of MEH-PPV soon after injection. As a result, for complete

intermixing the EL spectrum will only show orange emission of MEH-PPV and no blue emission of the SPB-02T. A similar observation was recently done for a 10 % MEH-PPV-90 % PFO blend, where all the electrons and holes in PFO energetically relaxed to MEH-PPV. In the resulting spectrum there was no blue emission of the PFO.(*1*)

In case that there is partial intermixing, resulting in a MEH-PPV concentration below the percolation threshold for transport (~5 %), holes and electrons will be injected into the SPB-02T and form excitons. However, these excitons will diffuse and will transfer their energy to MEH-PPV. It has been shown for MEH-PPV:PFO blends that even for very low concentrations of MEH-PPV of only 1 % the electroluminescence (EL) is still dominated by the orange emission of the MEH-PPV.(*2*) This example of partial intermixing is schematically sketched in Figure 5.1b), where the intermixing with a low MEH-PPV content is indicated by the dashed line. For this case there might be some residual blue emission from the region where the MEH-PPV did not penetrate. However, it should be noted that due to the unbalanced charge transport in MEH-PPV, caused by electron trapping, the recombination zone will be close to the MEH-PPV/PFO interface. The resulting EL spectrum will therefore still be dominated by the orange MEH-PPV emission (indicated by the orange arrows). Only if a bilayer with a sharp interface is formed there will a significant blue emission, additional to the orange MEH-PPV emission. This case is schematically shown in Figure 5.1c). In this case a thin layer of MEH-PPV will emit orange light and a thicker layer of SPB-02T will emit blue light. The emission is indicated by the orange and blue arrows, respectively. Furthermore, the emission of the blue light is expected to increase with increasing voltage, because the recombination zone will broaden across the layers. Analysis of the EL spectrum of the emissive bilayer can therefore be used to discriminate between fully or partially intermixed layers as well as the case of no intermixing.

In our PLED device structure the thickness of the MEH-PPV layer only amounts to 15 nm. This very thin layer of MEH-PPV was deliberately chosen in order to minimize the effect that blue emission coming from SPB-02T will be re-absorbed by MEH-PPV and subsequently emitted as orange light. By decreasing the thickness of MEH-PPV this absorption is decreased. Furthermore, to avoid quenching of excitons by the metallic cathode, a hole-blocking layer of PFO is spin-coated on top of the MEH-PPV:NOA83H blend layer. Typical quenching lengths are in the order of 10 nm.(*3*) If PFO would not be present, most excitons that are formed in the thin MEH-PPV will be quenched at the cathode and almost no

emission of MEH-PPV would be visible in the EL spectrum. The highest occupied molecular orbital (HOMO) of PFO is 5.8 eV below the vacuum level.(*4*) Compared to the HOMO of MEH-PPV which is reported to be around 5.0 – 5.3 eV(*5-7*) below the vacuum level, there is a big energy barrier at the MEH-PPV/PFO interface which blocks holes efficiently.(*8*)

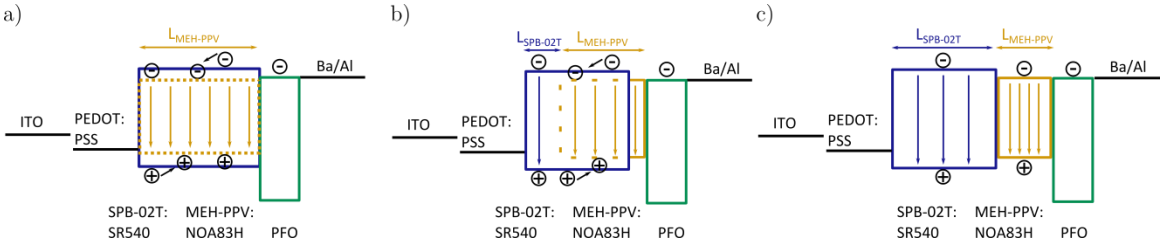

Figure 5.1: a) Schematic energy diagram of a completely intermixed layer of SPB-02T and MEH-PPV. The intermixing of MEH-PPV is indicated by the dotted line. In the intermixed region excitons in SPB-02T will energetically relax to MEH-PPV which results in orange emission solely. b) Energy diagram of partially intermixed emitting layers. Intermixing is indicated by the dashed line. In the intermixed region excitons in SPB-02T will energetically relax to MEH-PPV. This results in a strong orange and weak blue emission from the part where there is no MEH-PPV. c) Energy diagramm of a multilayer device without intermixing. Electrons and holes recombine and emit orange light in MEH-PPV which is indicated by the orange arrows. Additionally, there is a significant blue recombination in SPB-02T that is indicated by the blue arrows.

5.3 Results and discussion

To realize such a multilayer PLED, both the MEH-PPV and SPB-02T layers must be insoluble. It was already described that this can be achieved for MEH-PPV blends by blending it with 10% of a cross-linkable matrix without altering its electrical and optical properties.(*9*) For SPB-02T a similar procedure is followed. Since the NOA83H matrix deteriorated the hole injection from PEDOT:PSS into MEH-PPV and SPB-02T is the layer on top of PEDOT:PSS in the multilayer PLED, SR540 was used as matrix in order to avoid the hole injection problem. 2 wt. % of Irgacure 819 in relation to the total amount of material in the blend was used as a photoinitiator to activate the cross-linking.

To make the blend layer of SPB-02T and NOA83H insoluble 20 wt % of SR540 are needed. This is twice as much as compared to the MEH-PPV blends. The reason is the better solubility of SPB-02T in organic solvents than MEH-PPV, although the molecular weight of SPB-02T (M_w = 750000 g/mol) is higher than MEH-PPV (M_w = 370000 g/mol). If 100 nm of pristine SPB-02T is spin-coated on a glass substrate and chlorobenzene is spin-coated on top only around 20 nm of the film remains on the substrate, whereas for MEH-PPV typically 60 nm remains. If chlorobenzene is spin-coated on a 80:20 SPB-02T:SR540 or 90:10 MEH-PPV:SR540 blend after illuminating with UV light layer there is no wash off at all.

Hole-only devices of pristine SPB-02T and 80:20 SPB-02T:SR540 blends are made to analyze the hole mobility. The device architecture is ITO/PEDOT:PSS/SPB-02T:SR540/MoO_3/Al. The *J-V* characteristics (symbols) of pristine SPB-02T and 80:20 SPB-02T are shown together with drift-diffusion simulations, using a temperature, field and carrier density dependent mobility in Figure 5.2a) and b), respectively. The thickness of both samples is 115 nm. The mobility fit parameters are the prefactor μ_0, the site spacing a and the width of the Gaussian density of states (DOS) σ.(*10*) The obtained parameters together with the (zero-field, zero-density) mobility at 295 K are shown in the figures. The pristine device and the 80:20 blend device can be simulated with the same site spacing a and DOS σ, showing that the disorder is not affected by the presence of the SR540 matrix. The current density of the 80:20 blend devices is slightly lower as compared to the pristine devices. This can be simulated by lowering the mobility prefactor μ_0 from 220 m^2/Vs to 120 m^2/Vs. The effect that a and σ are not affected by the matrix and μ_0 is lowered with increasing amount of matrix has already been observed in MEH-PPV:SR540 hole-only devices.(*9*) The reduction of the zero field mobility of the 80:20 SPB-02T blend by almost a factor of 2 compared to pristine SPB-02T is also similar to the MEH-PPV blends. As a result, an insoluble layer of SPB-02T with nearly identical transport properties as the pristine material can be realized by adding 20% of a cross-linkable matrix.

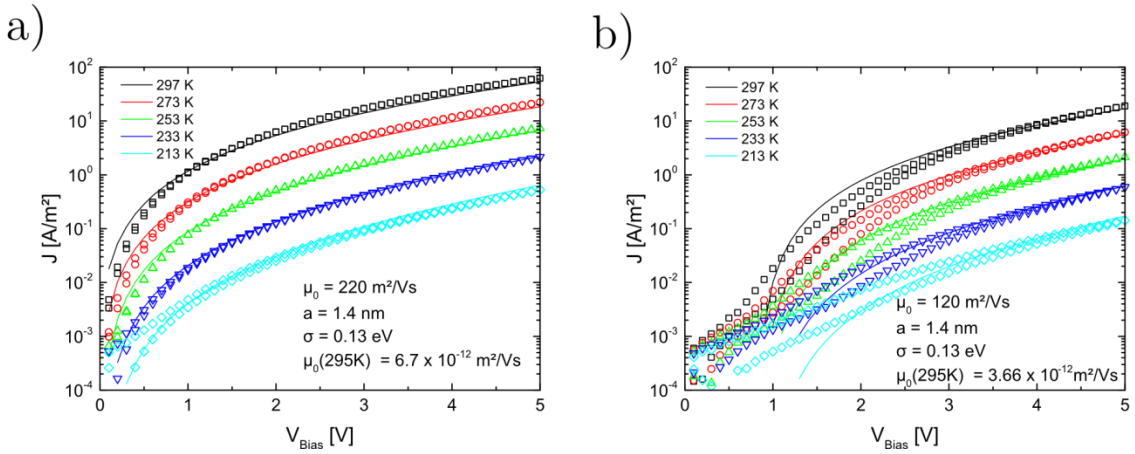

Figure 5.2: J-V characteristics (symbols) of pristine SPB-02T (a) and 80:20 SPB-02T:SR540 (b) hole-only devices together with simulations (solid lines)

As a next step the insoluble 80:20 SPB-02T:SR540 blend is used as a blue emitting layer in a multilayer PLED. To realize a multilayer PLED, the blend was spin-coated on top of a pre-patterned glass/ITO substrate that is covered with solution-processed PEDOT:PSS. The blend was then cross-linked under UV

illumination in a nitrogen atmosphere with a dose of 5 J/cm^2. Afterwards, a 90:10 blend of MEH-PPV and NOA83H, which is used as a different cross-linkable host matrix, was spin-coated on the SPB-02T blend and again cross-linked with a dose of 5 J/cm^2. For MEH-PPV blends with NOA83H we observed that the solubility was lower as compared to MEH-PPV blends with SR540. However, the hole injection from PEDOT:PSS into the MEH-PPV:NOA83H blend was deteriorated upon increasing amount of NOA83H blend. In the multilayer stack a SPB-02T:SR540 blend layer is in between the MEH-PPV:NOA83H and PEDOT:PSS such that this problem does not occur anymore and NOA83H can be used as matrix in combination with MEH-PPV. Finally, PFO was spin-coated as hole-blocking layer, and as a top contact barium with an aluminum capping layer were thermally evaporated.

A first measure to check the stack integrity is the thickness. The total thickness of the solution processed PEDOT:PSS/SPB-02T:SR540/MEH-PPV:NOA83H/PFO multilayer was 139 nm. Thickness of reference layers on glass substrates was 40, 50, 15 and 35 nm for PEDOT:PSS, SPB-02T:SR540, MEH-PPV:NOA83H and PFO, respectively. Comparing the sum of the thickness of the reference layers (140 nm) and the total thickness of the multilayer (139 nm), indicates that the layers are really stacked on top of each other. However, it still is possible that MEH-PPV and SPB-02T intermix or that the film formation on a glass substrate is different as compared to the film formation on another polymer layer. To analyze this further we measure the EL spectrum and calculate the relative emission of MEH-PPV and SPB-02T at different voltages.

The EL spectrum of the multilayer PLED device was measured from 4 to 8 V. The spectra were normalized to the maximum peak that is corresponding to MEH-PPV and shown in Figure 5.3. The MEH-PPV emission is mainly located between 550 and 650 nm. Additionally to that, between 400 and 550 nm there are three peaks that correspond to the blue SPB-02T emission. These peaks are increasing with increasing voltage which means that the emission shifts from an almost pure orange at 4 V to a white emission that consists of blue and orange at 7 V. This is illustrated by the photographs in the inset. The peak does not increase anymore after 7 V. Furthermore, the CIE (Commission internationale de l'éclairage) coordinates have been calculated for each voltage and are shown below the photographs. The coordinates shift from an orange value of x = 0.46 and y =0.45, towards an almost white color of x = 0.34 and y = 0.41. The CIE

coordinates of MEH-PPV and SPB-02T are x = 0.46, y = 0.55 and x = 0.19, y = 0.39, respectively.

Note that for complete intermixing only the orange peak of MEH-PPV would be visible. This is mainly because the energy level of the HOMO and LUMO of MEH-PPV is inside the HOMO and LUMO energy of the SPB-02T. It has been shown that in blends of 10 wt. % MEH-PPV and 90 wt. % PFO, where the energy levels of HOMO and LUMO are also inside the ones of PFO, the resulting EL spectrum is completely orange.(*1*) Additionally, at concentration of MEH-PPV above the percolation threshold, electrons and holes will be injected directly in MEH-PPV instead of SPB-02T. However, from the spectrum alone it cannot be distinguished if there is still a small intermixed region at the SPB-02T/MEH-PPV interface.

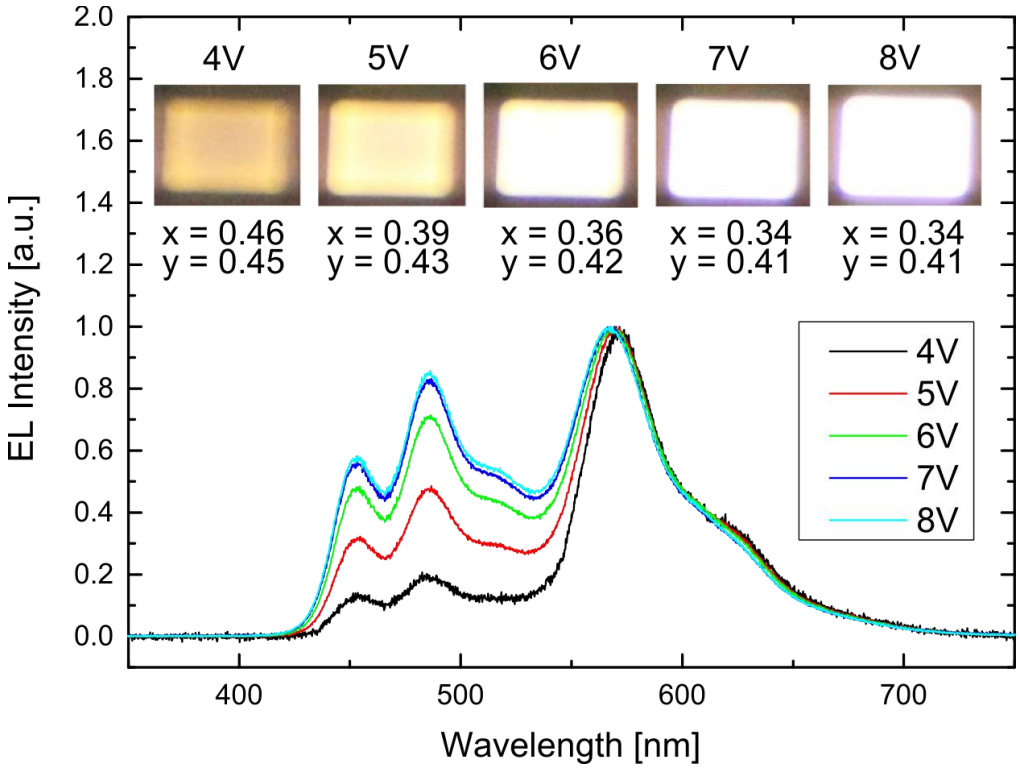

Figure 5.3: Normalized EL spectrum of SPB-02T/MEH-PPV/PFO trilayer for different applied voltages. At low voltages spectrum is dominated by the MEH-PPV emission (peak at 580 nm). At higher voltages there is additionally blue emission of SPB-02T and the emission color changes from orange to white. The inset shows photographs of the device at different voltages.

As a next step the relative contributions of the orange emission of MEH-PPV and the blue emission of the SPB-02T were determined at each voltage. Since the spectra of both materials overlap, the spectrum was deconvoluted by fitting Gaussian peaks to each peak in the spectrum. This is shown for the EL spectrum at 8 V in Figure 5.4a). The red, green and blue peaks correspond to the emission of

SPB-02T and the teal and pink peak correspond to MEH-PPV. The resulting EL spectrum (orange) that is obtained by the sum of the five peaks is shown in orange and is in very good agreement with the measured EL spectrum (black). The area of the peaks corresponding to SPB-02T and MEH-PPV were integrated and from the areas the relative contribution of both emissions was calculated. The relative contribution of the MEH-PPV and SPB-02T emission for each voltage is shown in Figure 5.4b) as symbols.

As shown in Figure 5.3 the EL spectrum is dominated by the orange emission of MEH-PPV at low voltages. More quantitatively, at 4 V 80 % of the emission originates from excitons that recombine in the MEH-PPV layer and only 20 % originate from SPB-02T. As the voltage increases the emission of MEH-PPV and SPB-02T gets more and more balanced. At 7 V 55 % of the emission comes from MEH-PPV and 45 % comes from SPB-02T. In organic semiconductors, the electron transport is limited by the presence of traps.(*11*) Especially at low voltages, when the trap states are not filled, the charge transport is strongly unbalanced. In a single layer PLED electrons mainly occupy a region close to the cathode such that most of the light is generated there. In the present multilayer PLED holes are blocked at the MEH-PPV/PFO interface and recombine with electrons in the MEH-PPV, giving rise to the emission of orange light. As the voltage increases, the traps get more and more filled. Electrons will penetrate beyond the 15 nm MEH-PPV layer into the SPB-02T and also recombine there. The spectrum will change with the applied voltage from almost pure orange to white emission that consists of a balanced orange and blue emission. The effect that the EL spectrum changes with applied voltage is a typical feature in organic LEDs.(*2, 12-17*) Most notably, a color shift from orange to yellow to green was found in a triple emissive layer PLED with a red, green and blue emitting layer.(*16*)

To quantify if SPB-02T and MEH-PPV form a bilayer with a sharp interface, the Langevin recombination across the device is simulated with a drift-diffusion model.(*18*) In this model a temperature, field and carrier dependent mobility according to the extended Gaussian disorder model is used.(*10*) In the simulation we assume a sharp interface without intermixing between SPB-02T and MEH-PPV. If a bilayer is formed then the measured relative emission obtained from the EL spectrum should be equal to the calculated relative emission as obtained from the Langevin recombination distribution.

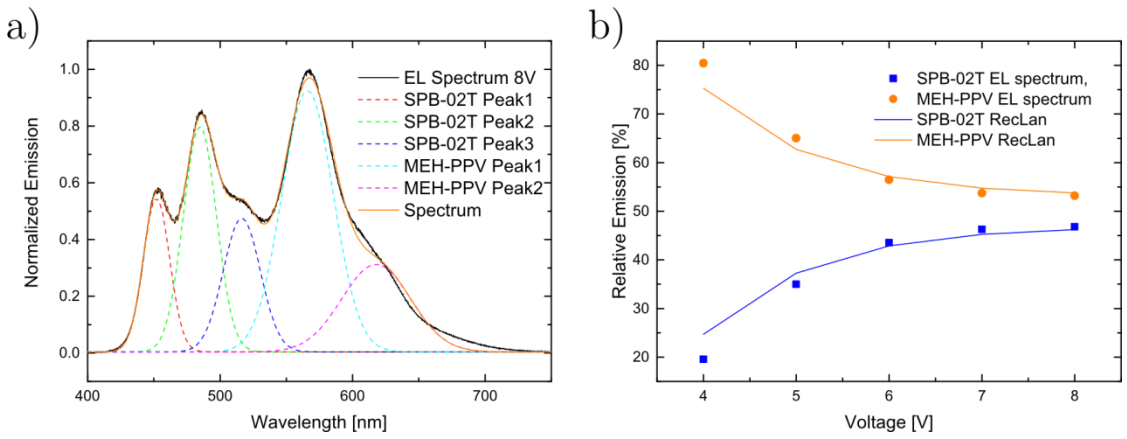

Figure 5.4: a) Deconvolution of the EL spectrum of the multilayer device (black) at 8 V by fitting Gaussian peaks in the spectrum. Integrating the peaks give the relative emission of the device. b) Measured relative emission obtained from the EL spectrum (symbols) and the calculated relative emission (solid line) obtained from Langevin recombination.

Because of the hole-blocking functionality of PFO, there is no recombination in the PFO layer. The HOMO and LUMO levels of MEH-PPV are reported to be -5.3 eV and -2.8eV, respectively.(*5-7*) The HOMO and LUMO values of polyspirofluorenes like SPB-02T are reported to be -5.6 and -2.6 eV, respectively.(*19, 20*) Due to their Gaussian shape, the tail states of both HOMOs and both LUMOs overlap and the small LUMO-LUMO offset at the MEH-PPV/SPB-02T has only a minor effect on the trap-limited electron transport. The calculated relative contributions of the MEH-PPV and SPB-02T emission as obtained from the Langevin recombination profile is shown in Figure 5.4b) as solid line. The calculation is in very good agreement with the relative emissions as determined from the experimental EL spectrum. This implies that there is no significant intermixing at the SPB-02T/MEH-PPV interface. A bilayer with distinct interfaces between the two emissive materials is formed.

5.4 Conclusion

In conclusion, a solution-processed multilayer PLED has been realized consisting of a hole injection layer, two emitting layers and one hole-blocking layer. To analyze if the two emitting layers intermix or if a real bilayer is formed, the relative emission of the two emitting materials was measured at different voltages. The Langevin recombination across the device was calculated at different voltages and compared to the relative emission of the spectrum. A good agreement between the measurement and calculation was found which supports that there is no intermixing at the interface and a bilayer with a sharp interface is formed.

5.5 References

1. D. Abbaszadeh *et al.*, Elimination of charge carrier trapping in diluted semiconductors. *Nat Mater* **15**, 628 (2016).

2. J. Huang, G. Li, E. Wu, Q. Xu, Y. Yang, Achieving High-Efficiency Polymer White-Light-Emitting Devices. *Adv Mater* **18**, 114-117 (2006).

3. D. E. Markov, P. W. M. Blom, Exciton quenching in poly(phenylene vinylene) polymer light-emitting diodes. *Appl Phys Lett* **87**, 233511 (2005).

4. Z. Zhu *et al.*, Polyfluorene Derivatives are High-Performance Organic Hole-Transporting Materials for Inorganic−Organic Hybrid Perovskite Solar Cells. *Adv Funct Mater* **24**, 7357-7365 (2014).

5. A. L. Holt, J. M. Leger, S. A. Carter, Electrochemical and optical characterization of p- and n-doped poly[2-methoxy-5-(2-ethylhexyloxy)-1,4-phenylenevinylene]. *The Journal of Chemical Physics* **123**, 044704 (2005).

6. Y. Li *et al.*, Electrochemical properties of luminescent polymers and polymer light-emitting electrochemical cells. *Synthetic Met* **99**, 243-248 (1999).

7. I. H. Campbell, T. W. Hagler, D. L. Smith, J. P. Ferraris, Direct Measurement of Conjugated Polymer Electronic Excitation Energies Using Metal/Polymer/Metal Structures. *Phys Rev Lett* **76**, 1900-1903 (1996).

8. T. van Woudenbergh, J. Wildeman, P. W. M. Blom, Charge injection across a polymeric heterojunction. *Physical Review B* **71**, (2005).

9. C. Kasparek, R. Rohloff, J. J. Michels, N. I. Crăciun, J. Wildeman, P. W. M. Blom, *Adv. Electron. Mater.* **3**, 1600519 (2017).

10. W. F. Pasveer *et al.*, Unified description of charge-carrier mobilities in disordered semiconducting polymers. *Phys Rev Lett* **94**, (2005).

11. H. T. Nicolai *et al.*, Unification of trap-limited electron transport in semiconducting polymers. *Nat Mater* **11**, 882-887 (2012).

12. A. Kohnen *et al.*, Highly color-stable solution-processed multilayer WOLEDs for lighting application. *J Mater Chem* **20**, 3301-3306 (2010).

13. X. Gong, S. Wang, D. Moses, G. C. Bazan, A. J. Heeger, Multilayer Polymer Light-Emitting Diodes: White-Light Emission with High Efficiency. *Adv Mater* **17**, 2053-2058 (2005).

14. S. Shao, J. Ding, L. Wang, X. Jing, F. Wang, White Electroluminescence from All-Phosphorescent Single Polymers on a Fluorinated Poly(arylene ether phosphine oxide) Backbone Simultaneously Grafted with Blue and Yellow Phosphors. *Journal of the American Chemical Society* **134**, 20290-20293 (2012).

15. J. Zou *et al.*, Simultaneous Optimization of Charge-Carrier Balance and Luminous Efficacy in Highly Efficient White Polymer Light-Emitting Devices. *Adv Mater* **23**, 2976-2980 (2011).
16. C. C. Huang *et al.*, Color-tunable multilayer light-emitting diodes based on conjugated polymers. *Appl Phys Lett* **84**, 1195-1197 (2004).
17. N. Aizawa *et al.*, Solution-processed multilayer small-molecule light-emitting devices with high-efficiency white-light emission. *Nat Commun* **5**, 5756 (2014).
18. L. J. A. Koster, E. C. P. Smits, V. D. Mihailetchi, P. W. M. Blom, Device model for the operation of polymer/fullerene bulk heterojunction solar cells. *Physical Review B* **72**, 085205 (2005).
19. D. Abbaszadeh, H. T. Nicolai, N. I. Craciun, P. W. M. Blom, Effect of arylamine hole-transport units on the performance of blue polyspirobifulorene light-emitting diodes. *Physical Review B* **90**, 7 (2014).
20. J. Yang, Y. Kwon, J. Kwak, C. Lee, P.119: High-Performance Polymer Light-Emitting Diodes with a Conjugated Polyelectrolyte. *SID Symposium Digest of Technical Papers* **44**, 1431-1433 (2013).

6 Efficiency of solution-processed multilayer polymer light-emitting diodes using charge blocking layers

Following the approach presented so far, in this chapter, a trilayer polymer light-emitting diode (PLED) consisting of a blend of poly[N,N'-bis(4-butylphenyl)-N,N'-bis(phenyl)-benzidine] (poly-TPD) and SR540 as electron-blocking layer, Super Yellow-poly(p-phenylene vinylene) (SY-PPV) blended with SR540 as emissive layer and poly(9,9-di-n-octylfluorenyl-2,7-diyl) (PFO) as hole-blocking layer is fabricated from solution. The trilayer PLED shows a 30% increase in efficiency at low voltage as compared to a single layer SY-PPV PLED. However, at higher voltage the advantage in current efficiency gradually decreases. A combined experimental and modelling study shows that the increased efficiency is not only due to the elimination of exciton quenching at the electrodes, but also due to suppressed nonradiative trap-assisted recombination due to carrier confinement. At high voltages, holes can overcome the hole-blocking barrier, which explains the efficiency roll-off.

6.1 Introduction

In the chapters 4 and 5 it was shown that by blending poly[2-methoxy-5-(2-ethylhexyloxy)-1,4-phenylenevinylene] (MEH-PPV) with a cross-linkable host matrix SR540 (ethoxylated (4) bisphenol a dimethacrylate) a blend layer can be made insoluble after cross-linking with only 10 wt. % of SR540. By fabricating a multilayer polymer light-emitting diode (PLED) with two emissive layers, namely a blue-emitting polyspirobifluorene (SPB-02T, Merck) and MEH-PPV, and analyzing the EL spectrum at different voltages, it was found that both layers do not intermix. In this chapter this is utilized to fabricate multilayer PLEDs with charge-blocking layers adjacent to the emissive layer.

In order to increase the efficiency of organic light-emitting diodes, charge-blocking layers are used. These blocking layers are typically adjacent to the emissive layer and confine electrons and holes in the emissive layer, such that they cannot leave the emissive layer without recombining. This is usually realized by materials with a deep highest occupied molecular orbital (HOMO) to block holes and materials with a shallow lowest unoccupied molecular orbital (LUMO) to block electrons. These multilayer structures can be easily fabricated by thermal evaporation.(*1*)

In this chapter, the effect of charge blocking layers on the efficiency of a multilayer PLED is investigated. An increase of around 30 % in current efficiency is found for the trilayer device at low voltages, which slightly reduces at higher voltage. By studying bilayer PLEDs in combination with a two-layer device model, it is found that not only the blocking layers eliminate exciton quenching, but also reduce nonradiative trap-assisted recombination due to charge confinement. The decrease in efficiency at high voltages is attributed to holes overcoming the hole-blocking barrier at high fields.

6.2 Results and discussion

Figure 6.1a) schematically shows the energy diagram of a single layer MEH-PPV PLED. The work function of the PEDOT:PSS hole-injection layer is well aligned with the HOMO of MEH-PPV at around 5.2 eV below the vacuum level. The barium cathode is equally well aligned with the LUMO of MEH-PPV of 2.7 – 3 eV below the vacuum level, such that both contacts can be regarded as ohmic contacts.(*2-4*) In MEH-PPV, like in most conjugated polymers, the electron transport is trap limited.(*5, 6*) By contrast, the hole transport is trap free, which leads to highly unbalanced charge transport. As a consequence, the electron-hole

recombination zone is not in the center of the layer, but very close to the cathode. The PLED light output originates from electrons and holes that form excitons and recombine radiatively. This is illustrated by the red arrows in Figure 6.1a). However, close to a metallic contact, excitons can be quenched, meaning that the excitons transfer their energy nonradiatively via long range dipole-dipole interactions to the metal.(*7*) This is indicated by the dotted line and black arrows in Figure 6.1a). Exciton quenching is especially pronounced at low voltages, where the trap states prevent electrons to drift deeper into the semiconducting layer, resulting in electrons situated mostly close to the cathode. In addition, the presence of trap states give rise to a second, nonradiative trap-assisted (Shockley-Read-Hall, SRH) recombination mechanism.(*8*) Both, SRH recombination and cathode quenching of excitons are important loss mechanisms in PLEDs and their magnitude depends on the applied voltage.(*9*) The SRH recombination events are indicated by the dotted blue arrows in Figure 6.1(a-c). The relative magnitudes of non-radiative losses (SRH recombination and cathode quenching) as a function of the applied voltage are shown for a 100 nm thick MEH-PPV PLED in Figure 6.1d). The plot was obtained using drift-diffusion simulations that include a density, field and temperature dependent charge carrier mobility.(*10, 11*) At low voltage, all electrons are captured by trap states and the efficiency is completely limited by SRH recombination of free holes with trapped electrons. As the voltage increases, the charge density increases, and more free electrons are available in the device due to trap-filling. However, because of the unbalanced charge transport, the recombination zone is still close to the cathode and the efficiency is additionally affected by cathode quenching. At low voltage (e.g. 2.3 V) the loss due to cathode quenching amounts to 13 % while the loss due to SRH recombination amounts to 58 %, resulting in only 29 % radiative exciton recombination. At high voltage (e.g. 5 V) the loss due to cathode quenching decreased slightly to 10 % and the loss due to SRH recombination strongly dropped to 21 %, giving rise to a radiative exciton recombination of 69 %. Due to the increasing amount of free electrons at higher voltage the relative contribution of SRH recombination is reduced, because more free electrons can recombine radiatively with a hole, following the Langevin mechanism.(*12*) Furthermore, the effect of cathode quenching reduces, since the recombination zone shifts away from the cathode due to trap-filling.

In order to avoid quenching at the electrodes and confine the excitons completely in the emissive layer, a trilayer PLED, consisting of poly-TPD as electron-blocking layer, SY-PPV as emissive layer and PFO as hole-blocking layer

is fabricated. The energy diagram is schematically shown in Figure 6.1b). The HOMO and LUMO of poly-TPD are reported to be at 5.1 and 2.3 eV below vacuum level, respectively.(*13*) The HOMO aligns well to the HOMO of SY-PPV located at -5.2 eV, and holes can be injected without a barrier from the ITO/PEDOT:PSS anode. The LUMO of poly-TPD is significantly higher than the LUMO of SY-PPV, which is reported to be at 2.7 eV below vacuum level.(*14*) Therefore, electrons are effectively blocked at the poly-TPD/SY-PPV interface. PFO has a deep HOMO, situated at 5.8 eV and the LUMO is around 2.7 – 3 eV below vacuum level.(*15, 16*). In the resulting trilayer device, holes are blocked at the SY-PPV/PFO interface and electrons are blocked at the SY-PPV/poly-TPD interface, forcing them to recombine in the SY-PPV layer. The chemical structure of the organic semiconductors is shown in Figure 6.1e-h).

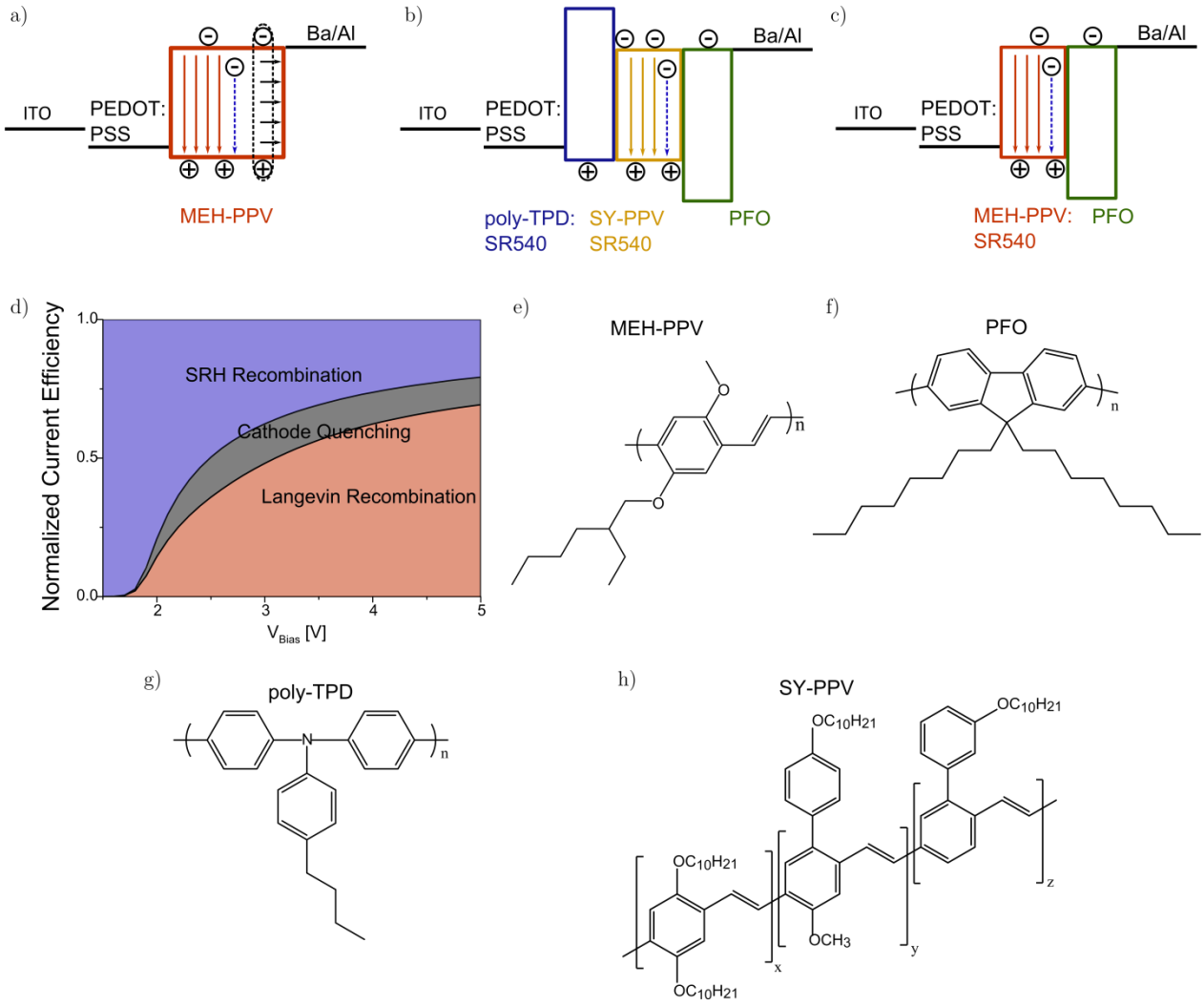

Figure 6.1: a) Energy diagram of a single layer MEH-PPV PLED. Electrons and holes are injected from the cathode and anode, respectively, and recombine by emitting light (red arrows). Trapped electrons recombine nonradiatively via SRH recombination (blue arrow).

Excitons close to the cathode are quenched and do not emit light (black arrows). b) Energy diagram of PLED consisting of poly-TPD:SR540 as electron-blocking layer, SY-PPV:SR540 as emissive layer and PFO as hole-blocking layer. Due to both blocking layers, the charges are confined in the emissive layer and forced to recombine there. c) Energy diagram of PLED consisting of MEH-PPV:SR540 as emissive layer and PFO as hole-blocking layer. Due to the deep HOMO of PFO, holes are blocked and quenching at the cathode is eliminated. d) Non-radiative losses (SRH recombination, blue, and cathode quenching, black) for a 100 nm thick MEH-PPV PLED calculated by a drift-diffusion model using a density-, field- and temperature-dependent carrier mobility. e-h) Chemical structures of MEH-PPV, PFO, poly-TPD and SY-PPV.

The electron-blocking and emissive layers have to be insoluble to achieve a multilayer structure. To obtain insoluble cross-linked films, poly-TPD and SY-PPV were blended with SR540 and Irgacure 819. A 100 nm layer of of SY-PPV:SR540 (90:10 by wt.) with 0.1 wt % Irgacure 819 as a photoinitiator, after cross-linking with UV-light (Dose 43 J/cm^2), showed a wash-off of 20 nm after spin-coating toluene on top of the blend layer. A crosslinked layer of poly-TPD:SR540 (90:10 by wt.) showed a similar wash-off, indicating that crosslinking was reasonably successful. The resulting trilayer device had a total thickness of 105 nm and consisted of a 20 nm 90:10 poly-TPD:SR540 electron-blocking layer, a 45 nm 90:10 SY-PPV:SR540 emissive layer and a 40 nm PFO hole-blocking layer. Including PEDOT:PSS, in total four layers were processed from solution on top of each other. The resulting current density J and luminance L versus the applied voltage V of a SY-PPV single layer (black) and poly-TPD:SR540/SY-PPV:SR540/PFO trilayer PLED (red) are shown in Figure 6.2a). It shows that at a given voltage the current density and luminance of the single layer SY-PPV PLED are higher than for the trilayer device. This originates from the electron and hole-blocking that causes a voltage drop across the charge-blocking layers.

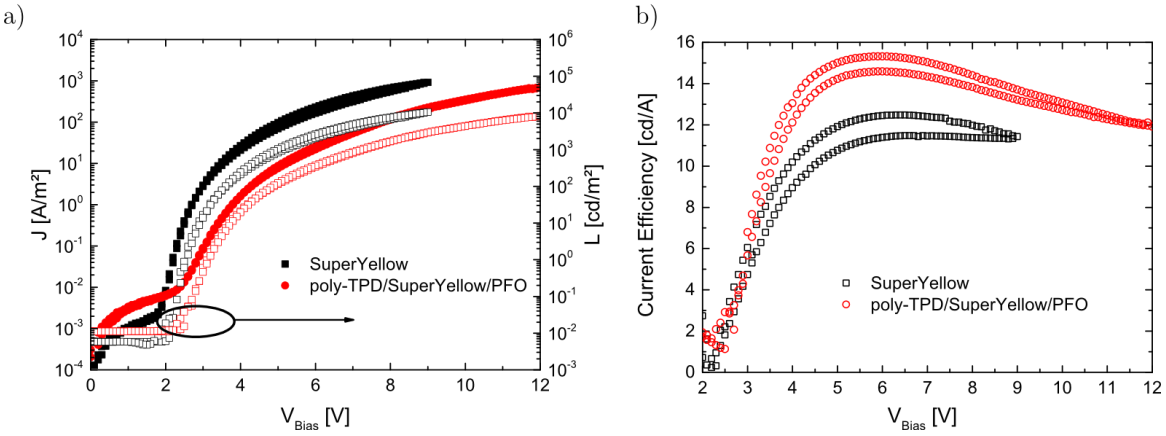

Figure 6.2: a) J-V-L characteristics of a single layer SY-PPV (black) and trilayer poly-TPD/SY-PPV/PFO PLED (red).b) Current efficiency of single layer SY-PPV and trilayer poly-TPD/SY-PPV/PFO PLED.

The resulting current efficiency (luminance divided by current density) is shown in Figure 6.2b) for a single layer SY-PPV (black) and trilayer 90:10 poly-TPD:SR540/90:10 SY-PPV:SR540/PFO PLED (red). The maximum current efficiency of the SY-PPV PLED is 12 cd/A at 6 V. For the trilayer PLED, the maximum value of the current efficiency is 15.5 cd/A at 6 V which is an increase in efficiency of 30 %. This increase is higher than expected for eliminating cathode quenching only as shown in Figure 6.1d). At applied voltages higher than 6 V, the efficiency advantage of the trilayer PLED gradually starts to decrease. For single layer PLEDs, the efficiency decrease at high voltages has been attributed to quenching of excitons at the anode.(*17*) Due to trap-filling, the emission zone is then spread across the whole semiconducting layer, leading to exciton quenching at the anode. However, in the trilayer device, the electron-blocking layer should prevent anode quenching.

In order to study the origin of the efficiency decrease at higher voltages, a simpler structure, consisting of MEH-PPV as emissive layer and PFO as hole-blocking layer, was fabricated. We have chosen MEH-PPV since a 90:10 MEH-PPV:SR540 blend layer is completely insoluble, meaning no wash-off, against chlorobenzene and toluene after cross-linking.(*18*) The energy diagram is schematically shown in Figure 6.1c). In this bilayer device, holes can be injected into the MEH-PPV blend layer and are transported to the PFO interface where they are blocked. Since the LUMOs of MEH-PPV and PFO are well aligned, electrons can be injected into PFO and are transported to the MEH-PPV blend layer where they can form excitons and recombine radiatively. Consequently, the recombination zone is shifted away from the cathode and the negative effect of cathode quenching is eliminated.

The device characteristics of single- and double-layer PLEDs of MEH-PPV and 90:10 MEH-PPV:SR540/PFO are displayed in Figure 6.3. The total film thicknesses of pristine MEH-PPV and the MEH-PPV/PFO double layer PLED were 95 and 85 nm, respectively. In the double-layer PLED, each individual layer is about 42 nm thick. Figure 6.3a) shows that the current density of the MEH-PPV/PFO double layer device is lower as compared to the single layer MEH-PPV PLED. This shift is stronger at voltages below 3 V and at 5 V the current density approaches the current density of MEH-PPV. Since holes get blocked at the PFO interface, the increased driving voltage is caused by the purely trap-limited transport in the PFO layer.(*19*)

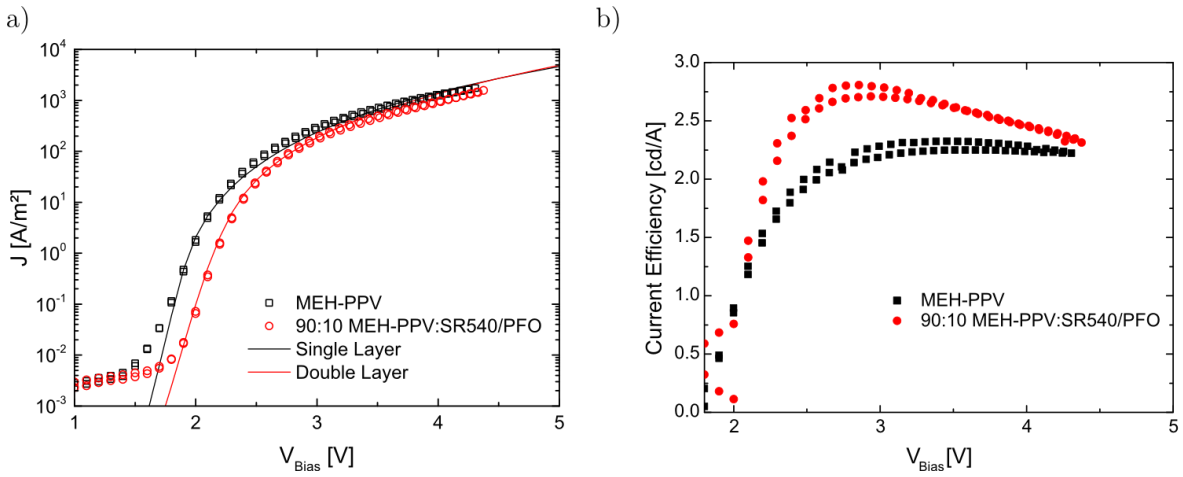

Figure 6.3: a) Current density *J* (open symbols) as a function of the applied voltage *V* of MEH-PPV (black) and 90:10 MEH-PPV:SR540/PFO (red) PLEDs. The lines show drift-diffusion simulations for a single layer (black) and double layer(right) device using field-depedent hole-blocking. b) Current efficiency as a function of the applied voltage of MEH-PPV and 90:10 MEH-PPV:SR540/PFO PLEDs.

The current efficiency as a function of the applied voltage of these devices is shown in Figure 6.3b). The current efficiency of the MEH-PPV PLED (black) gradually increases from 2 to 2.5 V and reaches a plateau of 2.2 cd/A after 2.5 V where it does not increase anymore. The current efficiency of the MEH-PPV:SR540(90:10)/PFO bilayer PLED is higher than the MEH-PPV device and has a peak of 2.8 cd/A at 2.8 V. At higher voltages, the current efficiency decreases gradually until it is almost the same as the MEH-PPV PLED at 5 V. The increase in current efficiency is about 30 % and the behavior is identical as observed in the trilayer device, shown in Figure 6.2b). The identical decrease in current efficiency at higher voltage shows that the decrease in current efficiency is caused by the hole-blocking layer.

To investigate the mechanism of the efficiency decrease at high voltages, drift-diffusion simulations were carried out. As a first step, the single layer MEH-PPV PLED device characteristics were modeled with drift-diffusion simulations(*32*) using a temperature-, electric field- and carrier density dependent mobility.(*10, 11*) The fit parameters describing the charge transport and Gaussianly distributed electron traps obtained from single carrier devices are given in Figure 2 in Appendix B and are identical to previously reported values.(*20*)

The model includes radiative Langevin recombination, nonradiative SRH recombination, and electrode quenching of excitons. Cathode quenching leads to a depletion of excitons in a region close to the cathode. Consequently, the resulting exciton density gradient leads to a diffusion of excitons from a region further away from the cathode towards the depleted region, thereby enhancing the effect of

quenching. (*21, 22*) To quantitatively describe the cathode quenching, the exciton diffusion coefficient and the exciton lifetime were measured using time-resolved photoluminescence (PL). The PL decay of a MEH-PPV film is shown in the Appendix B Figure 1. The diffusion coefficient was found to be $D = 1.3 \times 10^{-7} \frac{\mathrm{m}}{\mathrm{s}}$ and the exciton life time $\tau = 630\ \mathrm{ps}$. The drift-diffusion simulations for a single-layer MEH-PPV PLED are shown in the Appendix B Figure 2 and Figure 3, where the direct energy transfer range x_0 is set to 10 nm for this simulation.

In order to describe the current efficiency of the double layer device, a two-layer model for the hole transport was developed, where the hole transport was divided into two parts across the layer thickness. The mobility in the MEH-PPV layer was described as in the single layer device, using a conventional temperature-, field- and carrier-density dependent mobility.(*32*) To account for the hole-blocking, the hole mobility in the PFO layer was set to $\mu_{h,PFO} = 1 \times 10^{-15} \frac{\mathrm{m}^2}{\mathrm{Vs}}$. This value is more than three orders of magnitude lower than the zero-field mobility of MEH-PPV, which amounts to $\mu_{0,MEH-PPV} = 5 \times 10^{-11} \frac{\mathrm{m}^2}{\mathrm{Vs}}$ (*18*), resulting in holes being blocked at the MEH-PPV/PFO interface. Therefore, the current in the PFO layer is almost completely carried by electrons. By using a decreased mobility instead of an energetic barrier, the hole-blocking effect of the PFO layer is mimicked. For the electron transport, the same parameters were used as in the single layer device.

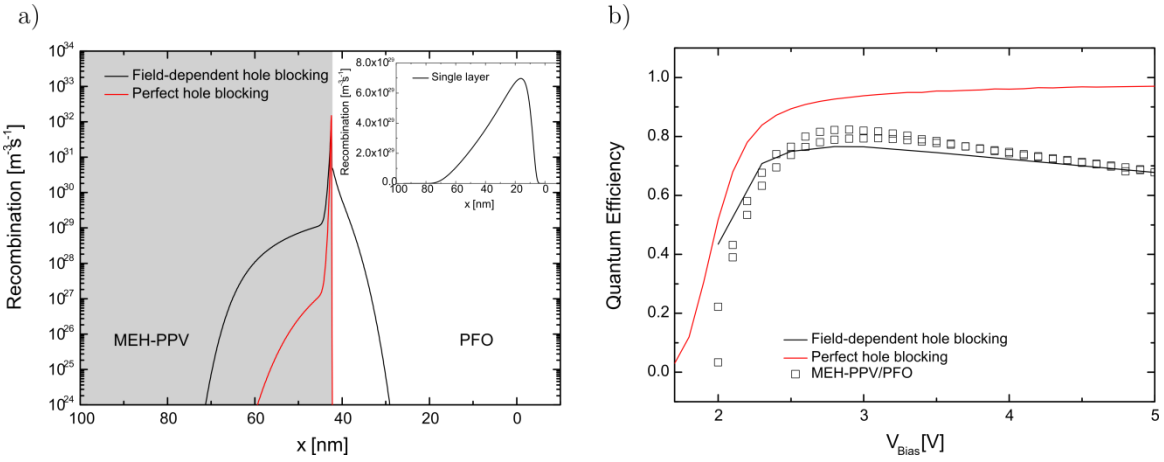

Figure 6.4: a) Simulated bimolecular recombination profiles for perfect hole-blocking (red) and field-dependent hole-blocking at the MEH-PPV/PFO interface at 5 V. The inset shows the recombination profile of a single layer MEH-PPV PLED on a linear scale at 5 V. b) Simulated (lines) quantum efficiency for perfect hole-blocking (red) and field-dependent hole-blocking (black). The experimental efficiency is normalized to the simulation. Only recombination in the MEH-PPV layer was assumed to be radiative in the simulations.

As shown in Figure 6.3a), the simulations are in agreement with the experimental current-voltage characteristics. In Figure 6.4a) the Langevin recombination as a function from distance to the cathode x at 5 V for the two-layer

simulation is shown. The heterojunction between PFO and MEH-PPV was set at 42.5 nm, similar to the experiment. A sharp peak (red line) in the recombination rate is observed at this junction, which is the combined result of the slow trap-limited electron transport through PFO, the trap-free hole transport through MEH-PPV and the hole-blocking effect of the MEH-PPV/PFO interface, leading to carrier accumulation at the interface. Basically, all recombination takes place at the MEH-PPV/PFO interface.

It is observed that the hole-blocking layer affects the efficiency in two ways. The elimination of cathode quenching is one reason for the efficiency enhancement in a bilayer device. However, the efficiency is further enhanced by the carrier confinement at the MEH-PPV/PFO interface. Due to the confinement, the carrier concentration at the interface is higher than the concentration in a conventional single layer device. Consequently, at the interface more electron traps are filled and more free electrons are available, resulting in an increased Langevin recombination as compared to nonradiative SRH recombination. The enhanced ratio of radiative to nonraditive recombination leads straightforwardly to an enhanced efficiency.

The simulated quantum efficiency as a function voltage is displayed in Figure 6.4b). Here, a quantum efficiency of 1 implies that all recombination is radiative, with no losses due to trap-assisted recombination or electrode quenching. After a steep increase at the built-in voltage of 2 V, the efficiency approaches unity and is almost voltage independent. This indicates that SRH recombination is almost completely suppressed due to the effect of carrier confinement.

However, in contrast to the simulation, the measured MEH-PPV/PFO double-layer PLED shows a decrease in current efficiency when a voltage higher than 3 V is applied, as shown in Figure 6.3b). The reason could be that above 3 V the electric field in the device is sufficiently high, such that holes can overcome the energy barrier of 0.5 eV. To account for this effect, the PFO hole mobility in the two-layer model was modified. Instead of a constant mobility, a field-dependent mobility was used(*23*)

$$\mu_{h,PFO} = \mu_0 \exp\left(\gamma\sqrt{E}\right),$$

to mimic field-enhanced hole injection. Here, μ_0 is the zero-field mobility, γ the field-dependent coefficient and E the electric field. The zero-field mobility was again set to $\mu_0 = 1 \times 10^{-15} \frac{\mathrm{m}^2}{\mathrm{Vs}}$, while $\gamma = 1.3 \times 10^{-3} \left(\frac{\mathrm{m}}{\mathrm{v}}\right)^{1/2}$. Again, the recombination profile as a function of the distance from the cathode x was calculated and plotted in Figure 6.4a) at 5 V in black. It appears that the

recombination is now less confined to the interface as in the simulation using a constant mobility, as expected for a reduced hole-blocking effect. Moreover, there is a small amount of recombination in the PFO layer, as observed for $x < 42.5\,\mathrm{nm}$. This shows that the use of a field-dependent mobility simulates the penetration of holes into the PFO layer. It should be noted that the weak recombination in the PFO layer is not visible in the electroluminescence spectrum because the blue light that is emitted by PFO is reabsorbed by MEH-PPV. Since the photoluminescence efficiency of MEH-PPV only amounts to 15%, 85% of the reabsorbed photons are lost. In addition, the decreased carrier confinement results in an increased contribution of nonradiative SRH recombination.

To simulate the efficiency, the recombination inside the PFO layer was treated as being nonradiative. The simulated quantum efficiency using the field-dependent mobility in PFO is plotted in Figure 6.4b). In agreement with the experiment, the simulation shows that the efficiency is increasing at low voltage and decreasing after a voltage higher than 3 V. The decrease of the efficiency can therefore be attributed to holes that overcome the energy barrier between the HOMO of MEH-PPV and PFO. With increasing voltage, more holes can overcome the energy barrier, resulting in a decrease in current efficiency.

What can be further noted from the simulated recombination profile is that anode and cathode quenching are completely eliminated, since most of the recombination is located at the MEH-PPV/PFO interface. As discussed above, the high carrier density at the interface leads to a larger contribution of Langevin recombination with respect to SRH recombination, resulting in a further increased efficiency. It is expected that the use of a better hole-blocking layer (deeper HOMO) can yield a highly efficient PLED without SRH recombination and electrode quenching.

6.3 Summary

In conclusion, it was demonstrated that by blending solution-processed conjugated polymers with a UV-crosslinkable host matrix (SR540) multilayer PLEDs could be achieved. A trilayer PLED was fabricated with poly-TPD as electron-blocking layer, SY-PPV as emissive layer and PFO as hole-blocking layer. The trilayer PLED showed an increased current efficiency at low voltage compared to a single layer SY-PPV PLED. However, at high voltage, the current efficiency gradually decreased. To study the efficiency in more detail, a bilayer PLED was fabricated consisting of MEH-PPV as emissive layer and PFO as hole-blocking

layer. The efficiency of the bilayer device showed identical behavior as compared to the trilayer PLED. It was shown that the increase in current efficiency was not only a result of elimination of exciton quenching at the electrodes, but also due to suppressed non-radiative trap-assisted recombination due to carrier confinement. At high voltages, holes can overcome the hole-blocking barrier, which explains the efficiency roll-off.

6.4 References

1. M. Ikai, S. Tokito, Y. Sakamoto, T. Suzuki, Y. Taga, Highly efficient phosphorescence from organic light-emitting devices with an exciton-block layer. *Appl Phys Lett* **79**, 156-158 (2001).

2. I. H. Campbell, T. W. Hagler, D. L. Smith, J. P. Ferraris, Direct Measurement of Conjugated Polymer Electronic Excitation Energies Using Metal/Polymer/Metal Structures. *Phys Rev Lett* **76**, 1900-1903 (1996).

3. A. L. Holt, J. M. Leger, S. A. Carter, Electrochemical and optical characterization of p- and n-doped poly[2-methoxy-5-(2-ethylhexyloxy)-1,4-phenylenevinylene]. *The Journal of Chemical Physics* **123**, 044704 (2005).

4. Y. Li *et al.*, Electrochemical properties of luminescent polymers and polymer light-emitting electrochemical cells. *Synthetic Met* **99**, 243-248 (1999).

5. H. T. Nicolai *et al.*, Unification of trap-limited electron transport in semiconducting polymers. *Nat Mater* **11**, 882-887 (2012).

6. M. M. Mandoc, B. de Boer, G. Paasch, P. W. M. Blom, Trap-limited electron transport in disordered semiconducting polymers. *Physical Review B* **75**, 193202 (2007).

7. R. R. Chance, A. Prock, R. Silbey, Comments on the classical theory of energy transfer. *The Journal of Chemical Physics* **62**, 2245-2253 (1975).

8. W. Shockley, W. T. Read, Statistics of the Recombinations of Holes and Electrons. *Physical Review* **87**, 835-842 (1952).

9. M. Kuik, L. J. A. Koster, A. G. Dijkstra, G. A. H. Wetzelaer, P. W. M. Blom, Non-radiative recombination losses in polymer light-emitting diodes. *Org Electron* **13**, 969-974 (2012).

10. W. F. Pasveer *et al.*, Unified description of charge-carrier mobilities in disordered semiconducting polymers. *Phys Rev Lett* **94**, (2005).

11. L. J. A. Koster, E. C. P. Smits, V. D. Mihailetchi, P. W. M. Blom, Device model for the operation of polymer/fullerene bulk heterojunction solar cells. *Physical Review B* **72**, 085205 (2005).

12. P. Langevin, *Ann. Chim. Phys.* **28**, 433 (1903).

13. Q. J. Sun *et al.*, White light from polymer light-emitting diodes: Utilization of fluorenone defects and exciplex. *Appl Phys Lett* **88**, 163510 (2006).

14. M. Zhang, S. Hofle, J. Czolk, A. Mertens, A. Colsmann, All-solution processed transparent organic light emitting diodes. *Nanoscale* **7**, 20009-20014 (2015).

15. S. Janietz *et al.*, Electrochemical determination of the ionization potential and electron affinity of poly(9,9-dioctylfluorene). *Appl Phys Lett* **73**, 2453-2455 (1998).

16. U. Scherf, D. Neher, *Polyfluorenes*. (Springer Berlin Heidelberg, 2008).

17. D. Abbaszadeh, G. A. H. Wetzelaer, H. T. Nicolai, P. W. M. Blom, Exciton quenching at PEDOT:PSS anode in polymer blue-light-emitting diodes. *J Appl Phys* **116**, (2014).

18. C. Kasparek, R. Rohloff, J. J. Michels, J. Wildeman, P. W. M. Blom, *Submitted*.

19. T. van Woudenbergh, J. Wildeman, P. W. M. Blom, Charge injection across a polymeric heterojunction. *Physical Review B* **71**, (2005).

20. C. Kasparek *et al.*, Solubility and Charge Transport in Blends of Poly-dialkoxy-p-phenylene Vinylene and UV-Cross-Linkable Matrices. *Adv Electron Mater* **3**, 1600519-n/a (2017).

21. A. L. Burin, M. A. Ratner, Exciton Migration and Cathode Quenching in Organic Light Emitting Diodes. *The Journal of Physical Chemistry A* **104**, 4704-4710 (2000).

22. D. E. Markov, J. C. Hummelen, P. W. M. Blom, A. B. Sieval, Dynamics of exciton diffusion in poly(p-phenylene vinylene)/fullerene heterostructures. *Physical Review B* **72**, 045216 (2005).

23. P. W. M. Blom, M. J. M. de Jong, M. G. van Munster, Electric-field and temperature dependence of the hole mobility in poly(p-phenylene vinylene). *Physical Review B* **55**, R656-R659 (1997).

7 Summary

State-of-the-art organic light-emitting diodes (OLEDs) consist of a stack of small molecule-based layers that each have a specific function. These include hole transport, electron-blocking, emission of one or more colors, hole-blocking and electron transport. Conventionally, such a stack is deposited by thermal evaporation in high vacuum, which is a slow and expensive process. The route towards lower cost is to process these multilayers from solution, such that cost-efficient roll-to-roll processes can be used. However, a major challenge is the stack integrity: when a second layer is coated on top of the previously deposited layer, the first layer will redissolve in the solvent of the second layer. Because of this, fabricating multilayers from solution is very difficult.

Lots of effort has been done to overcome this problem in the past years. However, most of the approaches rely on elaborate and cumbersome synthetic strategies. A universal approach, where common, commercially available organic semiconductors can be used is still lacking. Finding a universal approach for processing multilayer OLEDs is the main topic of this thesis. The main idea is to blend functional polymers with a cross-linkable host matrix. After spin-coating, the matrix is made insoluble by UV-light, rendering the whole blend layer insoluble against its initial solvents. Consequently, a next layer can be spin-coated on the now insoluble blend layer. In this way, the processability (matrix) is separated from the optoelectronic properties (functional polymer).

As a starting point, poly[2-methoxy-5-(2-ethylhexyloxy)-1,4-phenylene-vinylene] (MEH-PPV) is used as the functional polymer. Two different cross-linkable host matrices were tested: NOA83H and ethoxylated (4) bisphenol a dimethacrylate (SR540). Blends of MEH-PPV and matrix with different weight ratios, ranging from pristine MEH-PPV down to 20:80 MEH-PPV:matrix were spin-coated and subsequently cross-linked with UV-light in nitrogen atmosphere. To measure the solubility of the blend layers, chlorobenzene was spin-coated on top of the blends and the film thickness difference before and after spin-coating chlorobenzene was measured. It was found that for both matrices only 10 wt. % is sufficient to make the whole blend layer nearly completely insoluble. As a next step, the charge transport in these blends was analyzed. To this end, hole-only devices of blends with different weight ratio from pristine MEH-PPV to 10:90 MEH-PPV:matrix were fabricated. By comparing two hole-injecting contacts, ITO/PEDOT:PSS and MoO_3 an injection problem was found when holes were

injected from the ITO/PEDOT:PSS contact into the MEH-PPV:NOA83H blends, that markedly reduced the current density. This problem was not encountered in the MEH-PPV:SR540 blends. The hole injection from the MoO_3 contact was not affected by the presence of the matrix and the contact was ohmic at all times. The resulting bulk-limited hole transport was analyzed using a drift-diffusion model in combination with the Extended Gaussian Disorder Model for the charge carrier mobility. It was found that the mobility is decreasing with increasing amount of SR540. However, for a low amount of matrix of only 10 wt. %, that is sufficient to make the blend insoluble, the mobility is only slightly lowered. The electron current of these blends was hardly affected by SR540. Simulations showed that this is due to a dilution of the trap density that counters the effect of the reduced mobility. Finally, polymer light-emitting diodes (PLED) of pristine MEH-PPV and a 90:10 MEH-PPV:SR540 blend were fabricated that showed the same current and photocurrent. This demonstrates that the layer can be made insoluble without affecting its optoelectronic properties.

To extend this approach further, blends of the blue-emitting SPB-02T and SR540 were made. It was found that 20 wt. % of SR540 are necessary to make the blend layer insoluble. This higher amount of matrix was attributed to the increased solubility of SPB-02T in organic solvents. Multilayer PLEDs were fabricated with 80:20 SPB-02T:SR540 as hole transport/emissive layer, 90:10 MEH-PPV:NOA83H as emissive layer and PFO as hole-blocking layer. By combining the blue-emitting SPB-02T and the orange-emitting MEH-PPV, white light emission was achieved. The electroluminescence (EL) spectrum was changing from an almost pure orange light at 4 V to a balanced orange and blue emission at 8 V. The change in the spectrum was utilized to investigate the intermixing of both emitting layers. Although it was shown that the layers are insoluble, intermixing cannot be fully excluded and it is very difficult to experimentally prove the absence of intermixing. By comparing the change in the EL spectrum to a drift-diffusion simulation that assumes a sharp interface without intermixing a good agreement was found, that indicates that there is no significant intermixing at the interface.

Finally, the approach was utilized to fabricate multilayer PLEDs with charge blocking layers to increase the efficiency. A trilayer PLED was fabricated with poly-TPD as electron-blocking layer, SY-PPV as emissive layer and PFO as hole-blocking layer. In this structure, the charges are confined in the emissive layer. The trilayer device showed a 30 % increased efficiency at low voltage as compared

to a single layer device with SY-PPV as emissive layer. However, at high voltage, the current efficiency gradually decreased.

To study the efficiency in more detail, a bilayer PLED was fabricated consisting of 90:10 MEH-PPV:SR540 as emissive layer and PFO as hole-blocking layer. The efficiency of the bilayer device showed an identical behavior as compared to the trilayer device. To investigate this behavior, model calculations were done in which the MEH-PPV and PFO were given different mobilities. The hole mobility in the MEH-PPV layer was conventionally calculated using a temperature-, field- and density-dependent mobility. The hole mobility in PFO was assumed to be very low and field-dependent mimicking the hole-blocking functionality of PFO. It was shown that the increase in current efficiency was not only a result of elimination of exciton quenching at the electrodes, but also due to suppressed nonradiative trap-assisted recombination due to carrier confinement. At high voltages, holes can overcome the hole-blocking barrier, which explains the efficiency roll-off.

In conclusion, a generic way of making layers insoluble by blending commercially available functional polymers with a cross-linkable matrix was presented. For different polymers it was shown that only low amounts of matrix are necessary to make the blend layer insoluble, which did not affect the optoelectronic properties. Several different multilayer PLEDs have been presented in this work that show that this approach has the potential to be a generic way to realize solution-processed multilayer PLEDs.

8 List of publications

- C. Kasparek, R. Rohloff, J. J. Michels, N. I. Crăciun, J. Wildeman, P. W. M. Blom, *Adv. Electron. Mater.* 2017, 3, 1600519
- C. Kasparek and P. W .M. Blom, *Appl. Phys. Lett.* 110, 023302 (2017)
- C. Kasparek, I. Rörich, P. W. M. Blom, G. A. H Wetzelaer *in preparation*
- Lenz, T., Ghittorelli, M., Benneckendorf, F. S., Asadi, K., Kasparek, C., Glasser, G., Blom, P. W. M., Torricelli, F. and de Leeuw, D. M. (2016), *Adv. Funct. Mater.,* 26: 5111–5119

9 List of figures

10 Appendix

A Supplementary Information to Chapter 4

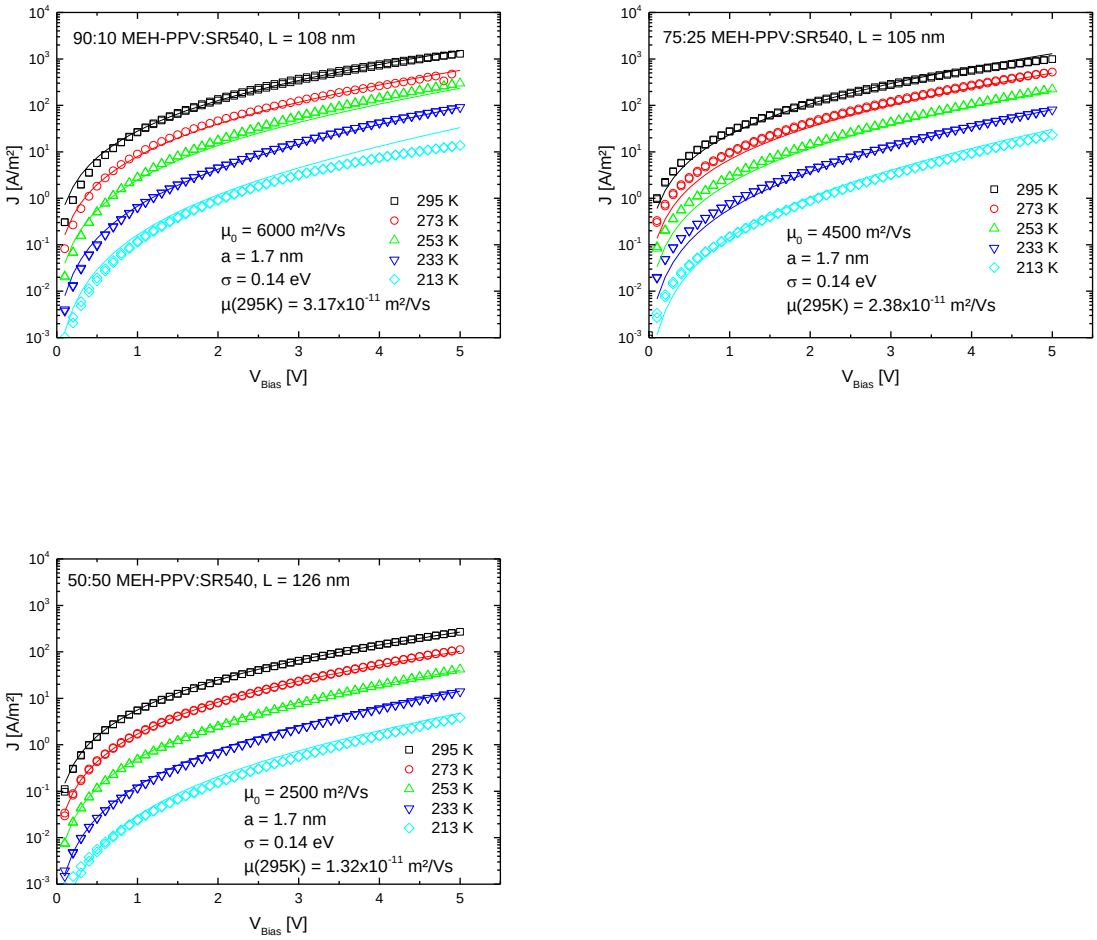

Figure 10.1: J-V characteristics and simulations for hole-only devices of MEH-PPV:SR540 blends for different blend ratios and temperatures. Fit parameters are listed in the figures.

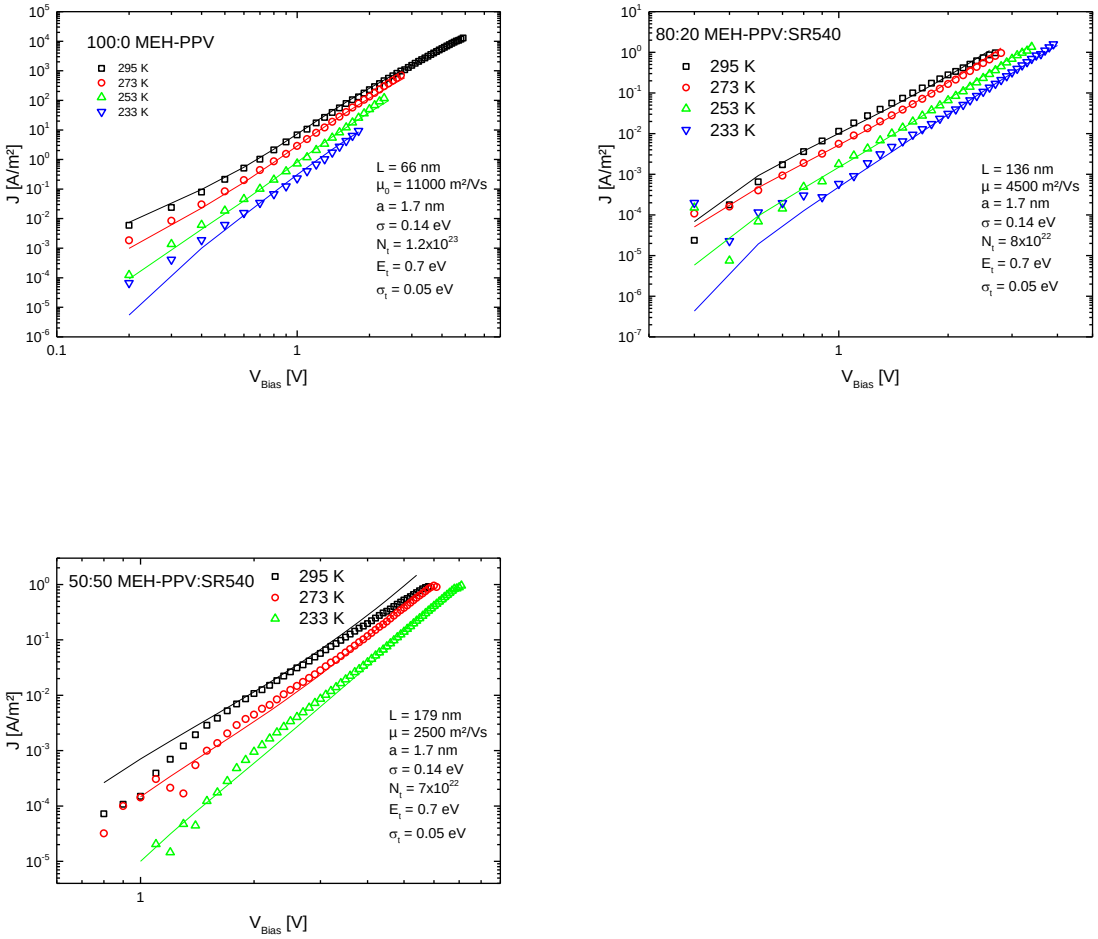

Figure 10.2: J-V characteristics and simulations for electron-only devices of MEH-PPV:SR540 blends for different blend ratios and temperatures. Fit parameters are listed in the figures.

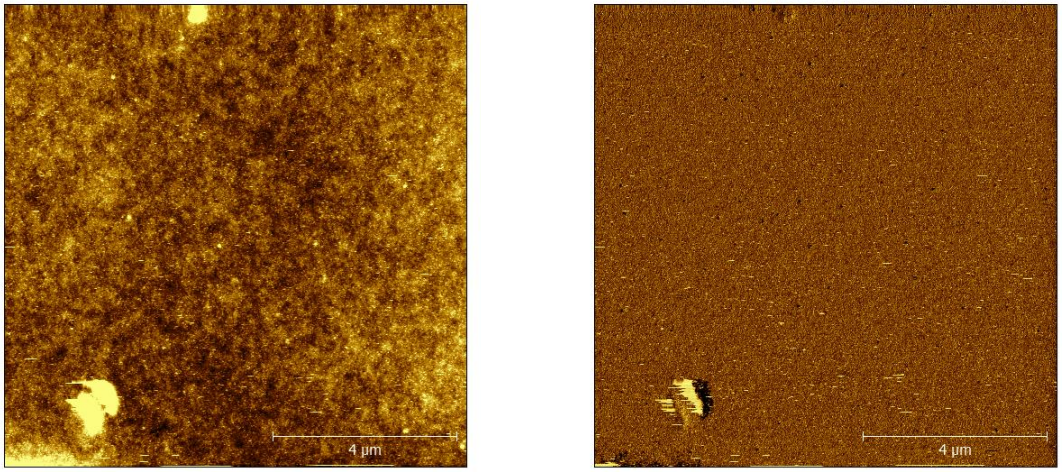

Figure 10.3: AFM of the topography (left) and phase (right) of a 50:50 MEH-PPV:SR540 blend showing a smooth and featureless surface

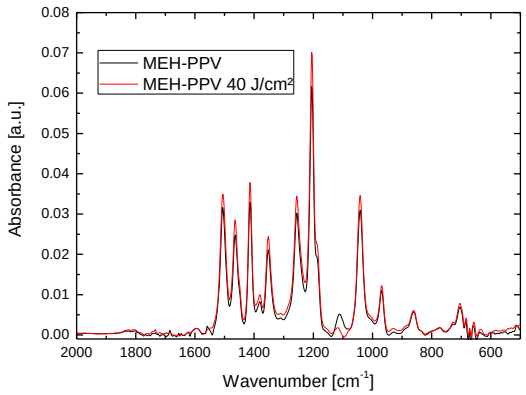

Figure 10.4: FTIR spectrum of MEH-PPV (black) and MEH-PPV that was illuminated with UV light with a dose of 40 J/cm²

B Supplementary Information to Chapter 6

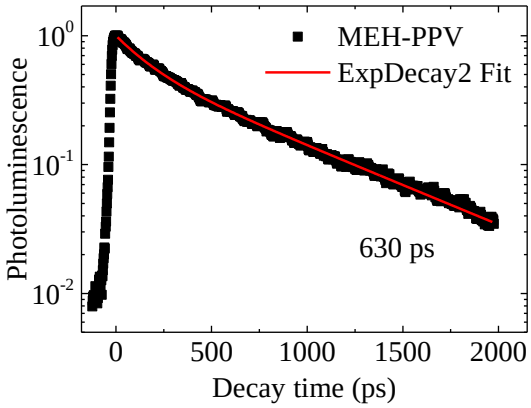

Figure 1: Photoluminescence decay times of MEH-PPV in a thin film measured at room temperature. The exciton lifetime has been determined by double exponential fit to 630 ps.

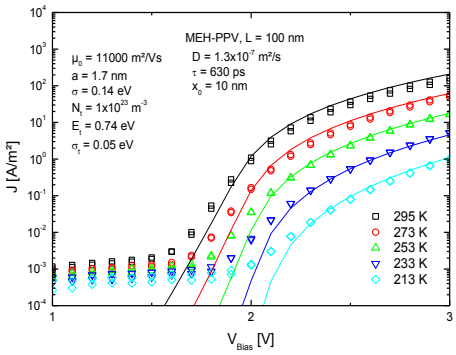

Figure 2: Drift-diffusion simulation of current density versus applied voltage of MEH-PPV PLED for different temperatures

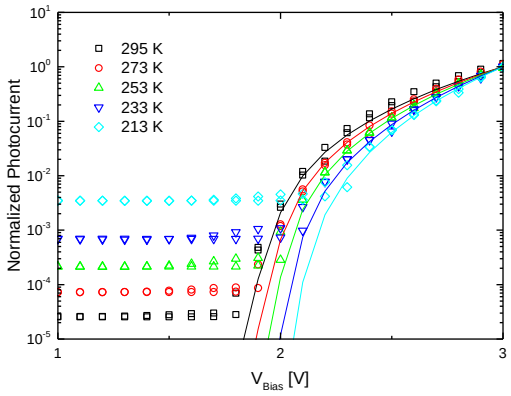

Figure 3: Drift-diffusion simulation of normalized photocurrent versus applied voltage of MEH-PPV PLED for different temperatures